FZR

Forschungszentrum Rossendorf

FZR - 77

Institute of Ion Beam Physics and Materials Research

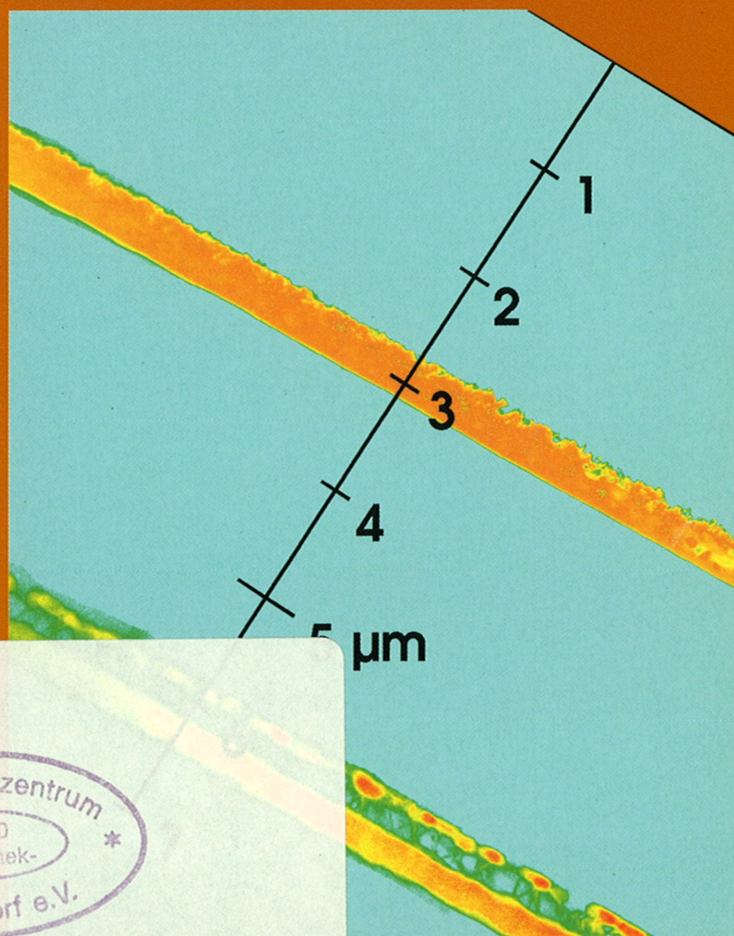

Forschungszentrum
D 120
-Bibliothek-
Rossendorf e.V.
BRD

Annual Report 1994

Postfach 510119
D-01314 Dresden, Germany
Tel. +49-351-591-22 45
Fax +49-351-591-32 85

FORSCHUNGSZENTRUM ROSSENDORF
INSTITUT FÜR IONENSTRAHLPHYSIK UND MATERIALFORSCHUNG

Annual Report 1994

Editors:
W. Möller, E. Wieser, S. Kirch

FZR-77
März 1995

For further information on the research projects described in the present annual report, please address the director or one of the authors at the institute.

The front cover shows a cross-sectional transmission electron micrograph of a double SIMOX structure (two buried layers of SiO_2 in Si), generated by implantation of 10^{18} O^+/cm^2 each at energies of 9 and 3.8 MeV and substrate temperatures of 400 °C and 300 °C, respectively, and subsequent furnace annealing for 12 h in dry nitrogen at 1300 °C.

Postal address:

Postfach 51 01 19
D-01314 Dresden
Germany

Telecommunication:

Tel.: +49 351 591 2245
Fax: +49 351 591 3285
E-mail moellerw
@fz-rossendorf.de

Contents

Seite

Preface 5

Highlights

Ion Beam Induced Crystallization of SiC - Kinetics and Morphology 7

Positron Studies of Defects in Ion Implanted SiC 11

Formation and Characterization of Double SIMOX Structures by Sequential High and Low Energy Oxygen Implantation into Silicon 16

A New Fabrication Method for Submicron $CoSi_2$ Dots and Wires Using Focused Ion Beam Implantation and Local Melting by Flash Lamps 20

IBAD Preparation of Films Containing Carbon Nitride 24

Sheath Dynamics in Plasma Immersion Ion Implantation 28

External PIXE-RBS Analysis of Book Paintings 31

A Novel Silicon Detector Structure with Internal High Field Region for Low Energy Heavy Ion Spectroscopy 34

New Microfluidic Components for the ISFET Microsystem 38

The Dependence of the Hydration Process of Hardening Cement on Temperature Studied by Small-Angle Neutron Scattering (SANS) 40

Structure and Diffusion of Self-Interstitials in Silicon Studied by Molecular Dynamics Simulation 44

Electronic Stopping of Heavy Ions in the Kaneko Model 49

Point Defect-Based Modeling of Diffusion and Electrical Activation of Ion Implanted Boron in Crystalline Silicon 53

Short Contributions

Basic Ion-Solid Interaction 56

Ion Beam Analysis 60

Ion Beam Surface Modification 62

Ion- and Plasma Assisted Deposition 68

Sensors and Microsystems 70

Structural Investigations 75

Ion Devices 78

Statistics

Publications 80

Conference Contributions 87

Lectures 97

Reports 101

Laboratory Visits 102

Patents 103

PhD Thesis 104

Diploma Theses 104

Meetings Organized by the Institute 104

Seminar of the Institute 105

Departments of the Institute 108

List of Personnel 109

Preface

Three years after its foundation at the beginning of 1992, the Research Center Rossendorf (Forschungszentrum Rossendorf, FZR) is on its way towards a modern and efficient establishment. Its five institutes of Ion Beam Physics and Materials Research, Safety Research, Bioanorganic and Radiopharmaceutical Chemistry, Radiochemistry and Nuclear and Hadron Physics are developing successfully towards new tasks on the basis of old activities and know-how acquired in the former institute of the Academy of Sciences in the German Democratic Republic. New research facilities have been and are still being installed. Still, a large number of local restorations remain to be done, and the removal of nuclear waste still presents a severe task. Nevertheless, Rossendorf's tendency towards an 'open' institution has been promoted in 1993 by a widely increasing number of external contacts and collaborations of regional, national and international character.

The Institute of Ion Beam Physics and Materials Research is devoted to the application of ion beams for the modification and the analysis of near-surface layers of solids. The research activities aim at combining closely basic studies and investigations of technological application. For the modification of materials, a broad range of ion-based techniques is available, such as ion implantation, and ion- and plasma-assisted thin film deposition. Correspondingly, characteristic ion energies being available range from about 10 eV for plasma processes to several 10 MeV for heavy ion implantation and ion beam analysis.

With ions provided in this energy range, the institute represents the largest organisation of this kind in Germany. Therefore, the German Research Council confirmed its role as a national ion beam center in the 1994 recommendation for the future of the FZR.

Main fields of application are the improvement of mechanical surface properties, defect engineering and the production of buried layers in semiconductors, and the preparation of special radiation detectors and ion-sensitive microsensors. Technical process development is accompanied by experiments which improve the understanding of the basic physical and chemical mechanisms. For this purpose, in-situ diagnostics play a prominent role. In connection with the experimental studies, theoretical investigations are being performed, in particular using computer simulation programs.

High-energy ion beam analysis is employed as an important tool for the characterization of near-surface layers, both for the institute's scientific program and for external services. The institute offers a broad range of such methods and is continuously improving the corresponding facilities and data reduction techniques.

For the above experimental and theoretical investigations, the institute can rely on a permanent total staff of 81 persons, including 33 professional scientists. In addition to 3 Post Docs, the institute succeeded in recruiting another 23 coworkers in 1993 from different external projects. These are of vital importance as the main source of integrating young scientists. The projects are being sponsored by a wide range of organizations such as the Saxony and the German federal governments, the European Union, and industry. 19 PhD students, more than half of which being supported from external sources, contribute essentially to the research activities of the institute.

In 1994, further relations were established both with industry and within regional, national and international programs.The institute is a member of the Dresden Materials Research Community, which represents about 300 professional scientists at the Technical University of Dresden, the Max-Planck and Fraunhofer societies, and other research institutions. Within programmes by the German Federal Minister of Education, Science, Research and Technology it offers its facilities to scientists in particular from universities. From the European Human Capital and Mobility program, long-term visitors contribute to the scientific program of the institute. Members of the institute played a leading role in the definition of a proposal for a new national program of ion beam application, and in different European networks on ion beam processing of semiconductors, analysis of art objects, and deposition of hard coatings.

A few larger experimental devices became available in 1994 which replaced out-dated machines and complete the ion-beam and diagnostic facilities. In the beginning of the year, a 200 kV high current implanter from DANFYSIK was commissioned and is now routinely in operation. A 500 kV implanter from HIGH VOLTAGE ENG. and a high resolution 300 kV transmission electron microscope (TEM) from PHILIPS have been delivered and will be set into operation in early 1995. Together with the institute of radiochemistry, a beamline for the European Synchrotron Radiation Facility (ESRF) in Grenoble has been designed and is now awaiting its approval by the ESRF board. A project study has been finished and the detailed design has commenced for an extension of the building of the institute, which will allow the combination of the different ion accelerators and implanters and the TEM.

Both in-house experimental activities and external services have significantly increased in 1994: Some machines run at the limits of time and service personnel. Appreciable process in science and application has been achieved, which shall be displayed below. The present annual report will first address some 'highlights', and after that give a complete overview in form of short displays of the results of the individual activities.

Ion Beam Induced Crystallization of SiC - Kinetics and Morphology

V. Heera, R. Kögler, W. Skorupa and J. Stoemenos*
* Aristotele University of Thessaloniki, Physics Department, 54006 Thessaloniki, Greece

SiC may exist in the amorphous and many crystalline phases (polytypes) [1]. Therefore, it is a very interesting candidate for basic studies of crystallization and polytype transformation in solids. Additionally, SiC offers an important potential for applications as a semiconducting material at elevated temperature, high frequency and high power [2]. However, standard technologies for silicon device production as ion implantation at room temperature and subsequent thermal annealing of radiation damage at moderate temperatures cannot be adopted, because the radiation damage in SiC is extremely stable [3]. For instance, recrystallization of ion implantation amorphized SiC needs temperatures higher than 1450°C [4]. One way to overcome this problem is to prevent the formation of radiation damage by high temperature ion implantation [5]. Another idea is to apply ion beam induced epitaxial crystallization (IBIEC), which is known to be a low temperature annealing process in Si [6].

Recently, we succeeded in partial IBIEC of amorphous surface layers in 6H-SiC at a temperature as low as 480°C [7]. This first investigation carried out by Rutherford backscattering spectrometry in combination with the channeling technique (RBS/C) revealed a much more complex kinetics of IBIEC in SiC than in Si. The two most pronounced differences found are that the mean growth rate is a non-linear function of ion dose and amounts only to about 1/100 of the magnitude of the related IBIEC rate in Si [8].

In order to gain a deeper insight into the mechanism of IBIEC in SiC the morphology of the recrystallized layers has been investigated by cross-section transmission electron microscopy (XTEM) [9,10]. Further, series of experiments have been performed to study the dose and temperature dependence of IBIEC in SiC by RBS/C analysis [11]. For the investigations 1" single crystalline 6H-SiC wafers (n-type, (0001) Si-surface) from Cree Research Inc. were used. Amorphous surface layers, about 170 nm thick, were produced by room temperature implantation of 200 keV Ge^+ ions at a dose of 10^{15} cm^{-2} [10]. The IBIEC process was stimulated by 300 keV Si^+ irradiation with fluences between $5 \cdot 10^{15}$ and $3 \cdot 10^{17}$ cm^{-2}. The target temperature was varied between 300°C and 1050°C. One part of the surface of each sample was covered by a piece of silicon wafer to prevent irradiation and, in this way, to have a direct comparison between the ion beam and the pure thermal effect.

The RBS/C measurements reveal a clear shrinkage of the amorphous surface layer in SiC after ion irradiation even at a temperature as low as 300°C, which is more than 1100°C below the threshold temperature for complete thermal recrystallization. In agreement with the results of Bohn et al. [4] a small regrowth could be observed also in the unirradiated reference region at this low temperature. Within the accuracy of the measurement, IBIEC in SiC is an athermal process up to a temperature of 1000°C and clearly dominates over the thermal regrowth below 500°C. However, the mean regrowth rate of about 2 nm/ $1 \cdot 10^{16}cm^{-2}$ is too small for technological applications. Interestingly, a very small temperature increase from 1000°C to 1050°C leads to IBIEC of the whole amorphous surface layer. This corresponds to a regrowth rate of at least 17 nm/ $1 \cdot 10^{16}cm^{-2}$.
The temperature dependence of the thermal part of the total regrowth can be described by an activation energy of about 0.1 eV. It should be emphasized that the thermal regrowth stops after a maximum thickness of about 25 nm and can not be continued by prolonged annealing

at temperatures below 1450°C [4,10], whereas IBIEC proceeds with increasing ion fluence [10]. As clarified by XTEM analysis, the thermally induced amorphous layer shrinkage found in the RBS/C analysis is only due to the annealing of a not completely amorphous transition region of about 25 nm thickness [10] (see also Fig. 2).

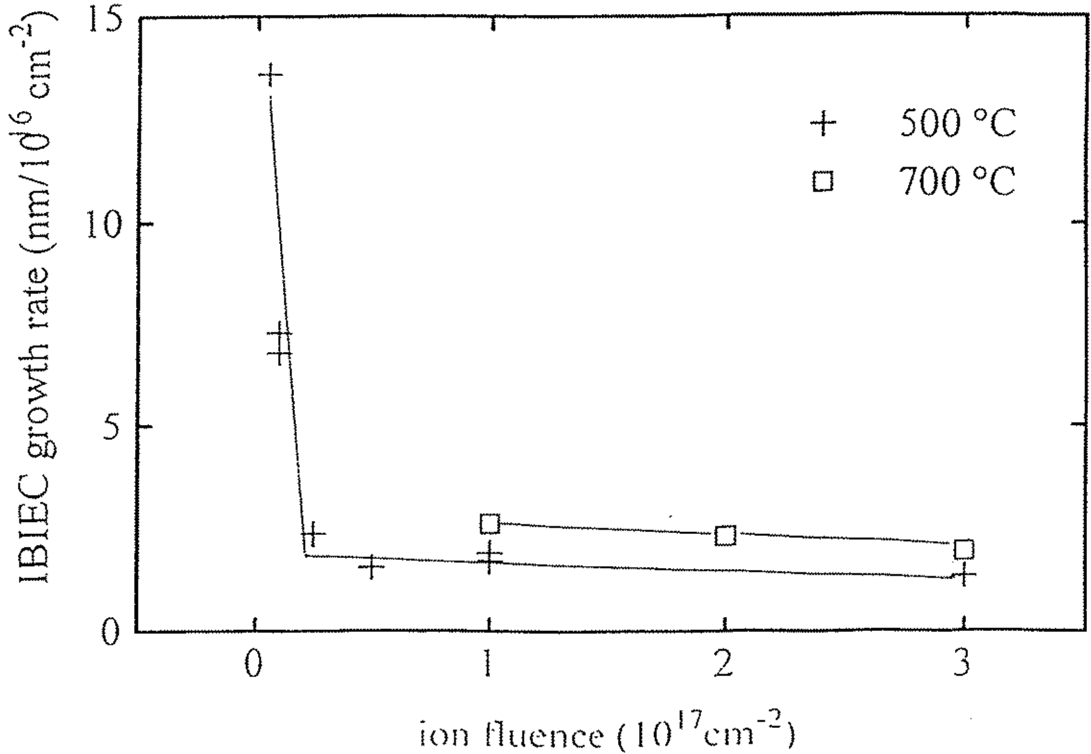

Fig. 1 The IBIEC rate as function of fluence

The fluence dependence of the IBIEC effect at 500°C is reported in Fig. 1. It should be mentioned that the IBIEC rate should be independent of the fluence for undisturbed epitaxial regrowth as known from IBIEC in Si [6]. Obviously, this is not the case for IBIEC in SiC. It decreases with increasing fluence from 14 nm/ $1 \cdot 10^{16}$cm^{-2} for a fluence of $5 \cdot 10^{15}$cm^{-2} to 2 nm/ $1 \cdot 10^{16}$cm^{-2} for $1 \cdot 10^{16}$cm^{-2}, respectively, and then remains almost constant.
As demonstrated by XTEM investigations, besides IBIEC also spontaneous nucleation and grain growth is stimulated by the ion beam irradiation. This effect is also known for Si [11]. Both the complex morphology of the ion beam recrystallized layers (Fig. 2) and the RBS/C results on the IBIEC kinetics can be explained by the competition between spontaneous nucleation and IBIEC [12]. At temperatures below 1000°C spontaneous nucleation of 3C SiC is more enhanced than IBIEC of 6H SiC. Therefore, the regrowth front which moves initially into undisturbed amorphous material meets small nuclei, which must be dissolved. This leads to an decrease in the IBIEC rate. Later the regrowth front is broken by bigger nuclei and epitaxial regrowth is only possible in columns. Finally, the regrowth of 6H SiC stops at the 3C polycrystalline surface layer. A quite different recrystallization regime was found for

temperatures above 1000°C. In this case the recrystallization is governed by epitaxial regrowth. No spontaneous nucleation disturbes the regrowth process. However, also in this regime the recrystallized material is not of a single polytype. In some regions the stacking sequence of the atomic layers is changed and a transition from 6H to 3C polytype occurs.

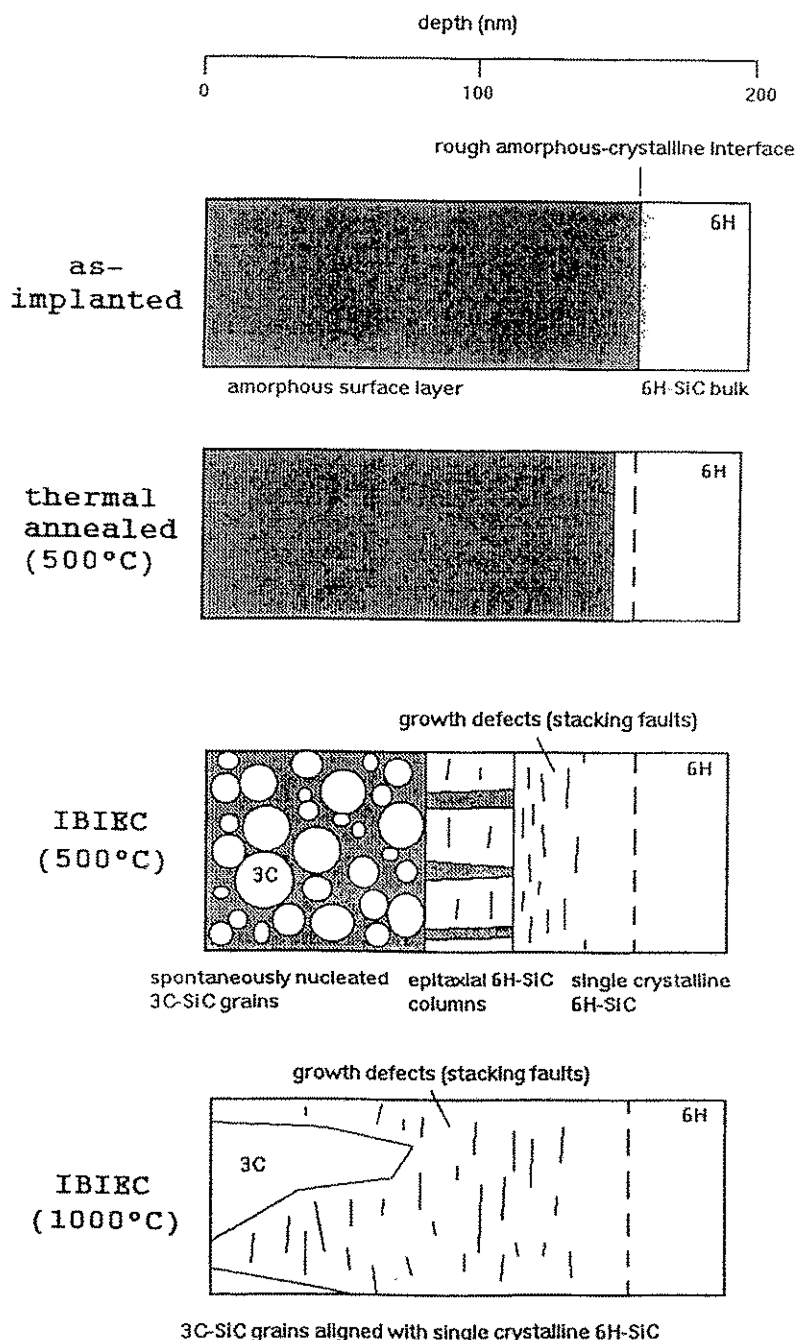

Fig. 2 Schematic of the layer morphology

In summary, our investigations have shown, that complete recrystallization of amorphous SiC layers is possible far below 1450°C, the threshold temperature of thermally stimulated solid phase epitaxy, by means of ion beam irradiation. However at temperatures below 1000°C ion beam stimulated spontaneous nucleation competes with IBIEC. This leads to a complex layer structure and a very small IBIEC rate. In principle, two ways are possible to overcome the problem of spontaneous nucleation, which retards the IBIEC process. The first one is to use a temperature exceeding 1000°C, where IBIEC dominates over spontaneous nucleation. The second one is to repeat a cycle consisting of low fluence IBIEC, where the growth is not yet disturbed by big nuclei, and post-amorphization of the remaining layer containing nuclei [13].

Acknowledgements

The authors which to express their thanks to M. Mäder and M. Voelskow for RBS/C measurements. Part of this work was supported by DFG (contract Ko1287/1-1) and by EMRS-Network 3: IBOS (contract ERBCHRX-CT93-0125).

References

[1] R.F. Davis and J.T. Glass, Advances in Solid State Chemistry **2** (1991) 1
[2] M. Ruff, H. Mitlehner and R. Helbig, IEEE Trans. Electron Devices **41** (1994) 1040
[3] R.F. Davies, G. Kelner, M. Shur, J.W. Palmour and J.A. Edmond, Proc. IEEE **79** (1991) 677
[4] H.G. Bohn, J.M. Williams, C.J. McHargue and G.M. Begun, J.Mater.Res. **2** (1987) 107
[5] R.F. Davis, Thin Solid Films **181** (1989) 1
[6] F. Priolo and E. Rimini, Mater.Sci.Rep. **5** (1990) 319
[7] V. Heera, R. Kögler, W. Skorupa and E. Glaser, Mat.Res.Soc.Symp.Proc. **316** (1994) 229
[8] V. Heera, R. Kögler, W. Skorupa and R. Grötzschel, Nucl.Instr.Meth. B80/81 (1993) 538
[9] V. Heera, R. Kögler, W. Skorupa and J. Stoemenos, Mat.Res.Soc.Symp.Proc. **339** (1994) 197
[10] V. Heera, J. Stoemenos, R. Kögler and W. Skorupa, J.Appl.Phys. 77 (1995) No. 7
[11] J.H. Shin and H. Atwater, Nucl.Instr.Meth. B 80/81 (1993) 973
[12] R. Kögler, V. Heera, W. Skorupa and M. Voelskow, submitted to Nucl.Instr.Meth.
[13] R. Kögler, V. Heera and W. Skorupa, in preparation

Positron Studies of Defects in Ion Implanted SiC

G. Brauer*, W. Anwand*, Y. Pacaud, W. Skorupa, F. Plazaola**, P.G. Coleman[+], A.P. Knights[+], J. Stöermer[++], P. Willutzki[++].
* TU Dresden c/o Forschungszentrum Rossendorf,Dresden, Germany
** Euskal Herriko Unibertsitatea-Zientzi Fakultatea, Bilbo, Spain
[+] University of East Anglia, Norwich, UK
[++]Universität der Bundeswehr München, Germany

Silicon carbide is a very promising material for special micromechanical applications, as well as for high temperature, high power electronic devices. This is due to its very interesting physical and electrical properties such as wide band gap, high thermal conductivity, high breakdown electric field and chemical stability even at high temperature [1]. Thus SiC is of significant interest and it is the purpose of an European Network to investigate its properties and applications in the field of semiconductor and electronic devices.

However, SiC is not an easy material to be processed. Especially, very high temperature is needed for the recrystallization of amorphous regions because of the high stability of defects induced by ion implantation.

The aim of this work is to understand the basic damage creation under irradiation. Therefore the investigation of these damages is also of interest to clarify Ion Beam Induced Epitaxial Crystallization (IBIEC) phenomena [2].

Commercially available 6H-SiC 1" wafers were implanted with 200 keV Ge^+ ions with fluences ranging from 10^{12} up to 10^{15} cm^{-2}. Many techniques, like XTEM, Raman spectroscopy, RBS, EPR, FTIR, and Positron Annihilation Spectroscopy (PAS) were used for the investigation.

PAS is a new technique in the field of SiC. However, it is now a well-established tool for the study of electronic and defect properties of solids [3, 4, 5]. Recent developments in slow positron beam methods [6] furthermore allow to investigate such properties for thin films, layered structures and even at surfaces [7].

Variable energy positron (E = (0.1-30) keV) measurements were performed for all specimens using a computer-controlled magnetic-transport beam system at UEA Norwich [7] at room temperature. Energy spectra of annihilation gamma rays were measured with a Ge detector having an energy resolution (FWHM) of about 1.2 keV at 511 keV. The Doppler broadening of the annihilation radiation is caused by the momentum of the annihilating electron-positron pair and can be characterized by the lineshape parameter S. The value of S is defined after background and shape corrections of the measured annihilation line as the integral of gamma ray intensity in the central energy region divided by the total intensity of the line. It is common to estimate S-E relations which are the base for further evaluations, like damaged layer thicknesses, defect profiles, etc., by the program package VEPFIT [8].

The S-E relations for all specimens are presented in Fig.1. It is obvious that three groups of curves may be defined as follows:

Group 1 : represents the virgin specimen which is characterized by a bulk parameter value $S_{bulk} = (0.4697 \pm 0.0001)$ and an effective positron diffusion length $L_{+,bulk} = (41 \pm 19)$ nm.

Group 2 : Fluence range from 10^{12} up to 10^{14} cm^{-2}, represents the ion implanted specimens where due to the damage caused by the ion implantation their crystalline structure has still not been lost. It shows already from the S-E relations that positrons are sensitive to the damage caused by different fluences of implanted ions and it should be possible to characterize such damage even at much lower fluences than 1×10^{12} cm^{-2}.

Group 3 : Fluences of $3x10^{14}$ and 10^{15} cm^{-2}, represents the ion implanted specimens where due to the damage caused by the ion implantation the crystalline structure has been lost in part and an amorphous layer at the surface exists. This is to be concluded from the large S values observed in the depth range (0 - 300 nm) compared to the measured S values observed at lower implantation fluences in the same range.

The thicknesses of the damaged layers were evaluated and are summarized in Table 1. As expected an increase of the damaged crystalline layer thickness with increasing fluence is found. In addition, for the two highest fluences applied an amorphous surface layer of about 100 nm thickness could be detected. This evaluated thickness corresponds well in its order of magnitude to the value estimated by TEM [2].

Φ (cm^{-2})	d_{DL} (nm)	d_{AL} (nm)
$1x10^{12}$	441	-
$3x10^{12}$	429	-
$1x10^{13}$	615	-
$3x10^{13}$	842	-
$1x10^{14}$	1050	-
$3x10^{14}$	976	94
$1x10^{15}$	977	98

Table 1 : Maximum thickness ($d_{DL,AL}$ = depth with respect to the surface as zero reference) of damaged (DL) and amorphous (AL) layers in 6H-SiC specimens implanted with 200 keV Ge^{+} ions to different fluences Φ.

In order to have an idea of the positron lifetimes to be expected in SiC polytypes calculations using the superimposed atom model [9] have been performed for perfect and several defected lattices, respectively. In the calculations the positron does not affect the electron structure beyond the short-range enhancement of the electron density at the positron. For the delocalized positron states, this is the correct limit of the two -component density functional theory [10] used to describe electron-positron systems. All results of the calculations are summarized in Tables 2 and 3, respectively. Eventhough the structures of the three SiC polytypes used in the calculations are different, the calculated bulk lifetimes are within 1 ps the same.
However, this result is not unexpected because the volume per atom in the three structures is very similar. Beside positron lifetimes the binding energies E_b for positrons trapped by a vacancy-type defect are collected in Table 3 too. The lifetimes calculated in the neutral, unrelaxed mono- and divacancies are also quite similar in the three polytypes. Therefore, the zincblende structure has been used also to perform the calculations in larger vacancy-agglomerates.

host	a (a.u.)	c (a.u.)	τ (ps)
3C-SiC	8.24	-	141
2H-SiC	5.81	9.54	142
6H-SiC	5.81	28.50	141

Table 2 : Lattice data and calculated bulk lifetime τ for SiC polytypes. The lattice constants a and c are given in atomic units (1 a.u. = $0.529177x10^{-10}$ m).

defect	3C-SiC		2H-SiC		6H-SiC	
	τ_d (ps)	E_b (eV)	τ_d (ps)	E_b (eV)	τ_d (ps)	E_b (eV)
V_C	150	0.28	151	0.26	150	0.28
V_{Si}	185	1.69	184	1.67	183	1.73
1-$V_{Si}V_C$	216	2.39	216	2.40	214	2.44
2-$V_{Si}V_C$	254	3.48	-	-	-	-
3-$V_{Si}V_C$	286	4.27	-	-	-	-
4-$V_{Si}V_C$	321	4.94	-	-	-	-

Table 3 : Calculated positron lifetimes τ_d in different types of neutral and unrelaxed vacancy-type defects in three SiC polytypes. The defect configuration n-$V_{Si}V_C$ (n = 1, 2, 3, 4) indicates a vacancy agglomerate with n missing divacancies. E_b indicates the binding energy of the positron in the corresponding defect.

Variable energy positron (E = (1-20) keV) lifetime measurements were performed on selected specimens (Samples implanted with fluences of 10^{13} and 10^{15} cm^{-2}, virgin 6H-SiC) with the latest timed-beam system at UBW Munich 11 at room temperature. The mean positron lifetime estimated for a certain positron energy E from the estimated -E relations yields the same information like the S-E relation. However, from a decomposition of the full lifetime spectra measured at each positron energy E it is possible to deduce useful additional informations about the type of defects involved. For the lifetime evaluations the program package POSITRONFIT 12 has been used.

In virgin 6H-SiC no straightforward one-component fit has been possible. However, regarding the energy range (5-20) keV only and averaging the mean lifetimes obtained in the different more-component fits finally a bulk lifetime τ_b = (140 $\pm$ 5) ps is obtained in rather good agreement with the theoretical estimation (see Table 2).

In case of specimen implanted with fluence of 10^{13} cm^{-2} from a two-component fit without any constraints an average longer lifetime component τ_2 = (235 $\pm$ 3) ps has been found in the energy range (1.5-14) keV that changes slightly into τ_2 = (242 $\pm$ 14) ps if the averaging is extended to the full energy range (1-20) keV. Therefore, we regard the lifetime τ_2 = (235 $\pm$ 3) ps to be representative of a vacancy-type defect created by ion implantation in SiC of still crystalline structure . According to the theoretical estimations given above (see Table 2) this defect most probably should be the divacancy.

The calculated positron lifetimes in this study correspond to neutral unrelaxed defects. However, the vacancies might be in different states of charge in semiconductors. It has been shown in the literature [13-15] that the charge state affects the positron lifetime through the changes in the atomic relaxation around the vacancy. Moreover, the relaxation around the defect is expected to increase with the number of vacancies in the agglomerate. Therefore, particularly in the case of larger vacancy agglomerates the calculated positron lifetimes may be shorter than the real ones. In case of specimen implanted with fluence of 10^{13} cm^{-2} an outward relaxation of the divacancy seems to be indicated from the experimental value of τ_2 which slightly exceeds the theoretical estimate (τ_{2v} = 214 ps).

In case of specimen implanted with fluence of 10^{15} cm^{-2} a two-component fit without any constraints gave a longer lifetime component τ_2 = (305 $\pm$ 6) ps with intensities up to about 80 percent in the energy range (1-5) keV. At higher energies this lifetime component rised up to 450 ps with its intensity decreasing thereby down to about 5 percent. This should not be regarded as an indication of increasing vacancy cluster sizes with depth because of very large errors implied in these values. On the other hand the shorter lifetime component decreases from about 220 ps to 163 ps in the energy range (5-20) keV. This suggests to interpret this lifetime component as an average of annihilations in the bulk and a defect having a lifetime of the order (200-250) ps, i.e. most probably the divacancy. This conclusion is supported from the obvious similarity of all S-E

curves at higher incident positron energies (see Fig.1). In order to have a more clear picture the evaluation of the sample implanted with fluence of 10^{15} cm^{-2} data has been repeated with the fixing: $\tau_2 = 305$ ps. According to the theoretical estimations given above (see Table 3) this lifetime should result from annihilations in vacancy clusters consisting of at least four but more probably six vacancies.

A more detailed presentation and discussion, especially regarding the extraction of true defect profiles from the lifetime data, is in progress for publication [16].

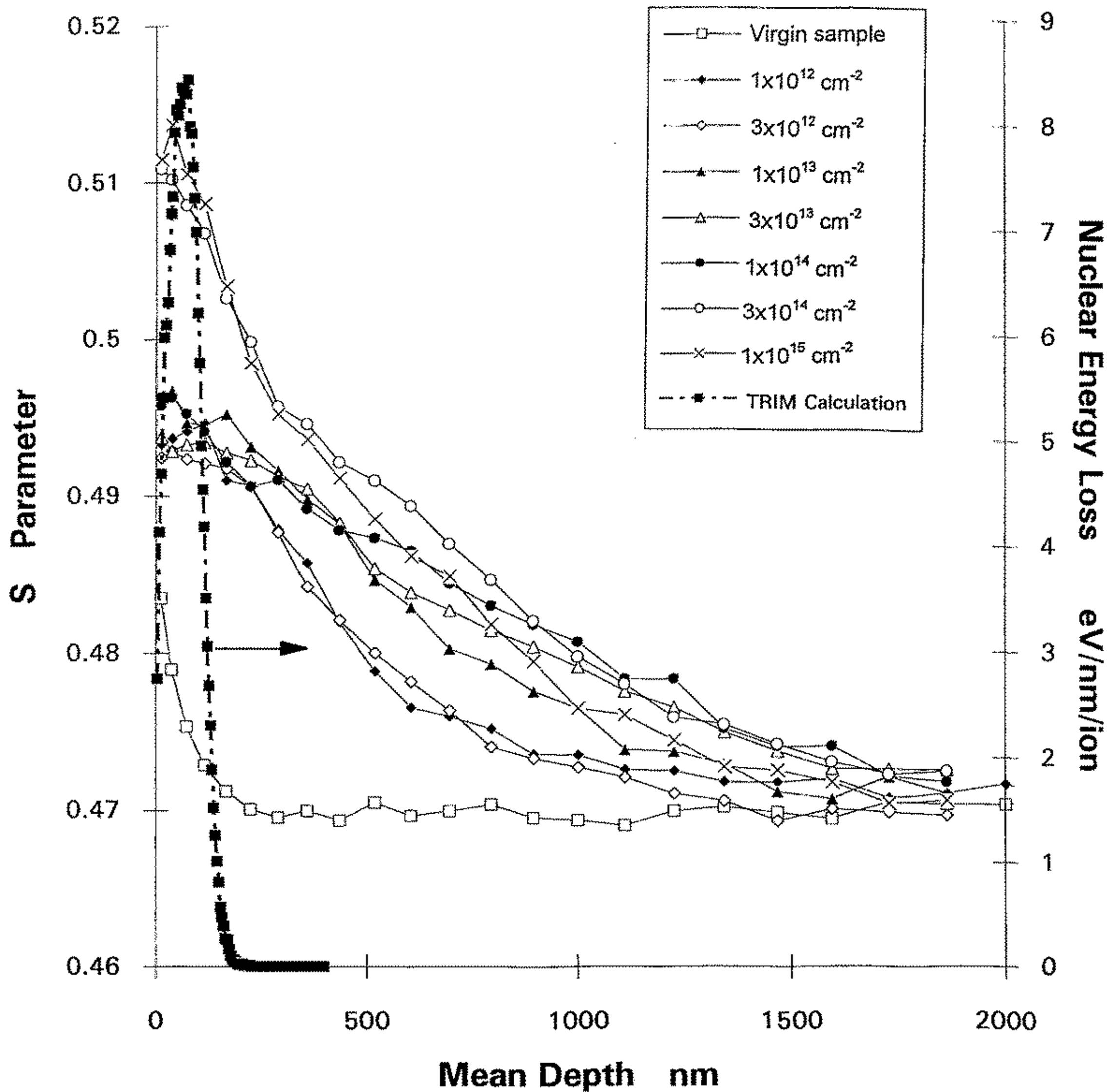

Figure 1 : In depth profile of positron annihilation spectra. The curve of the nuclear energy loss during implantation calculated by TRIM simulation is plotted for comparison.

[1] J.A. Powell, P. Pirouz, W.J. Choyke. Semiconductor interfaces, Microstructures and devices : Properties and applications (1993). pp 257-293. Publisher IOP Publishing Ltd, techno house, Redcliffe way.
[2] V. Heera, J. Stoemenos, R. Kögler, W. Skorupa. To be published in Journal of Applied Physics.
[3] Positrons in Solids. Topics in Current Physics, Vol.12. Ed.: P. Hautojärvi (Springer, Berlin, 1979)
[4] Positrons in Solid-State Physics. Proc. Int. School of Physics "Enrico Fermi", Course LXXXIII, Varenna, 1981. Eds.: W. Brandt, A. Dupasquier (North Holland, Amsterdam, 1983)
[5] P.J. Schultz, K.G. Lynn, Rev. Mod. Phys. 60 (1988) 701
[6] Positrons at Metallic Surfaces. Ed.: A. Ishii (Trans. Tech. Publications, Aedermannsdorf, 1992)
[7] N.B. Chilton, P.G. Coleman, Meas. Sci. Technol. 6 (1995) 53
[8] A. van Veen, H. Schut, J. de Vries, R.A. Hakvoort and M.R. Ijpma, in:Positron beams for solids and surfaces. AIP Conf. Proceedings 218. Eds.: P.J. Schultz, G.R. Massoumi, P.J. Simpson (American Institute of Physics, New York, 1990) p.171
[9] M.J. Puska, R.M. Nieminen, J. Phys. F13 (1983) 333
[10] E. Boronski, R.M. Nieminen, Phys. Rev. B34 (1986) 3820
[11] P. Willutzki, J. Störmer, G. Kögel, P. Sperr, D.T. Britton, R. Steindl, W. Triftshäuser, Meas. Sci. Technol. 5 (1994) 548
[12] P. Kirkegaard, M. Eldrup, Comput. Phys. Commun. 7 (1974) 401
[13] K. Laasonen, M. Alatalo, M.J. Puska, R.M. Nieminen, J. Phys.: Condens. Matter 3 (1991) 7217
[14] M.J. Puska, O. Jepsen, O. Gunnarson, R.M. Nieminen, Phys. Rev. B34 (1986) 2695
[15] S. Mäkinen, S. Mäkinen, Phys. Rev. B40 (1989) 12523
[16] G. Brauer et al. (to be published, 1995)

Formation and Characterisation of Double SIMOX Structures by Sequential High and Low Energy Oxygen Implantation into Silicon

N. Hatzopoulos, D. I. Siapkas*, P.L.F. Hemment+ and W. Skorupa
*Department of Physics, Aristotle University of Thessaloniki, Greece
+Department of Electronic and Electrical Engineering, University of Surrey, UK

The availability of a new generation of MeV implanters has sparked a new interest in high energy implantation and its potential applications [1]. High energy (MeV) SIMOX technology could find applications in the BiCMOS-SOI technology [2] and could be used as an alternative to standard SIMOX technology in order to reduce both the implantation temperature and the damage generated during implantation [3,4].

Optical waveguiding in SIMOX structures was first demonstrated by Soref et al. [5]. SIMOX structures have been produced and tested as waveguides [6] but the thick (> 1 μm) Si guiding layers needed, were produced by CVD growth of epitaxial Si. High energy SIMOX technology could be potentially used for the fabrication of Si based optical waveguides. In this respect, SIMOX technology in the low and high energy regimes allows the whole waveguiding structure to be fabricated with the use of the same implanter. The nature of ion beam synthesis permits the accurate control of the thickness of the individual layer through the ion energy and ion dose used. The fact that Si is transparent above 1.05 μm and that the values of the refractive indexes of Si and SiO_2 are 3.5 and 1.5 respectively, makes for strongly confined passive optical waveguiding structures. This technology is also suitable for the development of intrachip optical interconnects and dual waveguides, coupled or not, depending on the thickness of the SiO_2 cladding layers.

Since MeV implantation of oxygen in silicon creates structures with thicknesses in the order of micrometers, the most suited non-destructive analytical technique is infrared (IR) spectroscopy. In this work, the interference fringes region is studied and as a result of a multilayer modelling of the sample structure, based on a generalised matrix method [7], the reflectivity of the structure is calculated having as adjustable parameters the thicknesses and refractive index depth profiles. The refractive index profiles of the as-implanted layers were determined from computer fitting of the interference spectra. With the use of an effective medium theory [8], the oxygen concentration depth profile is the end result. The fitting function was a two-half-joined Gaussian-shape refractive index profile which was shown to mirror the oxygen concentration profile by means of RBS measurements. Therefore, the results of the computer fits were expressed as the depth of the maximum oxygen ion concentration, R_{max}, and the surface-side and substrate-side standard deviations of the oxygen profile, ΔR_1 and ΔR_2, respectively. From these values the first two moments of the range distribution, R_p and ΔR_p were calculated [9].

The formation and characterisation of a new, 5-layer Si-SiO_2-Si-SiO_2-Si structure, was reported [10]. This multilayer structure was fabricated by a double sequence of oxygen ion implantation and high temperature annealing. In order to analyse such complex structures, Fourier Transform Infrared (FTIR) spectroscopy was used, being the most suitable non-destructive technique to be able to give quick, accurate and quantitative information for thick Si structures [11]. In addition, the crystallinity of the Si layers is revealed. Proton beam RBS has been used to compare with, and to provide complementary information to IR data.

Oxygen ions ($^{16}O^+$) at an energy of 2 MeV were implanted into <100>, p-type, device grade Si wafers. The implantation temperature was at a minimum value of 600°C, kept constant

before and during the implant by a joule heated sample holder. The oxygen dose ranged from 0.1 to 2 × 10^{18} O^+ cm^{-2}. Samples were capped with SiO_2 and annealed at 1300°C for 6 hours. Then the cap was removed by HF etching and the wafer (sample DS1) was implanted with 90 keV O^+ ions, to a dose of 8 × 10^{17} at a temperature of 700°C. Again the wafer was capped with SiO_2 and subjected to high temperature anneal at 1300°C for 6 hours. Infrared reflection measurements were made using a Fourier spectrophotometer model Bruker IFS 113v (extended), working over the frequency range 10 - 20000 cm^{-1}, at the University of Thessaloniki. The angle of incidence was near normal and the accuracy was better than ± 0.3 %. A specially designed sample holder was used to take reflection measurements. A fresh front aluminised mirror was used as a reference. The samples were heavily lapped from the back side to avoid any reflection from the back side of the substrate. The H^+ beam RBS/Channelling was performed using 1 MeV energy protons with a scattering angle of 150°.

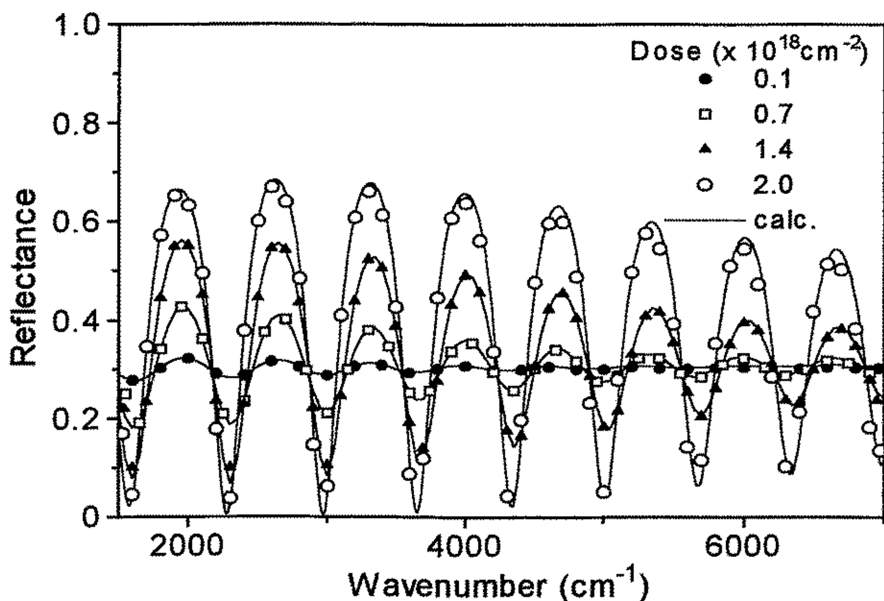

Fig. 1: Experimental infrared reflectance spectra (symbols) in the range 1500 - 7000 cm^{-1} from Si samples implanted at 700° C, with 2 MeV O^+ ions with doses of 0.1, 0.7, 1.4 and 2.0 × 10^{18} O^+cm^{-2}, compared to theoretical spectra (solid lines).

In fig. 1, the experimental IR spectra and the fits obtained using the methodology described above, can be seen for the high energy SIMOX samples implanted with doses of 0.1, 0.7 and 2.0 × 10^{18} O^+ cm^{-2}, all at a temperature of 700°C. The quality of the fits is extremely good, indicating that the only assumption of the model, the refractive index profile being of a two-half-joined Gaussian shape is true.

Fig. 2 shows the refractive index (taken at 3000 cm^{-1}) depth profiles used to produce the fits seen in fig.1, for the SIMOX samples implanted at 2 MeV. The value of $n(R_{max})$ for the highest dose is equal to 1.44. On the basis of information from RBS random spectra (not shown) for an energy of 2 MeV, the dose of 2.0 × 10^{18} O^+ cm^{-2} proves to be sufficient for the minimum of the Si dip to reach the value for stoichiometric SiO_2.

The value of the refractive index of stoichiometric fused silica, which has been shown to be the best fit for SIMOX produced SiO_2 [12], is 1.41072 at 3000 cm^{-1}, according to Malitson [13]. If it is assumed that the value of $n(R_{max})$ is that of stoichiometric SiO_2, then the discrepancy between this value and that of fused silica, can be explained as due to the

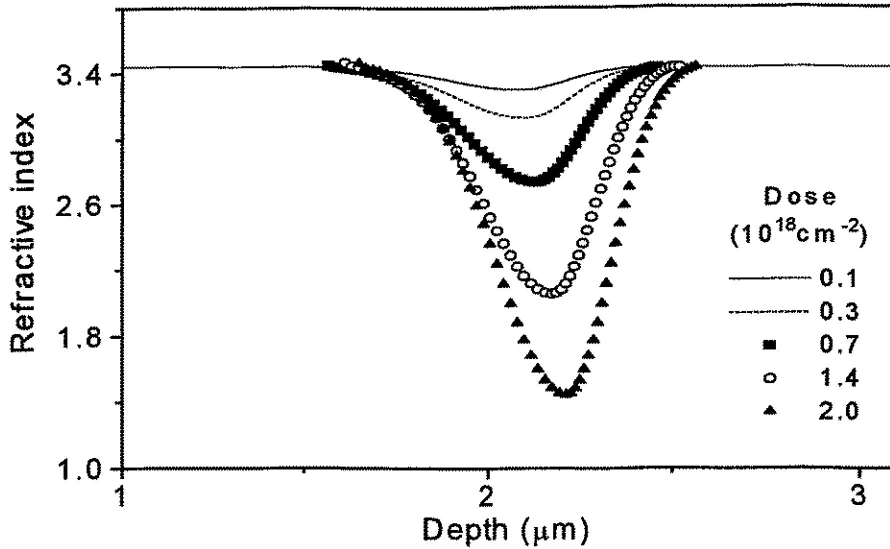

Fig. 2: Refractive index depth profiles obtained after the analysis of infrared reflectance spectra from Si samples implanted at 700° C, with 2 MeV O^+ ions (doses of 0.1, 0.3, 0.7, 1.4 and 2.0×10^{18} O^+ cm^{-2}).

higher strain bound to be present in a structure such as as-implanted SIMOX. The values of R_p and ΔR_p for 2 MeV oxygen in Si, obtained by IR measurements, TRIM92 [14], ref. [15], and ref. [3], can be seen in Table I. A very good agreement exists for the three experimentally obtained values of R_p and ΔR_p but the theoretical values are smaller than the experimental ones, with a larger difference in the R_p values.

Table I. Theoretical and experimental values of the first two moments of the range distribution for oxygen ions implanted into silicon with an energy of 2 MeV.

	this work	TRIM92 Ref. [14]	Kappert et al. Ref. [15]	Grob et al. Ref. [3]
R_p (μm)	2.039 ± 0.005	1.971	2.1 ± 0.05	2.02 ± 0.02
ΔR_p (μm)	0.16 ± 0.01	0.145	0.15 ± 0.01	0.17 ± 0.01

In fig. 3 the oxygen concentration depth profile from the sample DS1, can be seen. A comparison is made between the results of IR and RBS (spectra not shown). The agreement is quite good. The thickness of the in-between Si layer, is 1.63 μm, while that of the shallow SiO_2 layer is 0.175 μm. Also the Si overlayer thickness is 0.118 μm. The implantation and annealing sequence followed during the fabrication of the final structure, does not allow any oxygen diffusion to take place and so the final structure is accurately predictable, when the structures for the two individual samples are known. Depending on the thickness, one could have either a completely isolated dual waveguide or a completely or partly coupled dual waveguiding structure. Taking also in mind that waveguiding losses are dependent on the Si waveguiding layer thickness as well as its crystallinity, the ion beam synthesis capability to produce thick, bulk Si-like quality, Si layers becomes technologically very important.

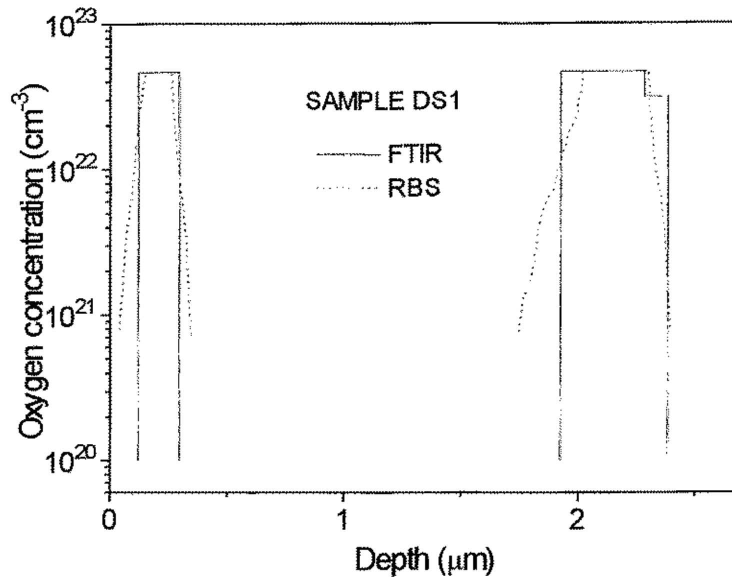

Fig. 3: Oxygen concentration depth profiles for sample DS1, obtained by IR (solid line) and RBS (dashed line) analysis.

In high energy SIMOX, an anneal of 12 hours at 1300°C is necessary, in order to achieve a uniform SiO_2 layer with almost planar interfaces. For double SIMOX structures the in-between Si layer as well as the top Si overlayer are of high crystal quality, with an oxygen concentration of less than 1×10^{20} O cm^{-3}. All the Si - SiO_2 interfaces are found to be quite sharp and so, one of the basic conditions for high quality waveguiding characteristics is met.

References

[1] Ziegler J.F. Nucl.Instr. and Meth. B6, 270 (1985)

[2] Matsumoto S., Ohno T. and Izumi K. Electron.Lett. 25, 904 (1989)

[3] Grob J.J., Grob A., Thevenin P., Siffert P., d'Anterroches C. and Golanski A., J.Mater.Res. 4(5), 1227 (1989)

[4] Ellingboe S., Ridgway M.C. and Schultz P.J. J.Appl.Phys. 73(3), 1133 (1993)

[5] Soref R.A. and Lorenzo J.P. in Integrated and Guided Wave Optics, 1989 Tech. Dig. Series, Opt. Soc. Amer., Washington DC, Feb. 6, 86 (1989)

[6] Soref R.A., Cortesi E., Namavar F. and Friedman L., IEEE Photon. Technol. Lett., 3, 22 (1991)

[7] Mitsas C.L. and Siapkas D.I., Appl.Opt. (1995)

[8] Aspnes D.E., Thin Solid Films, 89, 249 (1982)

[9] Gibbons J.F. and Mylroie S., Appl.Phys.Lett., 22(11), 568 (1973)

[10] Hatzopoulos N., Siapkas D.I., Hemment P.L.F. and Skorupa W., in Proc. 6th Int. Symp. on SOI Techn. and Devices, The Electrochem. Soc., May 1994, p. 123

[11] Hatzopoulos N., Siapkas D.I. and Hemment P.L.F., J.Appl.Phys., 77(2), 577, (1995)

[12] McMarr P.J., Mrstik B.J., Barger M.S., Bowden G. and Blanco J.R., J.Appl.Phys. 67(12), 7211 (1990)

[13] Malitson I.H., J.Opt.Soc.Am., 55(10), 1205 (1965)

[14] Ziegler J.F., Biersack J.P. and Littmark U., in The Stopping and Ranges of Ions in Solids, edited by J.F Ziegler (Pergamon, New York, 1985), Vol.1

[15] Kappert H.F., Heidemann K.F., Grabe B. and te Kaat E. Phys.Stat.Sol.(a) 47, 751 (1978)

A New Fabrication Method for Submicron $CoSi_2$ Dots and Wires Using Focused Ion Beam Implantation and Local Melting by Flash Lamps

L.Bischoff, K.-H. Heinig, J. Teichert and W. Skorupa

In recent years silicides from transition metals are playing an increasingly important role as conducting paths or as gate material in microelectronic and micromechanical devices as well as in quantum structures. A typical, well-studied representative is cobalt silicide. Continuous $CoSi_2$- films may be obtained by a stoichiometric implantation of cobalt into a heated silicon substrate and subsequent annealing (ion beam synthesis) [1]. By the substitution of the conventional broad beam technique by focused ion beam implantation a maskless resistfree process was demonstrated to write directly $CoSi_2$ - structures of arbitrary shape in the submicron region [2].
In this paper a new possibility for the formation of submicrometer $CoSi_2$ structures will be represented.

Flash lamp irradiation with milli-second pulses of sufficient intensity leads to a local melting process of a single crystalline silicon wafer with a polished surface [3]. This local melting at pulse heating is caused by the formation of melt nuclei on the Si surface followed by their facetted growth. The contours of the grown structures are strongly related to the crystal orientation. A surface breakup into solid and liquid areas is a result of the superheated silicon. The barrier for the formation of melt nuclei is lowest at the surface and melt 0nuclei appear there. On a cleaned polished surface they are distributed randomly because nucleation is induced by statistical thermal and density fluctuations. This process is called homonucleation. The barrier for the formation of melt nuclei may be decreased by surface defects like cracks or stratches or artificial structures acting as efficient nucleation centers. In this case it is called heteronucleation. This behavior is shown schematicly in Fig. 1. A detailled theoretical modelling of this process has been given elsewere [4].

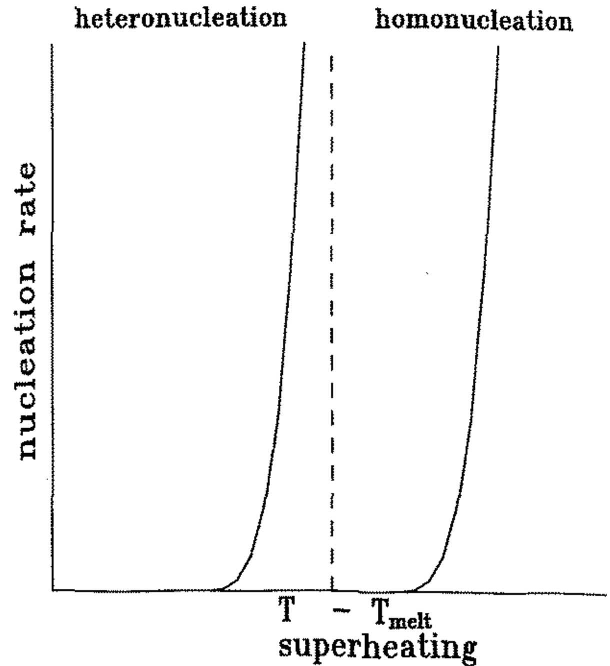

Figure 1: Possibility of controlled local melting by heteronucleation (schematicly)

In order to fabricate controlled molten regions by nucleation, efficient nucleation centers on a defect free surface must be created, which was done by writing implantation with the Focused Ion Beam IMSA-100 [5]. Along the <100> direction of a Si (001) wafer stripes, structures of arbitrary shape and dots have been implanted with a 35 keV Co^+ micro beam of about 200 nm diameter at doses of 0.5, 1.0 and 3.0 x 10^{17} cm^{-2}. The width of the stripes may exceed substantially the width of the wire to be fabricated. Than the whole silicon wafer was irradiated homogeneously with a light flash (120 Jcm^{-2}, τ = 20 ms). During the flash irratiation, grooves of molten silicon are formed selectively related to the implanted figures. Due to the rapid cooling of the wafer the monocrystalline resolidification of the molten regions lasts only a fraction of a second. The strong segregation of cobalt at the moving crystal - liquid interface results in an increase of the Co - concentration in the melt. This process stops when the eutectic concentration is reached which is close to the concentration of Co in the $CoSi_2$. The final width of the $CoSi_2$ - wires is proportional to the amount of implanted cobalt per unit length of the stripes. This mechanism of the sub micrometer $CoSi_2$ wire production can be clarified by on the phase diagramm of the cobalt - silicon system, see Fig. 2.

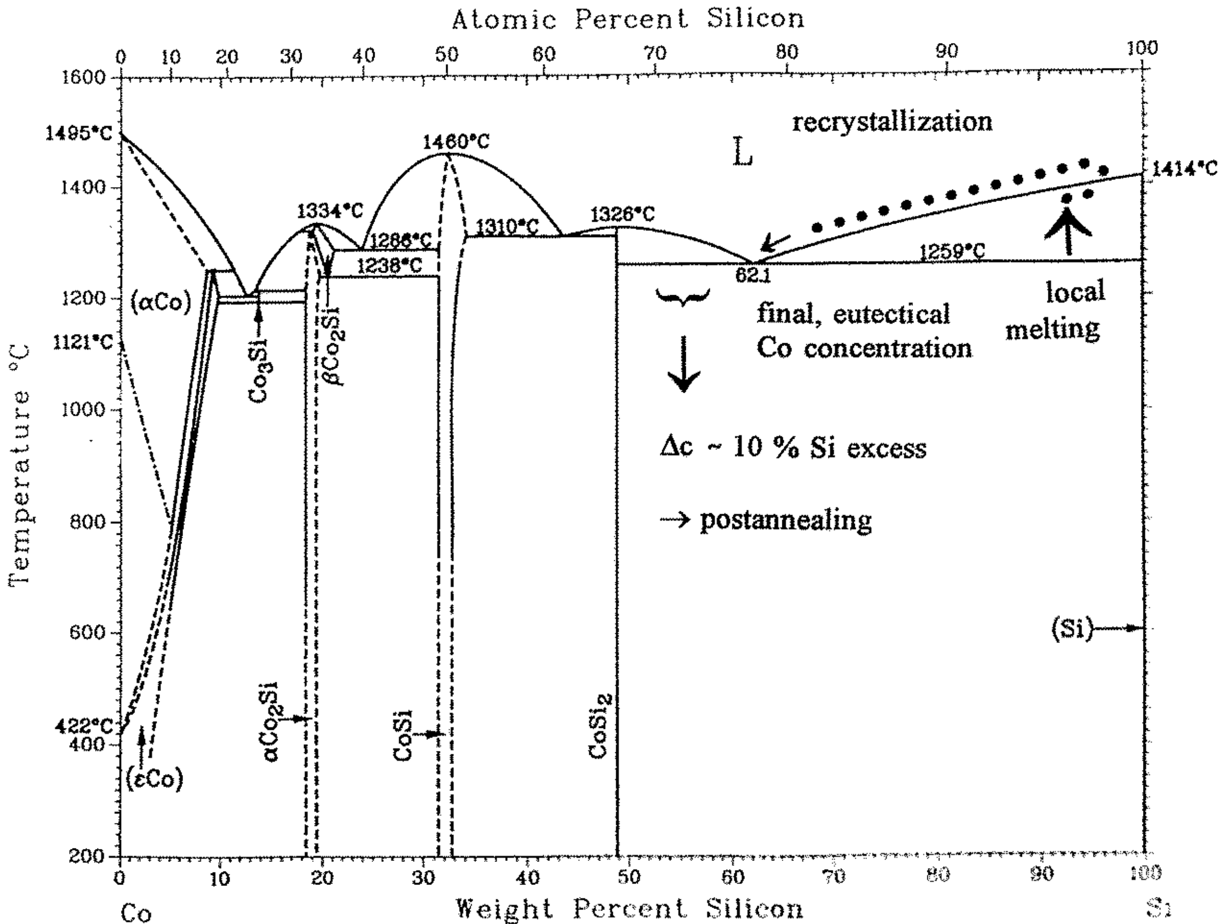

Figure 2: Mechanism of the sub-µm $CoSi_2$ wire fabrication, shown on the phase diagram

The obtained $CoSi_2$ - structures were analysed by SEM and EDX investigations. Co implanted lines of some dozens of µm length appear after the flash lamp pulse not as continuous wires but as several shorter parts of a wire. Fig. 3a shows such wire fractions with EDX line scans correlated to the Co - $K_{\alpha 1}$ line (E = 6.938 keV). Scan position (1) crosses a wire and (2) lies in a gap. At lower doses, a line of dots is formed, Fig. 3b. The length of these parts of wires depends on the implantation dose and, very sensitively, on the temperature profile at the surface of the wafer during the flash pulse. The longest wire part was 4 µm long and 200 nm in width. With the currently used pulse length (20 ms) it is difficult to fabricate continuous long wires. The reason is an instability driven by minimization of the surface energy. A solution may be to shorten the pulses to about 2 ms. This pulse length shortening lowers the time period of high temperatures at the surface by more than two orders of magnitude, which might prevent the development of that instability.

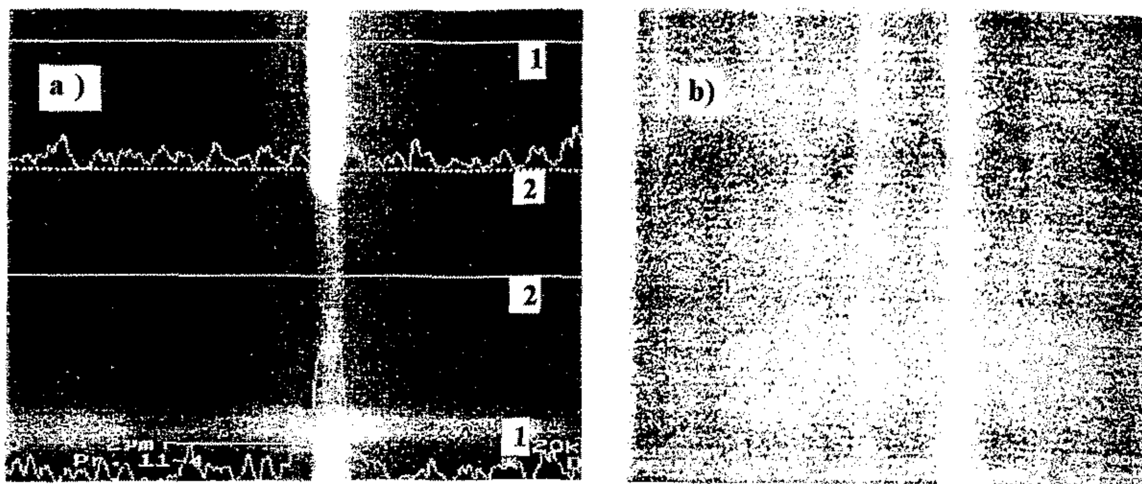

Figure 3: a) $CoSi_2$ wire parts after flash lamp annealing with EDX signals of the Co-$K_{\alpha 1}$ line over (1) and between wire parts (2)
b) line of $CoSi_2$ dots after low dose implantation and flash lamp puls

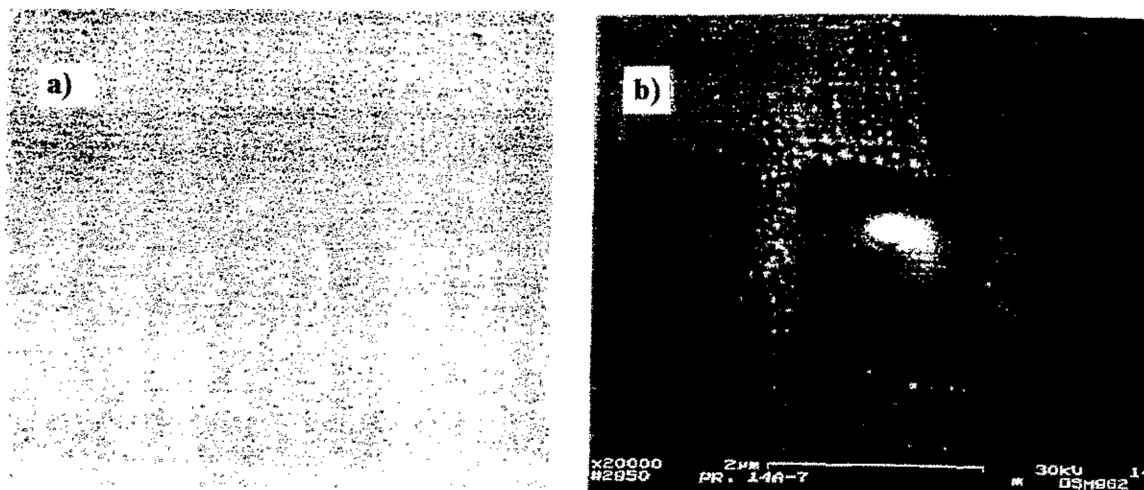

Figure 4: a) $CoSi_2$ dot matrix, b) detailled view of one micro dot

A second example of fabricated $CoSi_2$ microstructures are fields of dots, implanted (without beam blanking between the dots) and annealed under the same conditions like the micro wires above. Fig. 4 shows a dot matrix in overview (a) and more in detail (b). Most of the $CoSi_2$ is concentrated in the centre of a cone with a diameter of about 250 nm, but along the way of the quickly moving the ion beam during FIB dot implantation small precipitats are formed, too. This demonstrates the high sensitivity of the method with respect to the Co concentration. A post annealing at temperatures of about 1000 °C could be used to focus the small cobalt precipitates in the dot centres.
These preliminary results, obtained by this new method have shown, that $CoSi_2$ microstructures may be formed successfully in dimensions of about 100 nm and below. Shorter pulses will be tested in order to prevent the decay of the wires into short parts. Also the influence of different post-annealing treatments is promising. Further, the microscopic and macroscopic properties of the $CoSi_2$ microstructures will be investigated.
Promising applications of this new method to fabricate $CoSi_2$ micro dots and wires lie in the field of quantum devices.

References:

[1] A.E.White, K.T.Short, R.C.Dynes, J.P.Garno and J.M.Gibson; Appl. Phys. Lett. 50 (1987) 95

[2] L. Bischoff, J. Teichert, E. Hesse, D. Panknin and W. Skorupa; Mat. Res. Soc. Symp. Proc. 316 (1994) 741 and 320 (1994) 153

[3] K.-H. Heinig, M. Voelskow, J. Matthäi, A. Zetzsche and C. Treutler; Proc. Int. Conf. on Energy Pulse Modification of Semiconductors and Related Materials, EPM '84, Dresden, September 25 - 28 (1984) 280

[4] K.-H. Heinig; Proc. Int. Conf. on Energy Pulse Modification of Semiconductors and Related Materials, EPM '84, Dresden, September 25 - 28 (1984) 265

[5] L. Bischoff, J. Teichert, E. Hesse, D. Panknin and W. Skorupa; J. Vac. Sci. Technol. B12 (6) (1994) 3523

Acknowledgement

We are indebted to Dr. R. Müller, Mrs. E. Chistalle and Mrs. P. Schneider for SEM and EDX analysis, and R. Kliemann for the flash lamp processing.

IBAD Preparation of Films Containing Carbon Nitride

A. Kolitsch, E. Richter, U. Kreissig

In 1990, Liu and Cohen [1] presented a pseudopotential study of the structural and electronic properties of β-C_3N_4, a hypothetical compound with the structure of the well known β-Si_3N_4. The calculated bulk modulus of the predicted compound was found to be comparable to that of diamond. It was suggested that β-C_3N_4 may be metastable because of its moderately large cohesive energy.

Synthesis of β-C_3N_4 has recently been claimed, but in all cases the obtained film composition is not stoichiometric. The largest detected [N]/[C] ratio of the films is about 0.7. An explanation of that is the formation of very small β-C_3N_4 crystallites embedded in amorphous sp^2 bonded C_xN_y where y/x is typically between 0.2 and 0.5. At present a lot of different ways of β-C_3N_4 preparation are under investigation worldwide.

In our studies an ion beam assisted deposition (IBAD) system with a Kaufman ion source and an electron beam evaporator was used. The IBAD chamber is integrated in the high current beam line of a 20...200keV ion implanter system from DANFYSIK and allows to inject an additional mass-separated high energy and high current ion beam in-situ during the deposition or as post-implantation of the as-deposited films. The films were deposited by simultaneous carbon evaporation and bombardment with 600eV N_2^+ ions. The filmthickness ranged from 100nm to 300nm. Some of the 100nm films were post-implanted with 20keV N^+ ions (corresponding to a mean projected range of about 45nm) at fluences between $1x10^{17}$ cm^{-2} and $6x10^{17}$ cm^{-2}.

First experiments were devoted to the influence of the nitrogen to carbon transport ratio during the deposition process on the resulting nitrogen content and the obtained composition of the films. In a further step nitrogen post-implantation of the films was investigated in order to

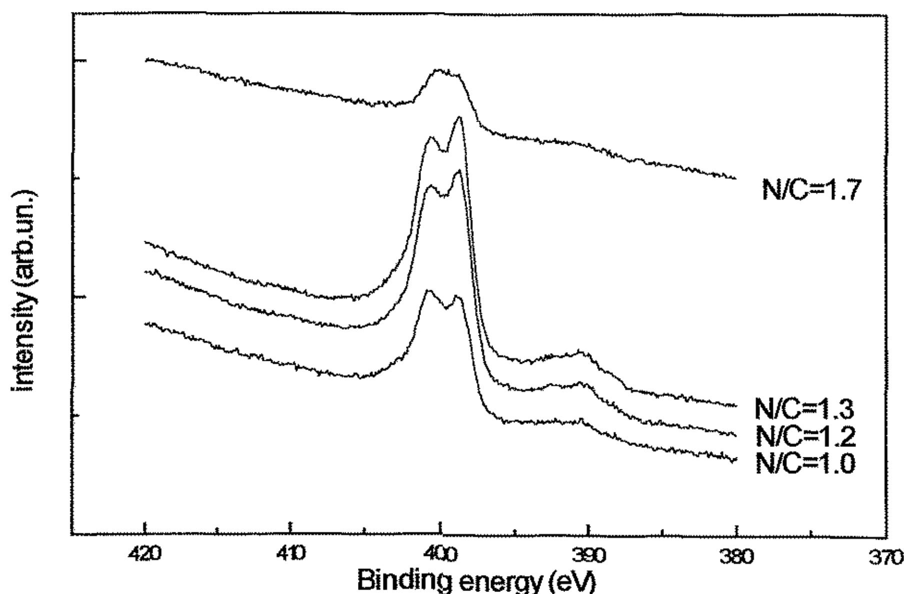

Fig. 1: Typical N 1s XPS spectra of β-C_3N_4 containing films deposited at various nitrogen to carbon transport ratios during the film growth

analyze the possibility of increasing the nitrogen content of the films or to change the structural properties.
The films were characterised by XPS, Raman spectroscopy and dynamical microhardness measurements.
XPS measurements were carried out with a FISONS MICROLAB 310F equipment using Mg K_α X-rays and 0.02% resolution of the kinetic energy.

Examples of N1s photoemission lines of the carbon nitride films are shown in figure 1. Four distinguishable peaks in the C 1s core level and three in the nitrogen spectrum can be resolved after inelastic background subtraction and Gaussian fit. The excellent resolution of the XPS measurements in multiple bumps is clearly to recognise.
The analysed features for the carbon spectrum correspond to carbon binding energies of 284.6eV, 285.9eV, 287.8eV, and 289.6eV. The nitrogen spectrum results in the energies of 398.8eV, 400.6eV, and 403.3eV. These energies agree very well with the results of Marton et al. [2] who first investigated films containing β-C_3N_4 by XPS to distinguish the binding energy of different C-N phases.

The correlation of the measured binding energies to different C-N structures follows:

C 1s XPS line		N 1s XPS line	
284.6eV →	„adventitious carbon and surface carbon that may have lost its nitrogen neighbours due to reaction with O_2 and/or CO from the air"[2]	398.8eV→	corresponding to carbon nitride phase 1
285.9eV →	predominantly sp^2-bonded carbon structure with a variable stoichiometry between C_5N to C_2N (Marton et al.[2] binding energy of carbon nitride phase 2)	400.6eV→	corresponding to carbon nitride phase 2
287.8eV →	assumed β-C_3N_4 structure with carbon atoms in tetrahedral sites and corresponding nitrogen in threefold positions (phase 1)	403.3eV→	N-O or N-N bonds
289.6eV →	typical CO bonds		

Thus the two carbon peaks at 285.9eV and 287.8eV reflect two binding states to nitrogen with the corresponding nitrogen peaks at 398.8eV and 400.6eV. The binding energy of carbon 1s electrons is insensitive to the co-ordination in the case of nonpolar bonds for instance in pure carbon phases or hydrogenated carbons [3]. But a small polarisation of the carbon bonds effects significant changes of the binding energy. The correlation of the measured binding energies with those of pyridine and urotropine by Marton [2] seems to be a good explanation for the large energy shift. The higher degree of polarisation of the urotropine bonds (tetrahedral bonded) results in a measured carbon binding energy of 286.9eV [2]. The nitrogen and carbon atoms in the predicted β-C_3N_4 structure occupy nearly the same sites as in the urotropine structure. The similar nitrogen binding energies of pyridine and urotropine of 399.8eV and 399.4eV, respectively, differ in the tetrahedral sites of nitrogen in the urotropine structure. The trigonal sites of the nitrogen atoms in the predicted β-C_3N_4 structure should lead to some de-

crease of the N1s binding energy by screening of the 1s orbital in comparison to the urotropine structure.

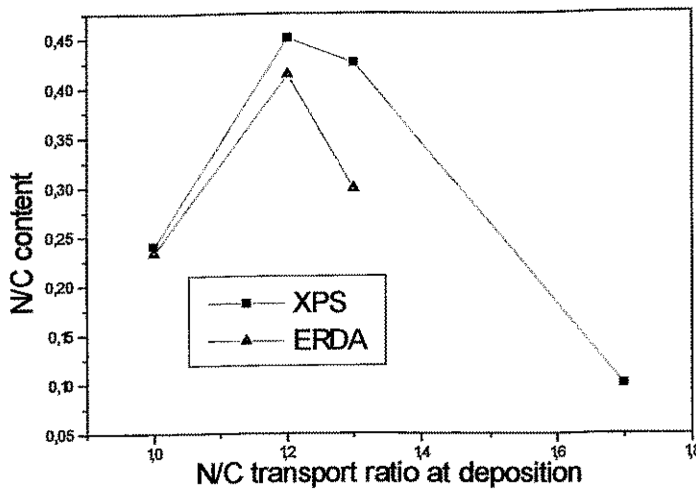

Fig. 2: Nitrogen to carbon content of the films as a function of the transport ratio of both species

To quantify the XPS peak intensity ratios of N and C elastic recoil detection analysis (ERDA) of the deposited films was carried out to measure the carbon and nitrogen content of the films. The measurements by ERDA agree reasonably with the peak intensity ratios N1s/C1s measured by XPS. No correction of the XPS peak intensities by using Scofield factors for the effective cross-section of the measurements was used. Figure 2 compares both results as a function of the ion/atom ratio of the deposition. These results show a maximum of the nitrogen content of the prepared carbon nitride films at a N/C transport ratio of the deposition process of about 1.2. Higher transport ratios result in higher sputter rates of the deposited films. A deposition experiment with a nitrogen/carbon transport ratio of 1.7 produces a very thin resputtered film with an altered shape of the XPS line.

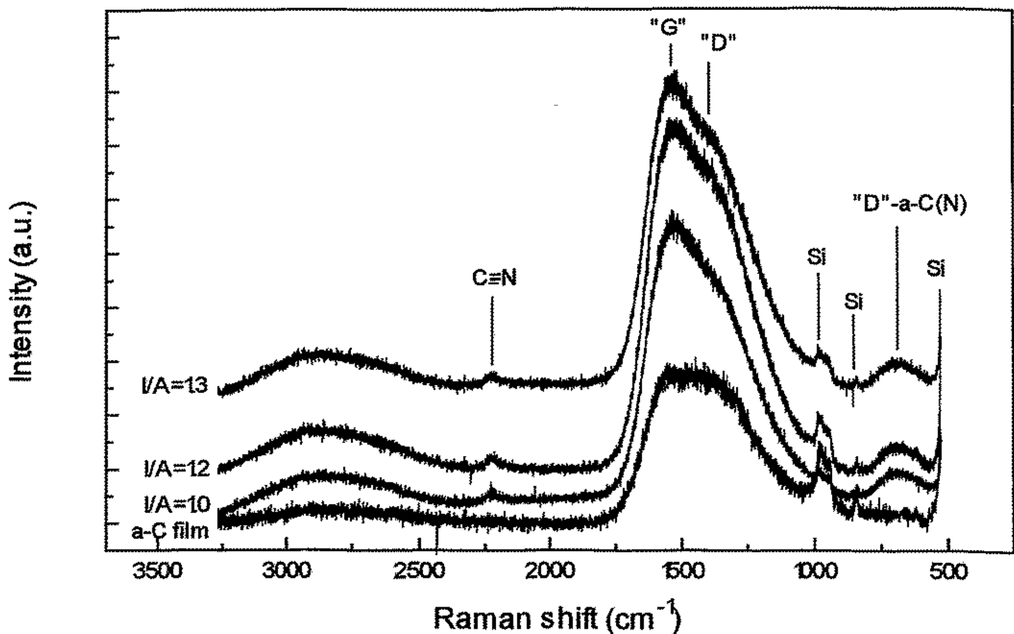

Fig. 3: Raman peak shift of C_xN_y films deposited with different N/C transport ratios in comparison to an a-C film

First results of Raman spectroscopy of carbon nitride films are presented in figure 3 in comparison to a spectrum of a nitrogen free amorphous carbon film deposited with assisting Ne^+ ions instead of nitrogen at the same parameters. Three effects are clearly visible. A new small „disorder" peak appears in the nitrogen containing films at 680-690cm^{-1}. The peak intensity ratio of disorder peak (1390cm^{-1}) to graphite peak (1560cm^{-1}) decreases drastically in comparison to a-C films without nitrogen. The 2229cm^{-1} bond indicates that nitrogen is chemically bonded to carbon (characteristic of nitrogen-carbon stretch). Apart from these differences Raman spectra of C_xN_y films resemble those of a-C films.
The hardness of the C_xN_y films slightly exceeds that of a-C films.
Post-implantation of 20keV nitrogen ions with different fluences clearly increases the bump at 403.3eV of the N1s peak of the XPS measurement (figure 4). This indicates an increase of

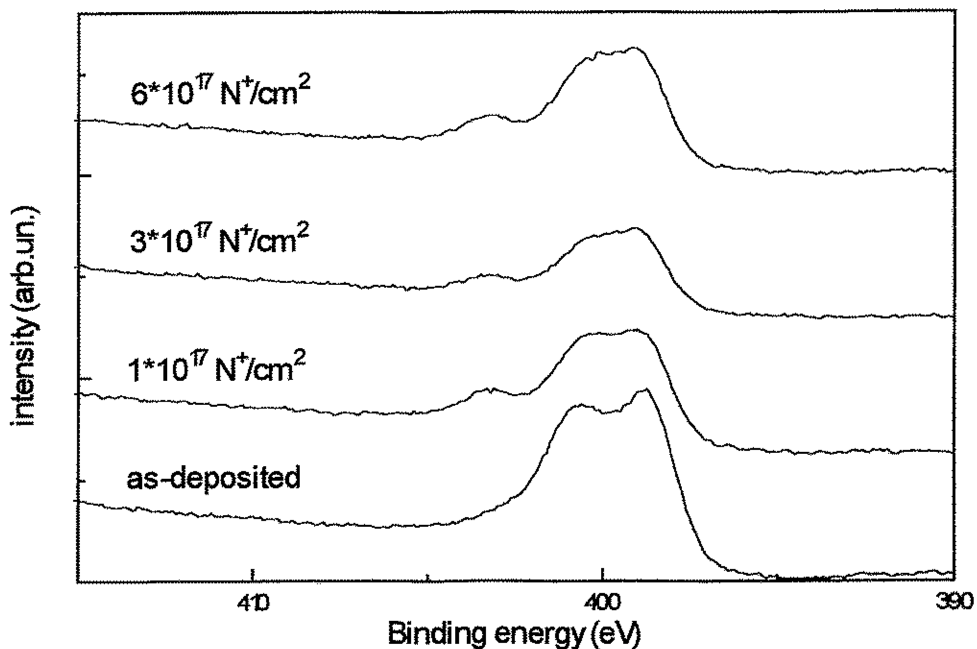

Fig. 4: XPS measurement of nitrogen 1s electrons of C_xN_y films post-implanted with 20keV nitrogen

carbon without bonding to nitrogen. Also a decrease of the global nitrogen content of the films is seen from the spectra. Therefore the post-implantation of nitrogen ions at the present parameters is unable to increase the nitrogen content or the content of the β-C_3N_4 phase in the film. On the contrary, high energy implantation breaks carbon-nitrogen bonds in the prepared films and results in an outdiffusion of nitrogen. To increase the concentration of the β-C_3N_4 phase in ion beam assisted deposited films, further parameters of the deposition remain to be investigated.

[1] A.Y. Liu, M.L. Cohen, Phys.Rev.B 41 (1990) 10727

[2] D. Marton, K.J. Boyd, A.H. Al-Bayati, S.S. Todorov, J.W. Rabalais, Physical Review Letters 73 (1994) 118

[3] S.R. Kasi, H. Kang, J.W. Rabalais, J. Chem. Phys. 88 (1988) 5914

Sheath Dynamics in Plasma Immersion Ion Implantation

J. Brutscher, R. Günzel

Plasma Immersion Ion Implantation (PIII) is a new method to implant ions into materials to modify surface properties. Gas ions as well as metal ions can be used [1-4]. Compared to conventional ion implantation, the characteristic advantage is that there is no need for an extraction system or other ion optics. In addition, PIII may be employed to treat large areas of three-dimensional objects. The sample is immersed into a plasma, and high voltage is applied to the sample. Ions are extracted from the plasma and accelerated directly to the sample. A pulsed voltage is used to reduce the thermal load and the possibility of arcing.

For this new technique, basic information is required on the plasma and sheath dynamics as well as the extraction of ions during high voltage pulses in the 10 μs range. The present paper describes the sheath formation both in stationary and dynamic mode.

The plasma was generated by a hot-filament assisted DC discharge with multipole magnets arranged around the chamber walls. For the plasma sheath measurements a 50 mm diameter aluminia disk was used as a sample. High voltage pulses were generated by discharging a high voltage capacitor through the plasma [5].

The plasma density was measured using an adjustable Langmuir probe.The plasma density is proportional to the discharge power in first order approximation. For time-resolved measurements, the probe was connected to a source of 2 V via a 50Ω resistor. The probe voltage was measured with a digital storage oscilloscope. This method allows a good time and spatial resolution and yields results similar to other much more complicated optical measurements [6]. In addition, measurements could be performed much closer to the sample (4mm at 13 kV) compared to other published data, and with a better time resolution [6,7]. For most of the plasma sheath measurements nitrogen gas with a pressure of 0.3 Pa was used, although the sheath width was nearly independent of the pressure in a pressure range from .08 to 2 Pa.

For the description of the behavoir of the plasma, the electrons can be considered inertialess because usual voltage rise times are much longer than the inverse electron plasma frequency. The space charge sheath forming around the sample which is biased with a negative high voltage can be described by the Child-Langmuir law because the flight time of the ions is usually also short compared to the rise time of the high voltage pulse. The ion extraction from the plasma is determined by the ions released from the retreating plasma and the quasistationary ion current density which can be extracted from the plasma. The sheat expands until there is a balance between the space charge limited current in the sheath and the stationary current from the plasma. The latter is determined by the Bohm sheath criterion [8], stating that ion current density is independent of the applied voltage and depends mainly on the plasma density. For calculating the sheath width in planar geometries, the Child-Langmuir equation is valid, wheras for spherical geometries a good analytical fit has been derived.

At moderate plasma densities, a DC voltage up to several kV can be maintained at the substrate. Fig. 1 shows the width of the sheath, as function of a stationary substrate bias. The experimental data were obtained from the langmuir probe measurement by the distance from the substrate surface, at which the electron density drops to 10% of the bulk plasma density. The theoretical curves have been calculated for the measured bulk density of $2\times10^{15}\mathrm{m}^{-3}$. Compared to planar geometry, a considerably better fit is obtained with the spherical approach for a curved substrate with a radius of 50 mm rather than the actual 50 mm diameter disk. This approximation appears reasonable as the plasma boundary establishes with a dome-like shape at larger sheath widths.

The extracted ion current density was calculated from the measured total electrical current by subtracting the secondary electron contribution (Secondary electron coefficients between 5 and 10 have been measured independently at an implanter at 10 to 40 keV for nitrogen using an

aluminium target, and extrapolated towards lower energy). The ion current density is nearly independent of the voltage and is consistent with the plasma density measurements.

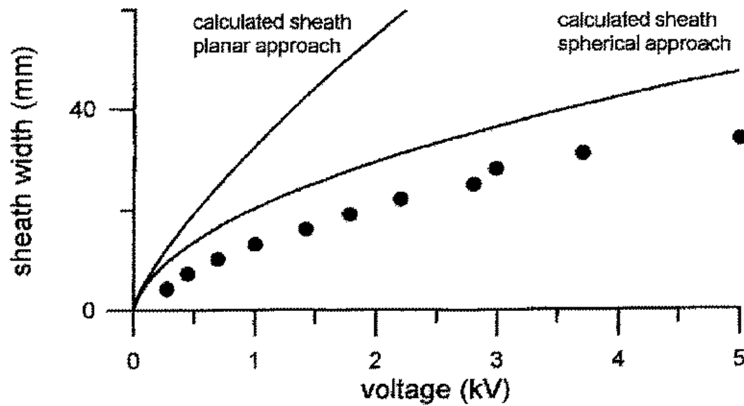

Fig. 1: Sheath width as function of sample bias. The experimental data (dots) are compared to calculations for a plasma density of 2×10^{15} m^{-3}, and planar and spherical geometry.

For the investigation of the sheath width evolution during the rise time of the voltage, the probe current was measured during a pulse at distances from the substrate of 4 to 32 mm. From this, the time-dependent sheath width was determined.

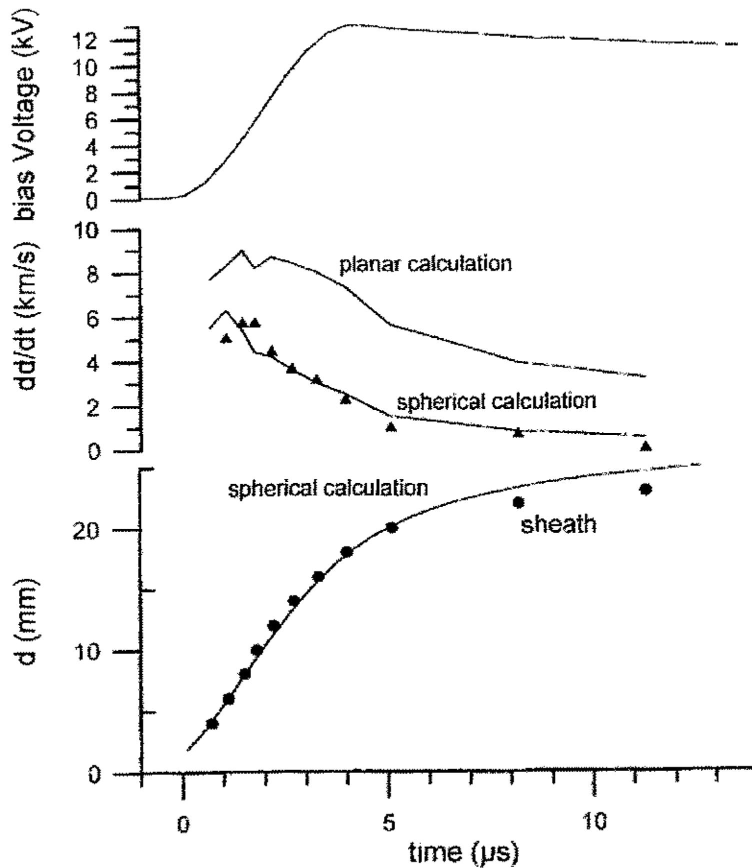

Fig. 2: Evolution of the sheath (bottom) and sheath velocity (middle) for a pulsed bias voltage (top) as a function of time.

Plasma density at 20 mm 3.5×10^{16} m^{-3}, electron temperature 0.85 eV.

For the given bias pulse shape, the width of the expanding sheath is in good agreement with the Child-Langmuir prediction again for a spherical geometry. The sheath velocity indicates an initial ultrasonic expansion: The ion 'acoustic' velocity amounts to 1.7 km/s at the present electron density and temperature.
During the expansion phase, the total ion current is composed of two fractions: The quasi-stationary contribution resulting from acoustic velocity and plasma density amounts to about $6\ A/m^2$. A time-dependent second fraction results from ions peeled off the moving boundary, i.e. given by the product of plasma density and sheath velocity, it decreases from about 30 A/m^2 to values below the stationary fraction during the first 5 μs. Therefore, the 'peeling-off' fraction represents only a minor contribution to the total implanted dose. Within a considerably uncertainty given by the uncertainty of the secondary electron yield, the measured electrical current is in reasonable agreement with the above model data.

References

[1] J.R.Conrad and J.R. Radke, J.Appl.Phys. 62 (1987) 4591
[2] R.J. Adler, Nucl. Instr. and Meth. B6 (1985) 123-128
[3] I.G.Brown, A.Anders u. a. J. Vac. Sci. Tech. B 12 (1994) 823
[4] R. Günzel, E. Wieser, E. Richter, J. Steffen, J. Vac. Sci. Tech. B12 (1994) 927
[5] G. Böhm, R. Günzel, J. Vac. Sci. Tech. B12 (1994) 821
[6] M.J. Göckner and Shamim M. Maik, Phys. Plasmas 1 (1994) 1064
[7] M. Shamin, J.T. Scheuer, J.R. Conrad, J. Appl. Phys. 69 (1991) 2904
[8] K.U. Riemann, J.Phys D: Appl. Phys. 24 (1991) 493

External PIXE-RBS Analysis of Book Paintings

C. Neelmeijer, W. Wagner, H.-P. Schramm, U. Thiel

On the occasion of Georgius Agricola's 500th birthday in 1994 attention has been focused on the paint material found in an issue of his famous book on mining and works "De re metallica". The very thin color coatings on the highly sensitive paper ground represent a challenge to the power and the guaranteed non-destructiveness of Ion Beam Analysis. Using external PIXE-RBS the substantial studies on the Freiberg (Municipal and Mining Museum) issue [1] aimed at: (i) confirming the age of origin of the coloration as a premise for (ii) conclusions on the real representation of colors regarding the painted garments.

In addition to the on-air PIXE arrangement [2] a light protected and cleanable silicon surface barrier detector (100 mm^2 active area, 300 µm depletion depth, ΔE_α=30 keV at 5.4 MeV) was implemented on the top of the graphite lined beam line end cup. Backscattered protons are incident at ϕ=135°. Protons of 4 MeV energy, 1 mm^2 spot size, 0.5 nA beam current and 30 s acquisition time guarantee a non-destructive analytical work. Examining 5 colors, 18 measurements took place on representative positions of the page numbers 118, 328 and 490.

The PIXE spectra were evaluated by the GUPIX program [3]. After subtracting the blank paper data and taking into account knowledge on paint techniques [4] the overall PIXE-RBS results represent a historical pigment palette: copper blue (azurite), copper green, mercury-sulfur red (cinnabar), carbon black and organic yellow dyestuff [4].

The red colorations on two positions differ significantly in shade and intensity.

(i) Position A: Light red clothes of the smelter (page 490)
(ii) Position B: Dark red of the roof (page 328).

Fig. 1 compares the PIXE spectra. Besides minor peaks (Ti, Mn, Fe, Zn) from the paper, cinnabar (HgS, ρ=8.9 g/cm^3) was identified at both positions. However, the stronger Hg(L) intensity at pos. B confirms a paint layer of larger thickness compared to pos. A. The cinnabar layer strongly attenuates the Ca(K) radiation from the paper substrate (Ca(K) in Hg: μ/ρ=1580 cm^2/g). Surprisingly, the Hg(M) and S(K) signals are missing at pos. B.

This can be understood from the RBS spectra given in fig. 2. Intense C and O continua (non-Rutherford cross sections [5]) arise from proton backscattering at the substrate. At pos. B (dark red) the substrate C surface edge shifts towards lower energy and a small peak structure from Hg of the cinnabar pigment layer appears near channel 450. Calibrations prove that Hg from the surface corresponds to channel 473. Consequently, cinnabar must be covered with a further layer which, in view of the missing fingerprint in the PIXE spectrum (fig. 1), is assumed to consist of organic dyestuff. Madder red on cinnabar [4] is known to enhance the optical color depth. Fig. 2 also includes the RBS spectrum of pos. A. Here, lower thicknesses of both cinnabar and the sublayer are reflected by smaller energy shifts. Quantitative estimation of layer thicknesses from the energy shifts mentioned at pos. B (dark red roof) yield 1.5 µm of e.g. madder red - hydrous Al_2O_3 (ρ=2.5 g/cm^3) was assumed to pigment the dyestuff - and 1.5 µm cinnabar as well.

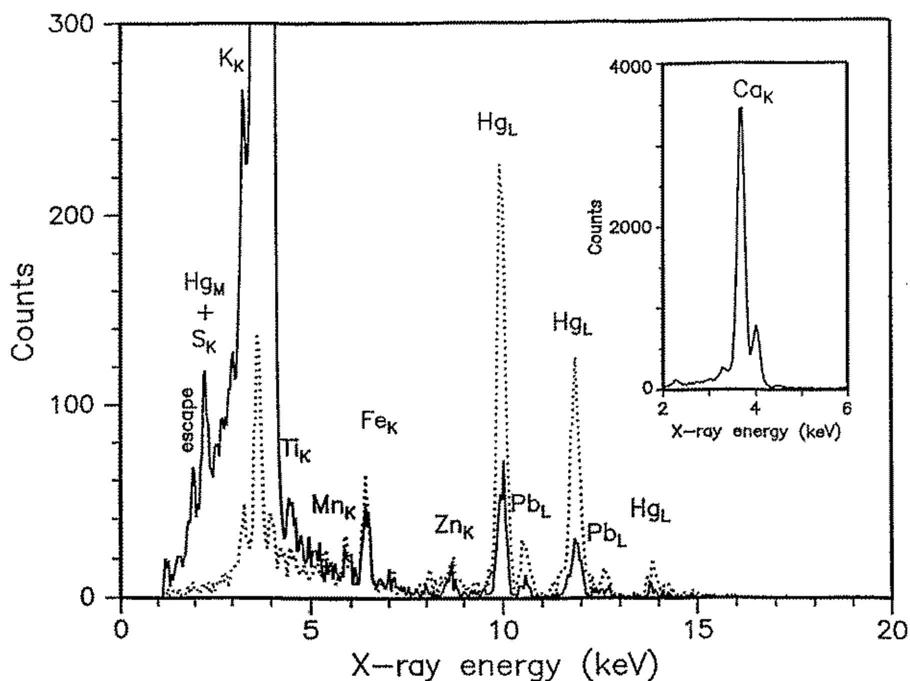

Fig.1: PIXE spectra (4 MeV primary protons) of red color: ——— pos. A, -------- pos. B (see text)

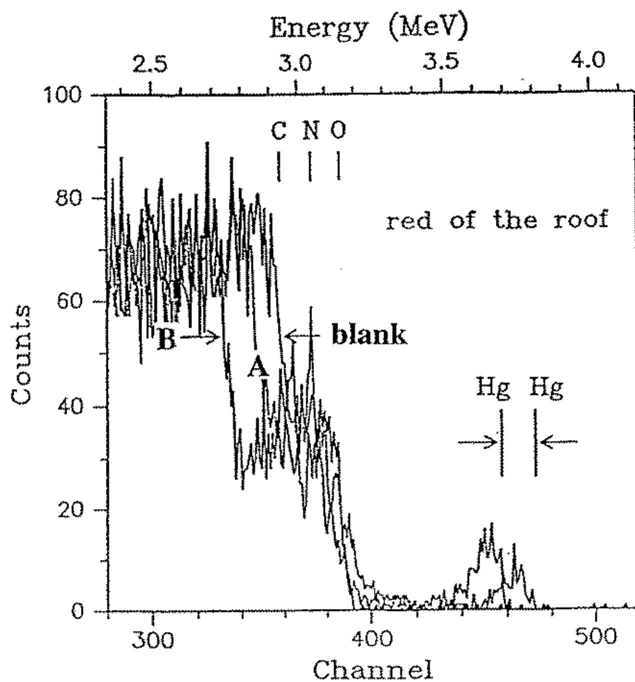

Fig. 2: Representative parts of RBS spectra simultaneously measured with PIXE, paper blank and red color: pos. A, pos. B (see text)

This paint layer arrangement is compatible with the observed 96% attenuation of the paper Ca(K) X-ray peak and the complete absorption of the cinnabar Hg(M) and S(K) lines in the PIXE spectrum (fig. 1). In fig. 1 the Pb X-radiation results from a minor admixture of red lead or white lead to the cinnabar.

This demonstrates that external PIXE-RBS [6] is excellently suited to characterize very thin layer arrangements of delicate book paintings in a non-destructive manner.

This work is supported by BMFT 215-4003-NE9ROS

References

[1] G. Agricola; De re metallica libri XII, Verlag J. Froben und N. Bischoff, Basel 1557
[2] C. Neelmeijer, H. Matthes, W. Pfestorf, H.-P. Schramm, C. Wendt; Nucl Instr. and Meth. B51 (1990) 140
[3] J. A. Maxwell, J. A. Campbell, W. Teesdale; Nucl. Instr. and Meth. B43 (1989) 218
[4] H. P. Schramm, B. Hering: "Historische Malmaterialien und ihre Identifizierung", (Berlin and Graz 1989)
[5] R. A. Jarjis, Nuclear Cross Section Data for Surface Analysis, Department of Physics, Schuster Laboratory, University of Manchester (1979)
[6] P.A. Mando, Nucl. Instr. and Meth. B85 (1994) 815

A novel silicon detector structure with internal high field region for low energy heavy ion spectroscopy

J. von Borany and B. Schmidt

Silicon detectors are widely used for the spectroscopy of charged particles. However, concerning the detection of heavy ions surface barrier detectors as well as modern ion implanted pn- junction detectors exhibit two drawbacks, namely the pulse hight defect and the plasma delay. It is well known, that the pulse high defect (PHD) is determined by three effects: the nuclear stopping, the energy loss in the detector dead layer and the recombination of charge carriers along the ionization track of the incident particle [1,2]. The amplitude deficit has been measured for different heavy ions as well as for fission fragments in a wide range of ion energy, and the corresponding data are usually included as correction parameters into the spectra analysis [3,4]. As PHD for heavy ions due to enhanced plasma recombination at ionization densities $\geq 10^{19}$ e/h-pairs per cm^3 is a function of the electric field strength [5], detectors with high internal electric fields are preferred for the spectroscopy of heavy ions. For detectors made of usually employed n-type silicon with resistivities of $400 \leq \rho_n \leq 5000$ Ωcm a maximum electric field of (2...25) kV/cm is obtained [6,7], which is insufficient to eliminate the recombination contribution to the amplitude deficit completely.

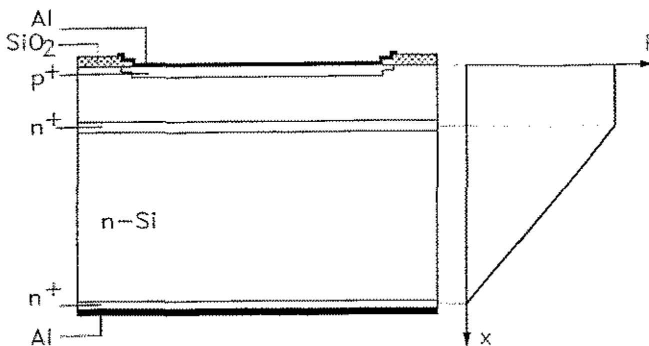

Fig.1: Schematic view of the modified detector structure

We propose a novel silicon detector with a possible high internal field strength up to 200 kV/cm, which is shown in Fig.1. The conventional diode structure based on high resistivity n-type material ($\rho_n \geq 1000$ Ωcm) is modified by a high energy, low dose ion implantation of donors (P^+, As^+), leading to a buried region of enhanced bulk doping. The calculation of the field distribution from Poisson's equation for a fully depleted detector indicates, that the local enhancement of the bulk doping due to the MeV implantation results in an increased and nearly constant electric field up to the depth of the buried implanted layer. Behind the n^+-layer the electric field linearly decreases analogous to the conventional detector configuration (see Fig.1). The dependence of the maximum field strength in the high field region on the applied detector voltage is shown in Fig.2.

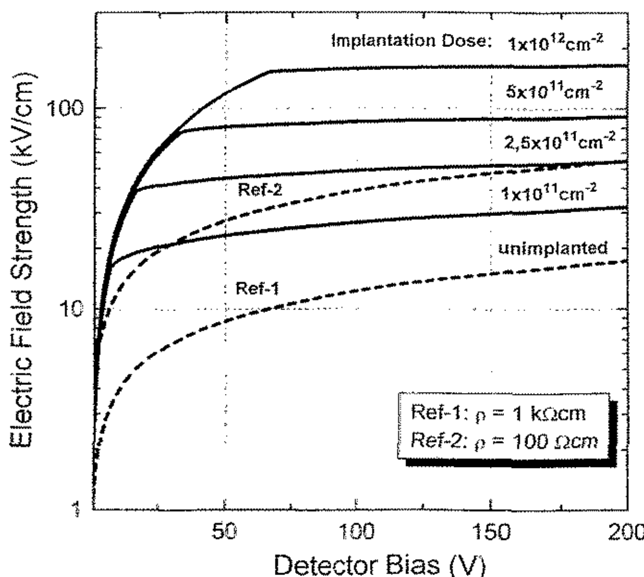

Fig.2: Calculated field strenght in the high field region. The dashed lines represent two conventional detectors made from different bulk materials.

Doses above $D \geq 2.5x10^{11}cm^{-2}$ result in high field regions with $F > 50$ kV/cm, which exceed those of conventional heavy ion detectors and for an implantation dose of $1x10^{12}cm^{-2}$ a field strength above 100 kV/cm can be realized, which is not far away from the critical field strength of ≈ 200 kV/cm for charge carrier multiplication (avalanche effect).
Detectors on high resistivity n-type material ($\rho_n \approx 1.5$ kΩcm) have been prepared including high energy ion implantation of phosphorous with E= 10 MeV and D= (2.5...10) · 10^{11} cm^{-2} in the standard planar process. The MeV-implantation results in a pearson-shaped doping profile with a maximum concentration of N_D = (2...10) · $10^{15}cm^{-3}$ in the depth of (4.9±0,2) μm, as determined by speading-resistance and capacitance-voltage profiling. For comparison conventional p^+nn^+-detectors without MeV- implantation but otherwise identically fabrication have also been prepared.

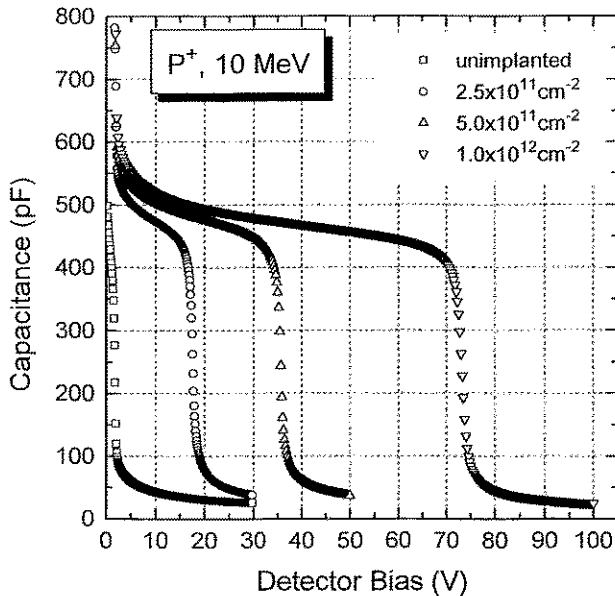

Fig.3: Detector capacitance characteristics of p^+n-junction detectors additionally implanted with different doses of phosphorous at 10 MeV

Measurements of the detector reverse current (IV) characteristics show no remarkable influence of the additional MeV- implantation step on the detector current even for internal electric fields of 150 kV/cm (U = 100 V, I < 30 nA). However, the buried implantation profile significantly changes the capacitance (CV) characteristics in comparison with conventional p^+-n-n^+-detector structures, as shown in Fig.3 for different implanted P^+-doses up to $10^{12}cm^{-2}$. The sharp transition in the CV- characteristics corresponds to the bias voltage at which the detector begins to be depleted over the maximum of the buried n^+- profile. These voltages agree with the expected values, which can be derived from the break points of the curves in Fig.2.

In contrast to conventional heavy ion detectors made from low resistivity silicon, the proposed detector structure enables a full depletion of (300...500) μm thickness. Therefore a detector is realized, which offers simultaneously enhanced field strength, large depletion depth and low capacitance (low electronic noise contribution). These detector properties seems to be very attractive for the simultaneous spectroscopy of light charged particles and low energy heavy ions.
First experiments have been performed at the Rossendorf Tandetron accelerator to characterize the behaviour of detectors with different high field regions for helium, oxygen and chlorine ions with ion energies of (0.9...8.5 MeV). For the reduction of the counting rate and the radiation damage of the detectors a backscattering arrangement (15 nm Au-layer on a C-target) was used. The ion energies for oxygen and chlorine correspond to projected ranges in silicon of (1...7) μm. The bias voltage for all detectors was changed from 5 V up to 200 V for covering the full electric field region (see Fig.1) and to obtain an overlap between detectors with different high field regions.
Fig. 4 shows the measured ion energies a function of the electric field strength for oxygen ions. Three regions can be clearly distinguished. The measured energy continuously increa-

ses with the electric field up to a constant value, which is obtained at around 35 kV/cm. The following nearly constant part of the curves can be interpreted as the region of maximum carrier collection from the window and the ionized track in the depletion zone. At electric fields above 100 kV/cm a significant rise of the pulse height was measured caused by the charge carrier multiplication. The beginning avalanche multiplication at moderate field strength of about (80...90) kV/cm is surprising and gives rise to the conclusion, that the electric field is strongly enhanced near the end of the "conducting needle" of the plasma track. As the multiplication is not characterized by a sharp transition, from these investigations it is difficult to define the maximum field strength suitable for heavy ion spectroscopy.

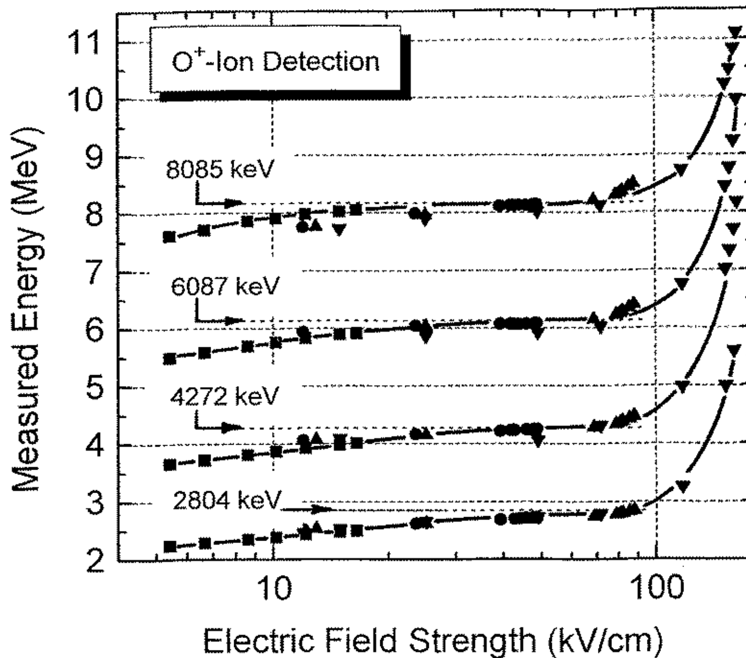

Fig.4:
Measured signal amplitudes of different high field region detectors in dependence on the electric field strength for various ion energies of oxygen (2.80 - 4.27 - 6.09 8.09 MeV)
Parameter: P^+, 10 MeV
■ : unimplanted;
● : $2{,}5\text{x}10^{11}\text{cm}^{-2}$;
▲ : $5{,}0\text{x}10^{11}\text{cm}^{-2}$;
▼ : $1{,}0\text{x}10^{12}\text{cm}^{-2}$

A comparison of the signal amplitudes for oxygen and chlorine ions, measured with different high field region detectors biased at a constant voltage (U = 100 V) is shown in Fig.5. All amplitudes are normalized to the energies, which were measured with the conventional p^+n-junction detector without MeV- implantation (F = 12 kV/cm). For high field region detectors a signal enhancement up to 25% has been obtained both for oxygen and chlorine ions in contrast to helium ions, where the effect is significantly smaller (0.80 MeV: 4%; 0.95 MeV: 2%; 2 MeV: < 0.5%). Generally, the signal enhancement increases with decreasing ion energy, which suggests a significant influence of the detector window on the PHD especially for low energies. Therefore, the detector dead layer was determined by the well known tilting technique [8], where the energy loss of ^{241}Am-α-particles (5,486 MeV) is measured as a function of the incidence angle (15°-60°). The effective silicon dead layer is found to be a strong function of the electric field strength and decreases from 130 nm to 35 nm with increasing field strength of 12 and 85 kV/cm, respectively. The effective dead layer thickness of (35±5) nm corresponds to the lowest values ever obtained for silicon pn-junction detectors. A simple estimation shows, that the signal enhancement both for helium and oxygen ions can be explained by the field dependent reduction of the effective dead layer window. As the electronic stopping power for oxygen in the investigated energy range depends only slightly from the energy (1-8 MeV: dE/dx = 130...170 eV/Å), the contribution of the detector dead layer to the relative amplitude deficit decreases with increasing

energy.

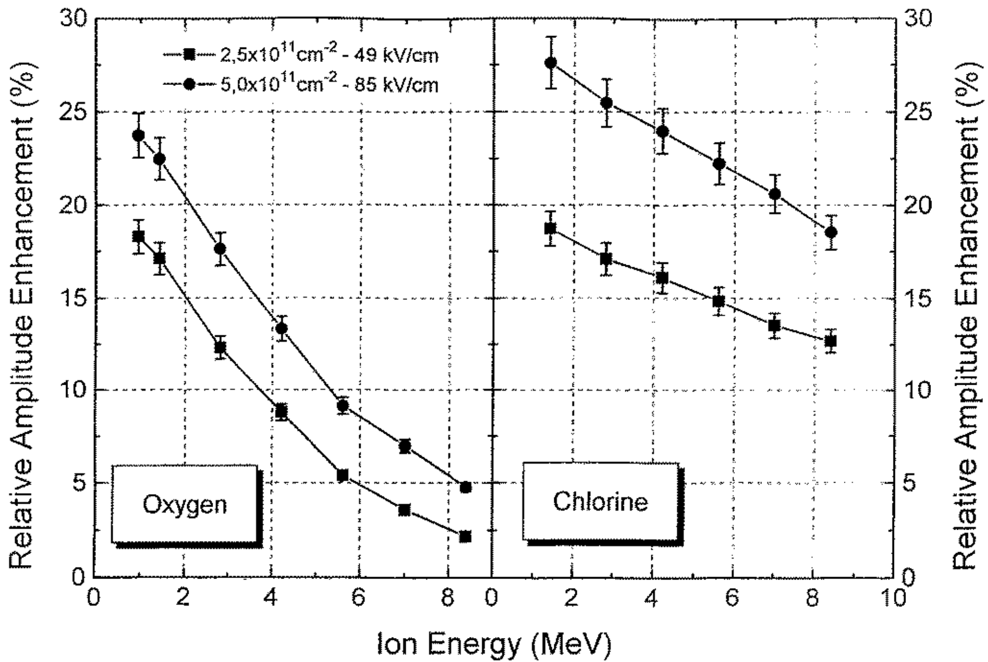

Fig.5: Amplitude enhancement in MeV- ion implanted high field region detectors compared to a conventional detector for various energies of ^{16}O and ^{35}Cl ions.

The situation is different for chlorine ions. The reduced effective dead layer can only explain a signal enhancement of 22% and 10% for an ion energy of 1 or 8 MeV, respectively. Therefore, additional charge carrier loss in the plasma track amplitude has to be taken into consideration, which can be reduced for detectors with electric high field regions. Further experiments will be done to seperate more clearly both the observed effects of the field dependent reduction of the effective silicon dead layer and the high field enhanced carrier collection from the plasma track of low energy heavy ions.

References:

[1] E.C. Finch, A.L. Rodgers, Nucl. Instr. and Meth. 113 (1973) 29

[2] S.A. Kassirov et al., Nucl.Instr. and Meth. 119 (1974) 301

[3] S.B. Kaufmann et al., Nucl. Instr. and Meth. 115 (1974) 47

[4] J.B. Moulton et al., Nucl. Instr. and Meth. 157 (1978) 325

[5] I. Kanno, Rev. Sci. Instr. 58 (1987) 1926

[6] E.C. Finch et al., Nucl. Instr. and Meth. 163 (1979) 467

[7] W. Bohne et al., Nucl. Instr. and Meth. in Phys. Res. A240 (1985) 145

[8] T. Maisch et al., Nucl. Instr. and Meth. in Phys. Res. A288 (1990) 19

New Microfluidic Components for the ISFET Microsystem

S. Howitz, H. Fiehn, S. Steinbach, T. Wegener, T. Gehring, M. Bürger

The Fluidic ISFET Microsystem (FIM) is a microinstrumentation for dynamic multiion detection of electrolyte solutions [1]. The modular designed FIM concept contains both sensors and actuators which may be combined flexibly according to the measuring purpose. The basic wafer of the FIM contains only fluidic channels and electrical conducting lines to ensure proper interconnections between the single components, which are made planarized by using standard methods of silicon micromachining. All silicon components are prepared separately in batch processes and have to be assembled onto the system wafer after cutting.

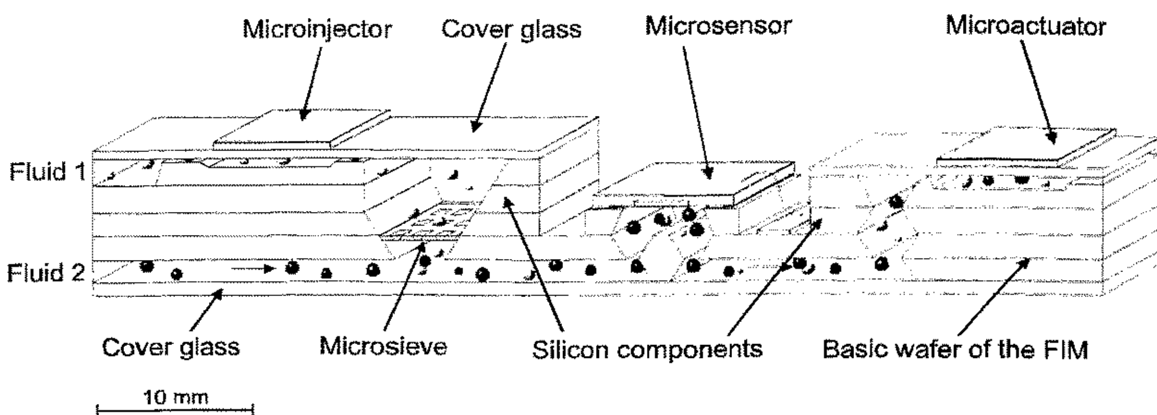

Fig. 1: Schematic description of the function of one measuring unit of the FIM. The ISFET-sensor arranged between two micropumps can be loaded alternatively with fluid 1, fluid 2 or mixtures of fluid 1 and fluid 2.

Due to the fact that microfluidic components are still not available commercially we have been forced to develop suitable devices to fit them to the FIM-system. Fig. 1 shows one measuring unit of FIM and illustrates the interaction of actuators and sensors. Manufacturing processes are based on the anisotropical chemical etching of (100)-silicon. The method of (micro)electronic photolithography has proven their suitability to design micromechanical and microfluidic structures. Closing and sealing of the fluidic structures are performed by anodic bonding of the silicon components with pyrex glass. The size of each single component is (20 x 10) mm^2 at most. The actuating devices are driven piezoelectrically by mounting piezo-actuators on elastic silicon or glass membranes to form bending compounds.

According to the requirements of the FIM two kinds of micropumps were developed for FIM, which can also be used as standalone components for other applications:

1. Many research activities around the world deal with micropumps providing a continuous fluid flow. Usually these pumps consist of a pump chamber with varying volume and in/outlets with unidirectional flow restrictions. Especially for FIM a new type of micropumps has been developed which does not need any flow restriction. It is based on the anisotropic flow resistance of flow channels formed as a nozzle or a diffuser. Such a pump has been realized by means of silicon micromachining for the first time. A yield of up to 400 µl/min at 50 V power is provided.

2. Chemical microsensors have to be calibrated periodically. This circumstance causes the problem to switch between the measuring and the calibration fluid on the sensor. It could be solved by the development of a microinjector - called microfluidic diode or micro drop emitter too - successfully. The microinjector is capable to apply incompressible fluids covering the range from 0.5 nl/impulse to 350 µl/min.

Conventionally fabricated piezo driven emitters for liquid drops are commercially available but very expensive and large in size. Miniaturized drop emitters are widely used in ink jet printers but there are no other applications known.

The developed microinjector is used both for the FIM (to switch fluid flows) and to inject liquid drops into air gaps, e.g. for dosing purposes. The left part of Fig. 1 illustrates the configuration of a microinjector as a microfluidic diode used by the FIM as a valve. With respect to the surface tension a microsieve with defined mesh size prevents the carrier fluid 2 in the injectorchannel from passing the sieve upward. The same effect enables the injected drops of fluid 1 hitting the sieve to join the carrier fluid and move with it. The flow resistance of the whole fluidic system has to be adjusted in such a way that no fluidic breakthrough occurs on the sieves.

The disadvantages of the open fluidic system can be related to the advantage caused by the ideal separation of injected and carrier fluid by the nozzle-air-sieve interface. Contamination induced microleaks - even in the nl range - well known from other microvalves are completely suppressed. The injection of one fluid into another through an air interface meets the demands of an ideal valve or an ideal mixing device.

The surface tension on the top of the nozzle is an essential requirement to ensure an anisotropic flow resistance to make the injector working. Both yield, drop size and drop form depend on voltage, frequency, impulse width and impulse form of the piezoactuator power supply as well as the design of inlets/outlets. Fig. 2 illustrates the correlations between some of these parameters.

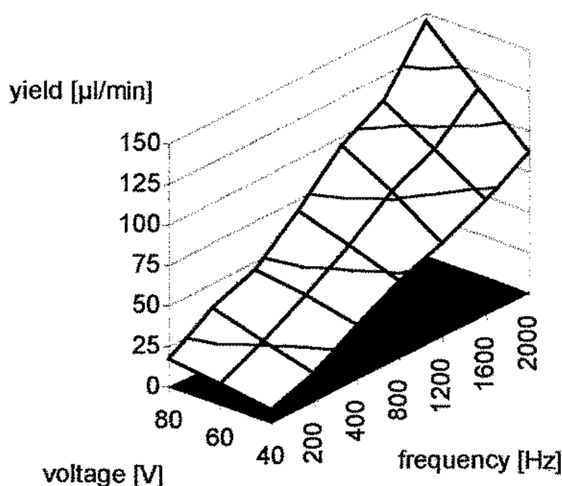

Fig. 2: The control of the parameters of the microdrop emitter makes it possible to provide either the dosing of some single drops or a continuos fluid flow.

References

1. H. Fiehn, S. Howitz, M.T. Pham, T. Vopel, M. Bürger, T. Wegener, Micro Total Analysis Work-shop, Twente, Netherlands, Nov. 21 - 22, 1994

The Dependence of the Hydration Process of Hardening Cement on Temperature Studied by Small-Angle Neutron Scattering (SANS)

A. Hempel, F. Eichhorn

Concrete is a widely spread construction material. Its technically relevant properties like strength, permeability for gases and liquids and corrosion resistance are essentially determined by the cement used and its curing during the hydration process. The ordinary Portland cement powder consists of some clinker phases, the major ones being calcium silicates, calcium aluminate, and calcium aluminoferrite [1]. The hydration of cement is quite a complex process because it depends on various external conditions. Obviously the most important ones are time and temperature: the latter influences the velocity of the chemical reaction. Therefore, the structure of such a system of different matrix phases (hydrates, unhydrated clinker grains) and pores must be considered as a function of time and temperature. So far the processes of structure development during the cement hardening are not understood in principle. Therefore, the aim of the present work is to use the small-angle neutron scattering method (SANS) with its specific scope for a deeper insight into the hydration process.

A known process to enhance strength or hardness of metallic materials is the generation and development of precipitates or fine grains. The sizes of these particles determine in a high degree the final physical parameters of the material, and often optimum material properties are correlated with particles of a defined size range. A similar dependence exists also for other materials especially for cement-containing building materials [2]. To demonstrate this, in Fig.1 a scanning electron micrograph shows structural details of the hydrated cement paste like pores and particles of various size. The existence of a hydrate shell formed around an initial clinker grain is evident.

There is a number of analysing methods for investigation of pores in cement pastes and concretes. Some of these methods are the capillary condensation method (BET method), the mercury intrusion porosimetry and the small-angle neutron or X-ray scattering (SANS, SAXS). The first two measuring procedures destroy the inner structure of the sample [3]. Using small-angle scattering the samples can be investigated in a non-destructive mode. Here the radiation is scattered if the beam crosses different phases. The intensity (contrast) of the scattered beam is determined by the difference of the scattering length densities of these phases. Unlike to small-angle X-ray scattering, SANS allows to vary the contrast between the hydration products. This is achieved by using a well-defined mixture of H_2O and D_2O for the hydration of cement. Then a material can be prepared which consists of one neutron-optically homogeneous matrix phase (all the chemically different hydrate phases have in this case the same neutron scattering length density) and pores [3]. In addition to this it is possible to investigate samples with greater thickness.

In cement paste the sizes of structural details lie in an extended region between some nm and mm. Therefore, different instruments are necessary for measurements over the whole size range. Several small-angle neutron scattering devices (like D11 at the HFR of the ILL Grenoble or MURN at the IBR-2 of the JINR Dubna) allow investigations in the higher momentum transfer range corresponding to the lower size region, whereas measurements with a small momentum transfer are only possible with the high-resolution double-crystal technique. For this purpose we installed a new version of such an instrument at a neutron guide at the BER-II reactor in the Hahn-Meitner Institute Berlin (Fig. 2).

Its main components are the two perfect silicon crystals in the (111) Bragg reflection. The crystals can be elastically bent down to a radius of 10 m. The maximum momentum resolution is obtained with a flat first crystal. The second (analyzer) silicon crystal reflects the neutron beam only in the case, that its net planes are parallel to the net planes of the first silicon crystal. If the analyzer crystal is cylindrically bent with an axis perpendicular to the scattering plane, then the Bragg condition is fulfilled only at a small part of the large crystal. With a sample positioned between both crystals scattering neutrons in the small-angle range, the Bragg reflection is spread out over a greater crystal part. A one-dimensional position sensitive detector records simultaneously the whole momentum transfer range [4]. This is the essential new capability of our double-crystal diffractometer what enables to investigate time-depending processes like the hydration of cement paste. In contrast to this the known variants only allow a step-by-step measurement of the scattering range.

The samples of hardening cement paste were prepared from ordinary Portland cement powder with a water-to-cement ratio of 0.38. This value enables a full hydration of all clinker phases. It determines the size and size distribution of pores, too. A mixture of 62 vol.% H_2O and 38 vol.% D_2O was used to prepare samples which have in this case only one neutron-optically homogenous matrix phase.
A thin aluminium slice was used as sample holder. The thickness of all samples was 0.5 mm. We started the evaluation of the microstructure in dependence on time and temperature.
The time-dependent hydration processes were measured at the temperatures of 23°C, 30°C, 39°C, and 48°C.

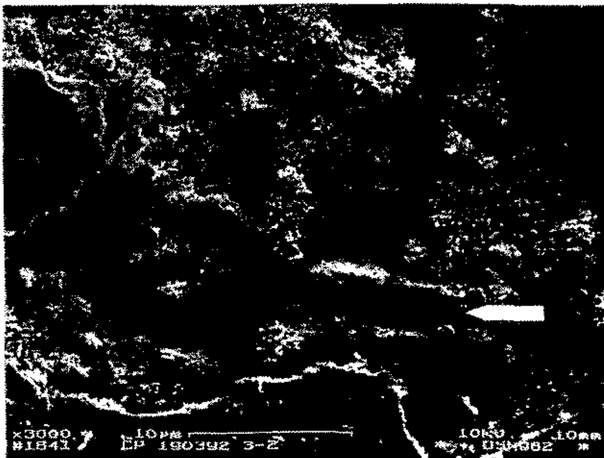

Fig.1 REM picture of hydrating cement, a clinker grain with a hydration shell is marked

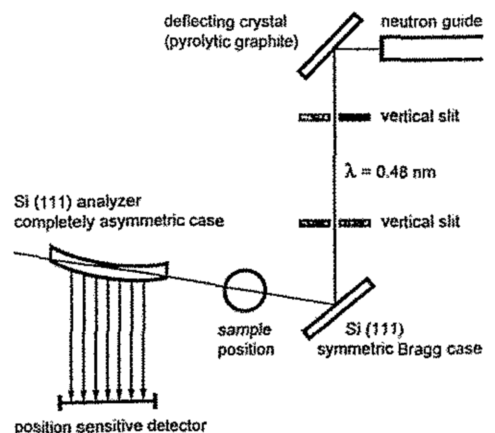

Fig.2 Sketched setup of the double-crystal diffractometer at the BER-II reactor of the Hahn-Meitner Institute Berlin

Fig. 3 shows the scattering curves at the temperature T=23°C for different times. It is obvious that at the beginning of the hydration the change of the scattering behaviour is stronger than after a longer hydrating time. There is a tendency to reach an asymptotic value. Similar results are obtained also at higher temperatures, but the scattering curve will reach its constant value quite earlier. At a temperature of 50°C this state will be achieved after some minutes (40 min) as against 48 hours at room temperature (T=23°C).

For describing the hydration process the particle size distribution (PSD) is more useful. The PSD represents the frequency to find particles in a defined radius range. The particle size distribution after different hydrating times at constant temperature was estimated by the indirect Fourier transformation of the scattering curve [5]. The resulting curves are shown in Fig. 4. The probability density of radii increases with longer hydrating times. The observed behaviour is caused by an increasing number of smaller particles and is a clear indication of increasing strength of cement. It seems that the latter is more correlated with a high nucleation rate and less with a growing rate of existent particles. The small oscillations around zero ordinate value at higher radii are artefacts of the evaluation procedure and do not have any physical meaning. The curve for radii below 200 nm is uncertain, because here the instrumental effect predominates the sample effect.

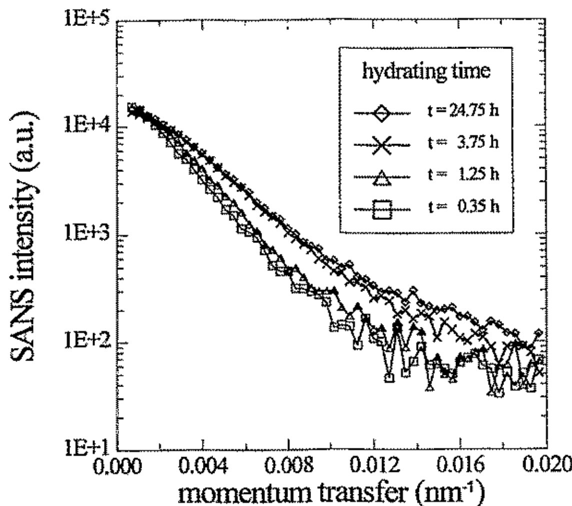

Fig.3 Scattering curves at different time for T=23 °C

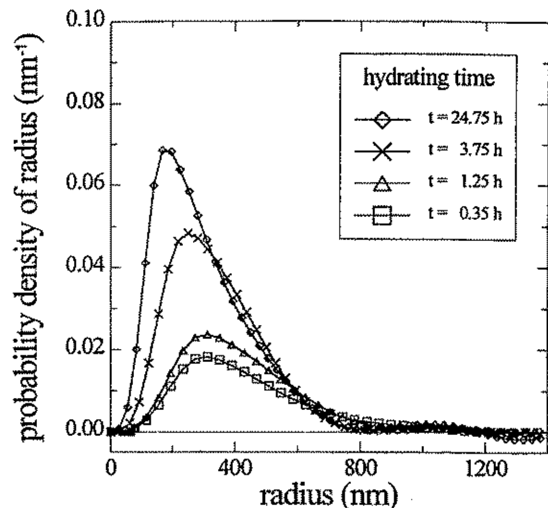

Fig. 4 Particle size distribution at different time for T=23 °C

In order to investigate the long-time effect of the structure development process, corresponding particle size distributions were considered, too. With time the particle size distributions at different temperatures become more and more similar to each other and do not show any significant difference after 48 h hydration. In the particle size range covered by the double-crystal diffractometer the final size distribution function seems to be independent on the hydration temperature.

It can be stated that the temperature only influences the process velocity but not the character of the microstructure.

Considering the results of the small-angle neutron scattering experiments at hydrating ordinary Portland cement paste a dependence of the structure development process on time and temperature could be identified. In particular we conclude that

-- the number of particles with radii in the range from 200 to 600 nm increases during the hydration,

-- in the investigated particle range the process velocity increases with the hydration temperature,

-- the final structure (nearly at the end of the initial hydration) is not influenced by the temperature during the hydration.

In a next step it would be interesting to investigate the hydrating behaviour at low temperatures (for instance at 10 °C) and the influence of humidity on the structural change.

This work is supported by the Bundesministerium für Forschung und Technologie under grant No. 03-EI3ROS.

[1] A. J. Allen et al.; J.Phys.D:Appl.Phys. 15 (1982) 1817

[2] K. Wesche; Baustoffe für tragende Bauteile, Vol. 2 , Wiesbaden and Berlin 1981

[3] F. Häußler, F. Eichhorn, S. Röhling, and H. Baumbach; Cement and Concrete Research 20 (1990) 644

[4] P. Mikula, P. Lukas, and F. Eichhorn; J. Appl. Cryst. 21 (1988) 33
A. Hempel, F. Eichhorn, and P. Reichel; BENSC Experimental Reports 1994 (Hahn-Meitner-Institut Berlin, Berlin Neutron Scattering Center) in preparation

[5] O. Glatter; J. Appl. Cryst. 13 (1980) 7

Structure and Diffusion of Self-Interstitials in Silicon Studied by Molecular Dynamics Simulation

K.-H. Heinig and V. Konoplev

The elementary point defects in silicon, the vacancy (V) and the self-interstitial (Si_i), have been a subject of intense studies for several decades. Despite of this, their diffusivities are not well-known. Different experiments give results varying over seven orders of magnitude [1]. Very recently, the Si_i came again in the spotlight of actual research because of its central role in the process of transient enhanced diffusion (TED), e.g. of TED of boron in silicon [2]. TED is caused by the formation of mobile [B-Si_i] complexes. A source of Si_i for the complex formation are extended defects (Si_i-clusters) produced during the implantation and the post-implantation annealing stages. Si_i are emitted from these defects into the B-doped region by further annealing.

The uncertainty in the diffusivity of Si_i precludes both an understanding of the kinetics of TED and the development of a reliable process simulator applicable at various implantation and annealing conditions [2]. In the present work we report new approaches for studying (i) the formation of Si_i configurations and (ii) the mechanisms of their diffusion. Molecular dynamics (MD) simulations were performed with the many-body Stillinger-Weber (SW) potential. The simulation cell was a 1000-atom crystallite ($5a_o \times 5a_o \times 5a_o$ size, a_o – lattice constant) with periodic boundary conditions.

For the study of Si_i configurations an additional atom was placed near the center of the simulation cell, and 128 independent MD simulations were performed by delivering 8 eV kinetic energy to the additional atom at random directions. The resulting agitation and consequent relaxation of target's atomic structure leads to the formation of definite Si_i configurations. This new approach for determining the Si_i configurations imitates processes occuring at the final stage of a collision cascade.

The difference $\Delta E^I = E^I - E^0$ between the potential energy E^I of the annealed simulation cell (i.e. cooled down to T= 0 K), containing an interstitial, and the energy of the perfect lattice without an interstitial, E^0, is shown in fig. 1 for MD simulations performed at T = 300 K and 1000 K.

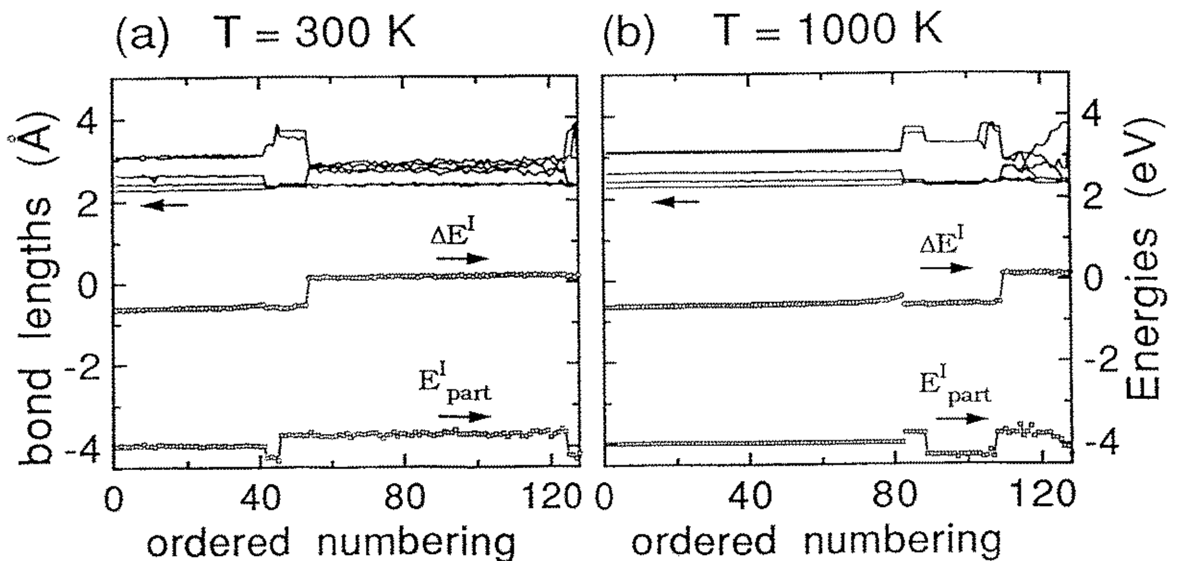

Fig. 1. The energies and the bond lengths characterizing the Si_i configurations found.

The numbering of MD simulations (abscissa in fig. 1) does not reflect the sequence of simulated "events". By this order the Si_i configurations are arranged into two groups with similar potential energy shifts ΔE^I. A detailed study of the structures of Si_i has revealed that each of the two ΔE^I values corresponds to a definite Si_i configuration presented in fig. 2. We denote by $I^{Jack}_{<110>}$ the ground state configuration (lower ΔE^I, fig. 2b), and by $I^{Dumb}_{<110>}$ - the excited Si_i configuration (fig. 2a). The formation energies E_f of $I^{Jack}_{<110>}$ and $I^{Dumb}_{<110>}$ interstitials were found to be equal to 3.72 eV and 4.47 eV, respectively. At 300 K, more $I^{Dumb}_{<110>}$ than $I^{Jack}_{<110>}$ configurations have been produced, namely, 59 % and 41 % (fig. 1a). This makes clear that the "reaction path" of the system in its configurational space is attracted quite frequently to a metastable state, and that the Si_i configurations found are separated from each other by an energy barrier. Fig. 1b shows that at $T = 1000$ K the ratio between the numbers of $I^{Dumb}_{<110>}$ and $I^{Jack}_{<110>}$ has changed in favor of the ground state configuration (17 % to 83 %).
The 3-dimensional images (fig. 2) of the two Si_i configurations show three $(1\bar{1}0)$-oriented atomic planes. They are looked from two perpendicular directions – along the $< 1\bar{1}0 >$-direction (upper frames), and along the $< 00\bar{1} >$ direction (bottom frames). The larger spheres present the atoms located at the intermediate plane. The black spheres belong to the specific interstitial configurations. The two black atoms in fig. 2a share one lattice site and form an $< 110 >$-oriented dumbbell. This interstitial configuration distorts substantially the surrounding lattice, producing notable shifts of even rather distant atoms out of their lattice sites (see fig. 2a, bottom frame), what seems to be the reason of the larger E_f of this Si_i structure.

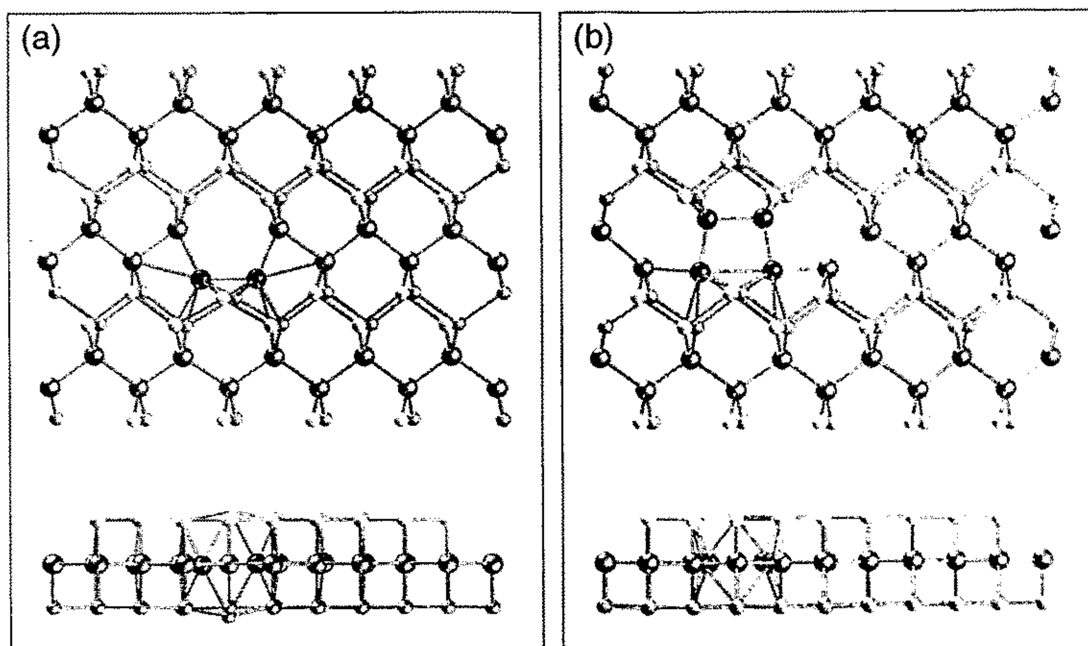

Fig. 2. The $I^{Dumb}_{<110>}$ and the $I^{Jack}_{<110>}$ self-interstitial configurations observed from two perpendicular directions.

The ground state configuration $I^{Jack}_{<110>}$, shown in fig. 2b, is produced by a replacement of three lattice atoms, forming a fragment of zig-zag chain, by the trapezoidal construction of the four black atoms. The bond between the atoms sharing one lattice site, corresponding to the base of the trapezoid, is weak (bond length of 3.05 Å). Disregarding of this bond reveals that these four

atoms form two fivefold rings with the atoms located at the upper and the lower (110)-planes. This procedure of creation of the $I^{Jack}_{<110>}$ interstitial is similar to that suggested by Jackson [3], where the replacement of the pyramid of four lattice atoms by a symmetric fivefold atomic ring is considered.

The extended nature of $I^{Dumb}_{<110>}$ and $I^{Jack}_{<110>}$ configurations means that one cannot identify any specific atom as an interstitial. The additional atom in this case is a virtual one with a volume distributed over a certain region that relates to the Si_i configuration. However, this virtual atom has a center of mass that we consider as interstitial position. We determine this position by a pattern recognition program, which allows us to calculate the diffusional random walk of Si_i. This is an important new feature in diffusion studies, since previously (for instance, in ref. [4]) the Si_i diffusion was estimated by calculating the relocations of target atoms induced by the Si_i motion.

In fig. 3 we show a fragment of the diffusional path of the Si_i corresponding to a time period of 100 ps and to a temperature of T = 1200 K. The circles in this figure mean positions of the Si_i at times separated from each other by 0.1 ps. The dense clouds of circles show the regions where the Si_i stays near the local energy minima. The average time between jumps of the Si_i is about 20 ps at this temperature. A motion between the local minima (jump duration) takes much less time (0.5 ... 1 ps). One important new feature in our diffusion study consists in observation that the lengths of jumps vary in the range of approximately 3...8 Å, i.e. both the jumps between neighboring local minima as well as between rather distant local minima occur. This implies that the Si_i diffusion is characterized by a wide diversity of diffusion jumps, and that these jumps have a collective nature.

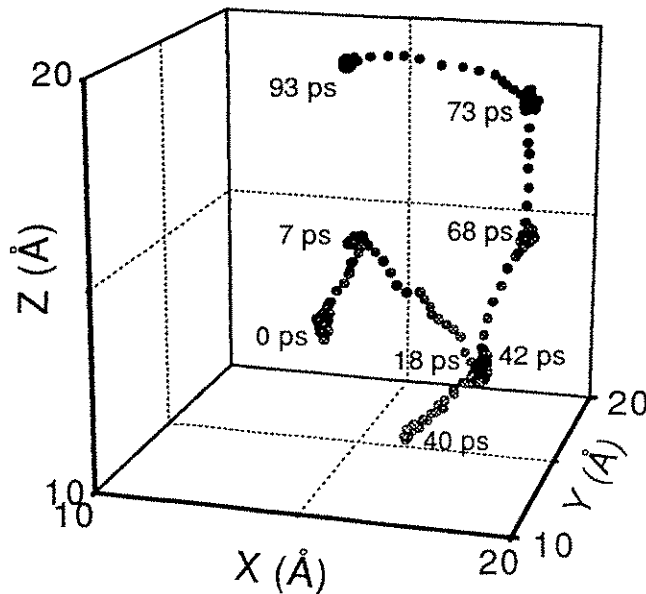

Fig. 3. A fragment of the diffusional path of Si_i at T = 1200 K during 100 ps time interval.

We illustrate in fig. 4 the details of the jump that corresponds to Si_i relocation from its position at t = 0 ps to that at t = 7 ps, for the diffusional path shown in fig. 3. The initial Si_i configuration is $I^{Dumb}_{<110>}$ (fig. 4a), and it transforms, due to the jump, into $I^{Jack}_{<110>}$ (fig. 4b).

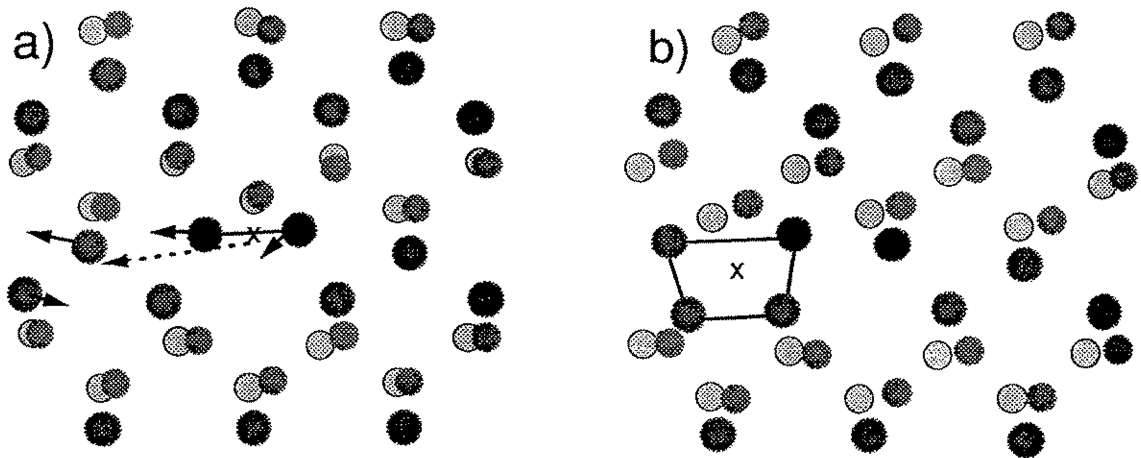

Fig. 4. Collective atomic redistribution in the region containing Si_i that results in a diffusional jump of a virtual atom.

The dashed arrow in fig. 4a shows the relocation of the center of mass of Si_i, and the short solid arrows indicate the displacements of the atoms participating in this Si_i jump. We should stress here that for a collective mechanism of Si_i diffusion the square of the relocation distance of Si_i does not equal to the sum of the squares of atomic relocations. In particular, for the event illustrated in fig. 4, these quantities approximately equal to 14 Å^2 and 8 Å^2, respectively. Large distance jumps, of the lengths of the order of 10 Å, can be interpreted as a short jump followed immediately, without complete relaxation in an equilibrium Si_i configuration, by one or more other jumps. In other words, the long jumps can also be imagined as a result of disordering, due to an energy fluctuation, of relatively large local region containing the virtual atom, followed by a reordering of this region, what leads to a collective atomic redistribution and, finally, to the appearance of the virtual atom at another equilibrium position of Si_i far apart from the former one.

In fig. 5 we compare our simulation results with the largest among reported experimental diffusivities of Si_i. The MD results at various T are shown by circles, and the thick solid line

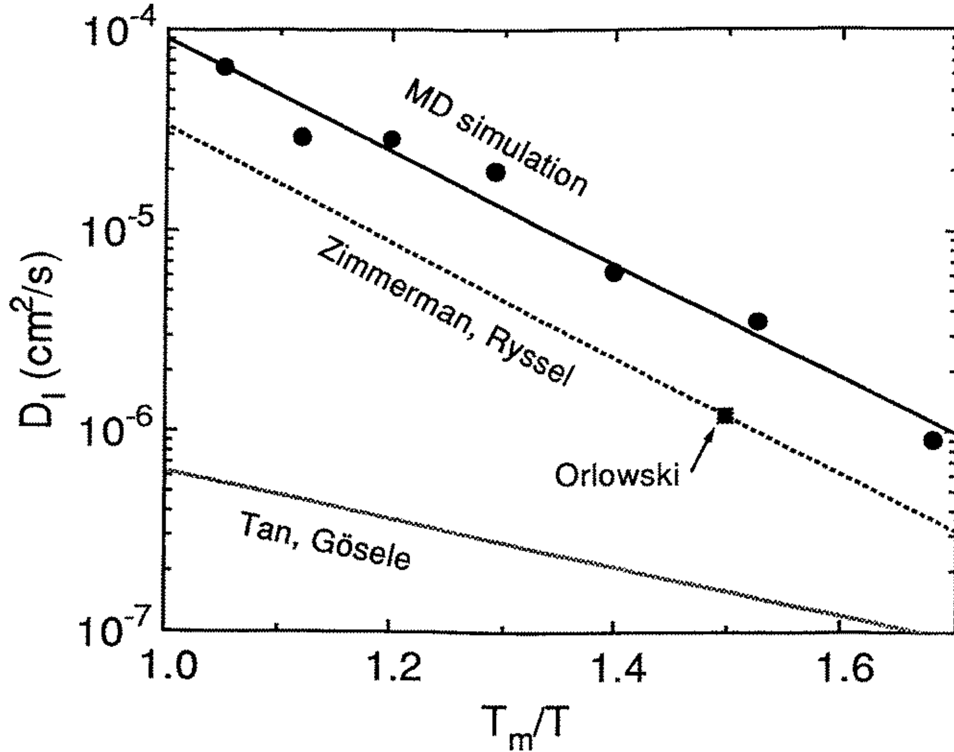

Fig. 5. The calculated and experimental diffusivities of Si_i at various temperatures (T_m is the melting temperature of Si). Only the largest of the reported experimental diffusivities were taken for the comparison.

is their exponential least square fit. A slope of the fitted line gives the value of 0.88 eV for the activation energy of diffusion. Agreement of our results with the experimental data of refs. [5,6] is good. The significantly smaller diffusivities obtained by other authors [1,7] can be explained by presence of a relatively high concentration of traps for Si_i in silicon crystals.

Supported by the Saxonian Government and by the Bundesminister für Forschung und Technologie through contract 211-5291-03-HE3ROS.

References

[1] W. Taylor, B.P.R. Marioton, T.Y. Tan and U. Gösele, Rad. Eff. and Def. in Solids, 111 & 112 (1989) 131.
[2] D.J. Eaglesham, MRS Bulletin, XIX, No. 12 (1994) 57.
[3] L.C. Kimerling, Inst. Phys. Conf. Ser. No. 46 (1979) 56.
[4] P.E. Blöchl, E. Smargiassi, R. Car, D.B. Laks, W. Andreoni and S.T. Pantelides, Phys. Rev. Lett. 70 (1993) 2435.
[5] H. Zimmerman and H. Ryssel, Appl. Phys. A55 (1992) 121.
[6] M. Orlowski, Appl. Phys. Lett. 58 (1991) 1479.
[7] U. Gösele and T.Y. Tan, Mat. Res. Soc. Symp. Proc. 36 (1985) 105.

Electronic Stopping of Heavy Ions in the Kaneko Model

R. Mathar and M. Posselt

Two quantities determine the electronic stopping of heavy ions from the point of view of effective charge theory: (i) the radial charge distribution of the electrons that are bound to the ion, or rather its wave number representation. The ionization fraction as a function of the ion velocity and atomic number is the key entry. (ii) The dielectric function of the target as a function of wave number and frequency. Together they define the polarization charges that are created by the moving ion, and finally the force (stopping power) that these charges exert on the ion. The name 'effective charge' points out that, under the restriction of a linear susceptibility of the target, the stopping cross section of partially stripped ions is not simply the squared ion atomic number times the proton stopping cross section at the same velocity, but effectively smaller.

The familiar theory based on the work of Brandt et al. [1, 2] deals with the target model of a homogeneous free electron gas (FEG). The essential contribution of the inner target shells to the target polarization is therefore missing, and experimental proton data, which evidently contain this piece of information, are scaled to obtain reliable results.

A more fundamental theory has been set up by Kaneko [3]. It delivers formulas for the susceptibilities of individual shells of bound electrons of target atoms. They may be roughly interpreted as a generalization of the calculation of the susceptibility of a FEG [4] to lowest order, but the momentum distribution of the wave packets of bound electrons is approximated by a Gaussian instead of the 'Fermi ice block.' The total stopping power is finally written down as a sum of target subshell contributions. Theories of this kind can compute heavy ion stopping powers without recourse to proton stopping powers. Nevertheless, the model has almost exclusively been applied to light ion stopping. Searching for improvements of the theory and its application to heavy ion stopping we discussed four aspects [5]:

(1) **Energy gaps of target shells.** We included a correction to the susceptibilities of shells

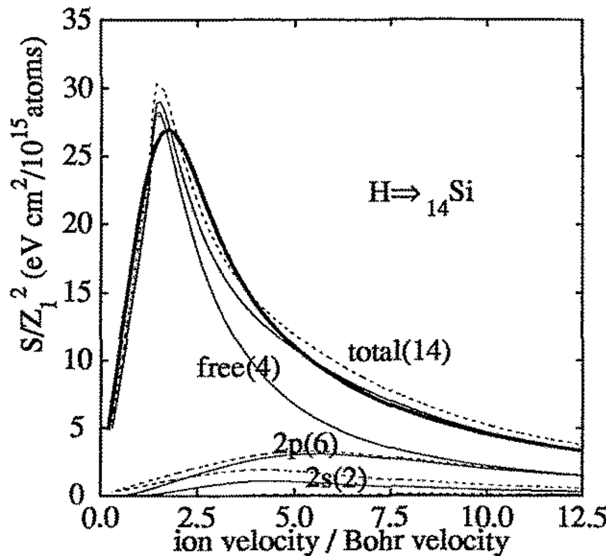

Figure 1: Total and per shell proton stopping cross sections in $_{14}$Si. Dotted lines: Original Kaneko theory. Bold: ZBL [2]. Thin solid lines: theory with energy cuts of the Si $1s^2$, $2s^2$ and $2p^6$ shell. Occupation numbers of the shells are given in parentheses.

of bound electrons to take into account that an electromagnetic field must at least transfer the energy of the individual excitation gap of the bound target electron [6] in order to create a (real) electron-hole pair. Polarizations and stopping powers are diminished by this kind of low-energy cut of the imaginary part of the susceptibilities, and the stopping powers of the subshells concerned no longer rise linear at low ion velocities. Looking at the stopping powers of protons, the general 5 – 10 % overestimation of their high-velocity stopping is removed (fig. 1). Because energy gaps change only features of the target model, protons are chosen here to remove the uncertainty on the projectile charge distribution from the theory. The action on heavy ion results is equivalent (cf. fig. 2).

(2) **Dead sphere of polarization.** The Kaneko theory more and more overestimates heavy ion stopping powers at their maximum, when the ion atomic number increases. We discovered that this corresponds to the feature of the familiar formulas to allow a target polarization without restriction on space. In a more realistic calculation, the electrons bound to the ion occupy some domain. We call it a 'dead sphere', since the excitation of a target polarization of either sign is suppressed there: target electrons cannot penetrate into this sphere, because the electron density inside is already fixed by the atomic theory; target electrons are not scattered from inside the sphere, because there are hardly any inside. This model to remove the polarization at the close neighbourhood of the ion nucleus lets the ion no longer 'skim over' but 'plough through' the target electrons. It is strongly supported by the observation that fits of the radii of these dead spheres are roughly equal to the radii of the outer shells of partially stripped heavy ions (fig. 2).

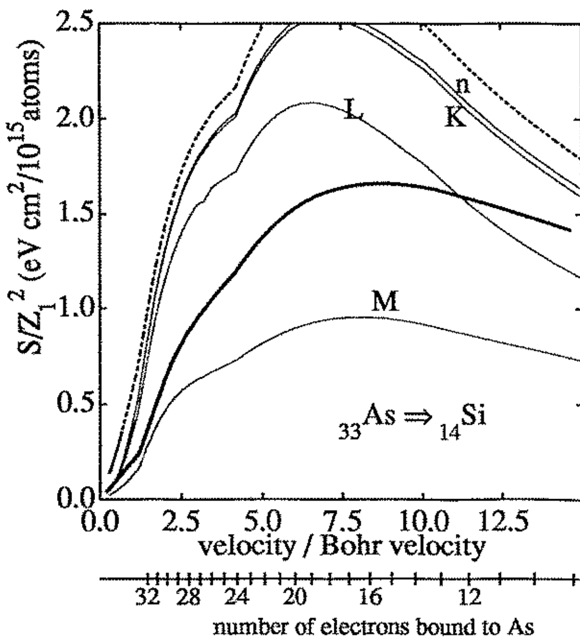

Figure 2: $_{33}$As electronic stopping in $_{14}$Si. Bold line: ZBL [2]. Dotted: original Kaneko theory with ZBL ion parameters. Thin solids: Kaneko theory with energy cuts of Si shells. Line 'n': no dead sphere. Lines 'K', 'L' and 'M': dead sphere radius set to the corresponding ion shell radius. Z_1 is the ion atomic number. Fig. 3 presents an example, where the dead sphere radius is dynamically shrunk with the ion size.

In the framework of effective charge theory, which defines the effective charge from the statistics of close and distant collisions between the ion and the target electrons, our rejection of some contribution to the 'close' channel inevitably reduces the effective charge. The calculation defines some effective new ion form function and is therefore not tied up with a special target model.

Light ions — at least up to $_5$B — are best fitted by the original model without dead sphere, even if some electrons are bound. Obviously, the expulsion of target electrons from the ion core needs a minimum interior electronic density to become effective.

(3) **Susceptibilities of target p and d subshells.** Height and location of the stopping maximum of *light* ions are dominated by the contribution of the free target electrons, the maximum of *heavy* ions more by the next inner, usually 2p and 3d, shells (fig. 1 vs. fig. 3, for example). We therefore checked another prospective reason for a new treatment of p and d subshells to explain the different success of the previous light and heavy ion computations.
The Kaneko theory assumes a Gaussian momentum distribution of the electron ground state of target shells as a starting point. This kind of wave packets was derived from thermodynamics without reference to an atomic theory. If we look at Fourier representations of free-atom Roothaan–Hartree–Fock electronic densities [6], and average over the directions of the momentum, this ansatz is confirmed for s shells, but a multiplication of the Gaussian with powers of the momentum is superior for shells with non-zero angular momentum quantum number. We recalculated the susceptibilities of these generalized ground states within the random phase approximation, but the change of the stopping powers turned out to be small (fig. 3).

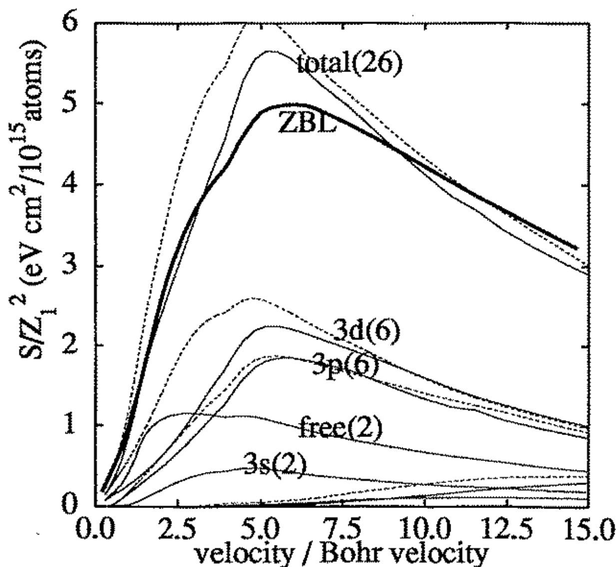

Figure 3: Total and per shell $_{15}P$ stopping cross sections in $_{26}Fe$. Bold line: ZBL [2]. Dotted: Kaneko theory with the plain Gaussian form of the electron wave packets in the ground state of Fe shells. Thin solid lines: Theory with the modified susceptibilities of the $2p^6$, $3p^6$ and $3d^6$ Fe shells. All non-ZBL results used a dead sphere radius of 1.1 times the ZBL ion size parameter, and cut energies for Fe shells.

The representation of d bands of solid transition metal targets by free-atom d orbitals, however, is questionable. Our (with respect to the angular momentum quantum number of the target shell) non-degenerated new formulas are therefore thought not advisable, and a better tuning is desirable in these cases.
(4) **Mutual (anti)screening and interaction of target shells.** The Kaneko theory sums up the polarization charges of all target shells independently. One artifact of this procedure is, for example, the overcompensation of the ion charge by the total polarization charge. We have tested an improved version of the theory, where the target polarization is not solely invoked by the field of the passing ion, but by the total field of the ion plus the remaining shells. It means building the target dielectric function by one plus the sum of all shell susceptibilities, and is equivalent to switching on a (Hartree) interaction between the polarization charges of different target shells. The overall change of stopping powers is modest, except for the extinction of the contribution of free-electron plasmons in transition metals — the concurrence and overlay of their excitation spectra with the damped excitations of the 3d shell makes them effectively decay into 3d single-particle excitations.

The Kaneko theory provides a computation of electronic stopping powers in random targets which is parameter-free with respect to the target. Our most essential contribution to the

dielectric theory was the installation of a polarization-free sphere around the nuclei of partially stripped ions to explain the systematic overestimation of the stopping power of heavy ions as a function of atomic number.

This work is supported by the Bundesministerium für Forschung und Technologie under Grant No. 211-5291-03-HE3ROS.

References

[1] B.S. Yarlagadda, J.E. Robinson and W. Brandt, Phys. Rev. B 17 (1978) 3473; W. Brandt and M. Kitagawa, *ibid.* 25 (1982) 5631; F. Schulz and W. Brandt, *ibid.* 26 (1982) 4864.

[2] J.F. Ziegler, J.P. Biersack and U. Littmark, Vol. 1 of *The Stopping and Range of Ions in Solids*, (Pergamon, New York, 1985).

[3] T. Kaneko, Phys. Rev. A 40 (1989) 2188; phys. stat. sol. (b) 156 (1989) 49; Nucl. Instrum. Methods B 48 (1990) 83; At. Data Nucl. Data Tables 53 (1993) 271; Nucl. Instrum. Methods B 90 (1994) 58; T. Kaneko and H. Tsuchida, J. Phys. B 27 (1994) 97.

[4] J. Lindhard, Dan. Mat. Fys. Medd. 28 (8) (1954) 1; J. Lindhard and A. Winther, Mat. Fys. Medd. Dan. Vid. Selsk. 34 (4) (1964) 1; J. Berger and S.G. Eckstein, Phys. Rev. B 26 (1982) 4305.

[5] R.J. Mathar and M. Posselt, Phys. Rev. B 51 (1995) 107; in *Arbeitstreffen des Verbundes "Festkörperphysik und Materialforschung mit nuklearen Methoden"*, Braunschweig, 4 – 6 Oct. 1994 and to be published in Phys. Rev. B.

[6] E. Clementi and C. Roetti, At. Data Nucl. Data Tables 14 (1974) 177; A.D. McLean and R.S. McLean, *ibid.* 26 (1981) 197; J.M. Garcia de la Vega and B. Miguel, *ibid.* 54 (1993) 1; 58 (1994) 307.

Point Defect-Based Modeling of Diffusion and Electrical Activation of Ion Implanted Boron in Crystalline Silicon

H. U. Jäger

The formation of very shallow p-type regions in silicon is becoming a problem in present-day microelectronics. The boron penetration depth and electrical activation found after ion implantation and subsequent annealing depend strongly on the specific process conditions. This applies, in particular, to the low-temperature annealing of non-amorphizing boron implants which has been considered in these investigations [1].

A system of diffusion-reaction equations is solved to model the depth profiles of boron atoms in interstitial (B_i) and substitutional (B_s) positions as well as the distributions of silicon self-interstitials I and vacancies V. The boron-containing diffusing species are assumed to be point defect impurity pairs (B_sI), (B_sV). To simulate electrical activation, we adopt the idea [2] that interactions between a substitutionally dissolved boron atom B_s and a self-interstitial I may lead either to the formation of a diffusing pair (B_sI) ("modified interstitialcy mechanism") or to the kick-out of the boron atom onto an interstitial site. The isolated boron interstitial B_i is considered, however, to be inactive and immobile, and the reactions

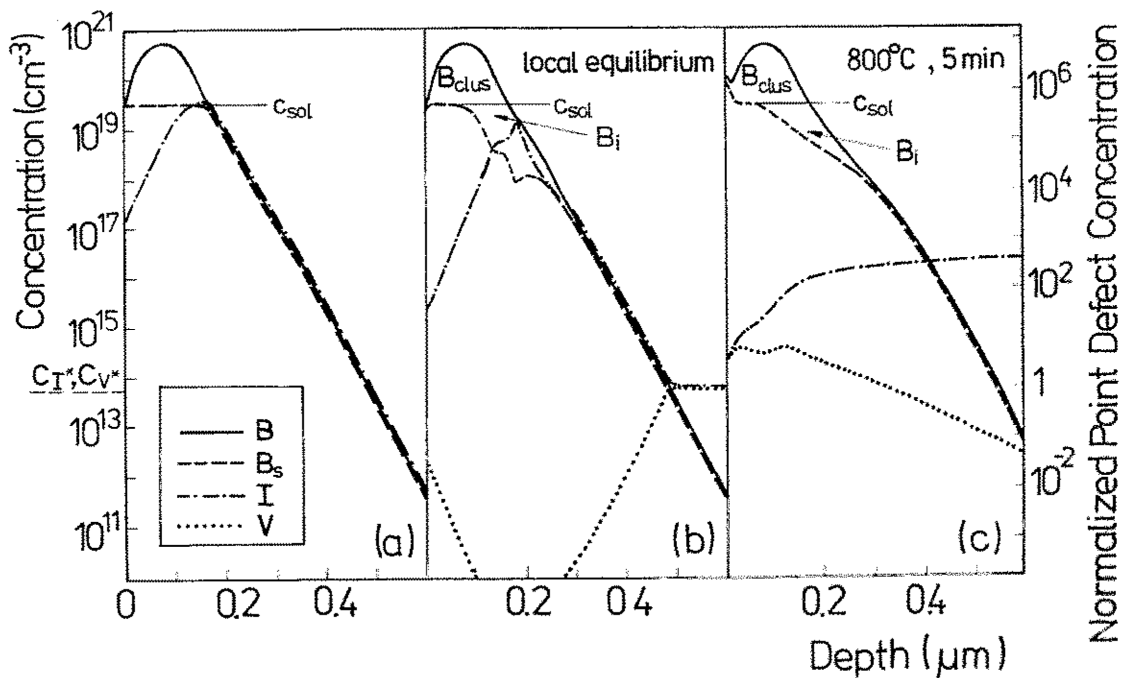

Fig. 1: Illustration of the model components and of the predicted relations between boron profiles (left-hand scale) and point defect profiles (left- and right-hand scales) for an 800°C, 5min annealing after 20keV, $5\times10^{15}cm^{-2}$ B ion implantation. The total (B) and electrically active (B_s) concentrations of boron are given explicitly. The difference between these two concentrations is assumed to consist of a completely clustered boron fraction B_{clus} above the solubility limit c_{sol} and of boron atoms B_i on interstitial sites. (a) The profiles used to determine the initial conditions. (b) The initial conditions defined by local equilibrium between the reacting species B_s, B_i, I, and V. (c) The effect of annealing.

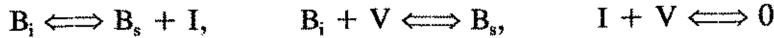

$$B_i \Longleftrightarrow B_s + I, \qquad B_i + V \Longleftrightarrow B_s, \qquad I + V \Longleftrightarrow 0$$

are used to model incomplete boron activation in the presence of implantation-induced, non-equilibrium point defect distributions. This concept is new. It is used instead of the idea of dynamic clustering in foregoing investigations [3,4]. Our approach allows to explain the different time periods observed at temperatures of about 800°C for transient enhanced diffusion (~30min) and for electrical activation (~10h). In addition, it provides a possibility to combine a nonequilibrium activation model with a diffusion model characterized by pair formation under equilibrium conditions.

In the case of low-dose boron ion implantation, when the boron peak concentration does not exceed the solubility limit c_{sol}, we start from an interstitial excess distribution of Gaussian shape with one interstitial per implanted boron atom ("+1 approximation"). For higher boron doses, the area density of this interstitial distribution is assumed to be constant, but the depth position of its peak depends on boron dose (Fig. 1a). Local equilibrium (Fig. 1b) for the reactions between the point defects and the boron species is postulated to be realized before the onset of diffusion (Fig. 1c). According to our investigations, the outdiffusion of implantation-induced self-interstitials and the reaction $B_i \Rightarrow B_s + I$ prove to be the leading mechanisms for boron activation.

The calculations have been performed using the module for point defect-based diffusion of the process simulator TESIM [5]. The computed boron depth profiles have been compared with data from the literature. Implantation doses from $2 \times 10^{14} cm^{-2}$ up to $5 \times 10^{15} cm^{-2}$ have been analyzed, annealing temperatures and times have been considered over the ranges 700 - 1000°C and 10s - 8h, respectively. Though our approach is charaterized by a number of simple assumptions, essential deficiencies are only found in certain cases of annealing subsequent to high-dose boron implantation. Trapping of free interstitials by extended defects seems to become important at low temperatures (~800°C) and for annealing times of several

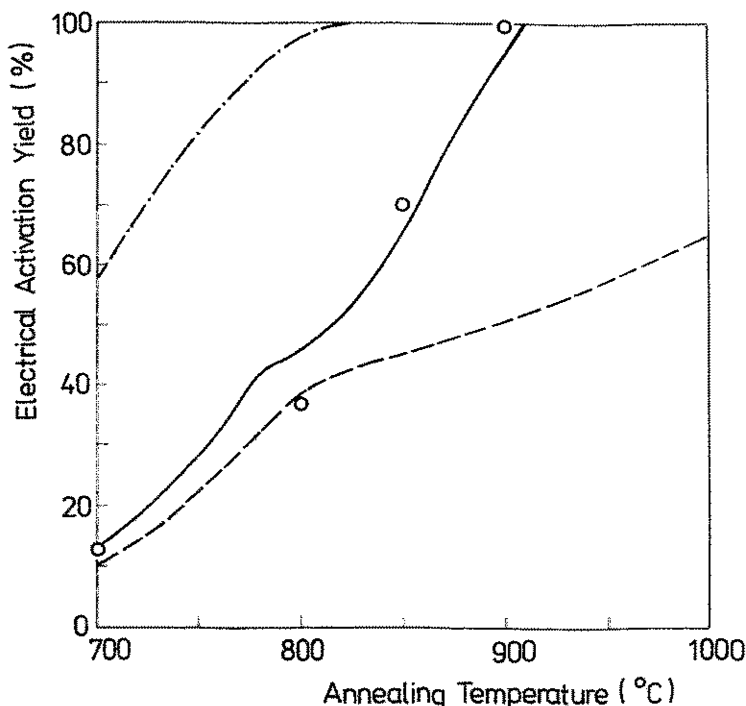

Fig. 2: Electrical activation versus temperature for 30-min annealings of samples implanted with 50 keV, B ions to a fluence of $5 \times 10^{14} cm^{-2}$. The model predictions (solid line) are compared to data [6] (circles) from sheet resistivity and Hall measurements in Van der Pauw devices. There are also given the initial activation assumed (dashed line) and the results in the case of complete activation of the as-implanted boron concentrations up to the solubility limit (dashed-dotted line).

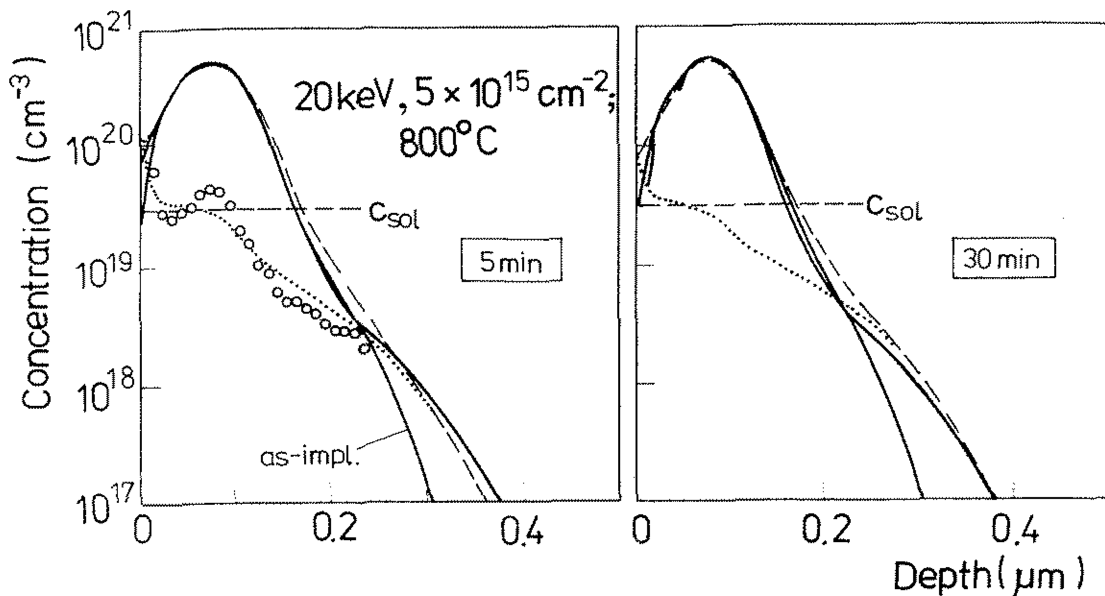

Fig. 3: Depth profiles in silicon samples implanted with 20keV boron ions to a dose of $5x10^{15}cm^{-2}$ and annealed at 800°C. The boron atomic (dashed lines) and electrical (dotted lines) profiles simulated are compared to experimental profiles [7] which were measured using SIMS (solid lines) or anodic stripping followed by incremental sheet resistivity and Hall measurements (circles). The as-implanted distribution (SIMS) is reported as a reference in each part of the figure.

hours. If the depth region with maximum boron concentration is in its as-implanted state close to amorphization, a boron overactivation which is beyond the present model can be found. For all other cases it is possible to achieve a reasonable modeling of electrical activation (Figs. 2, 3) and of transient enhanced diffusion (Fig. 3).

Acknowledgements
This work was supported in part by the Bundesministerium für Forschung und Technologie under Grant No. 211-5291-03-HE3ROS. Thanks are also due to the Fraunhofer-Institut für Mikroelektronische Schaltungen und Systeme Dresden for the possibility to work in this institute as guest scientist.

References

[1] H. U. Jäger, submitted to J. Appl. Phys.
[2] P. M. Fahey, P. B. Griffin, and J. D. Plummer, Rev. Mod. Phys. 61 (1989) 289
[3] N. E. B. Cowern, H. F. F. Jos, K. T. F. Janssen, and A. J. H. Wachters, Mat. Res. Soc. Symp. Proc. 163 (1990) 605
[4] M. Hane and H. Matsumoto, IEEE Trans. Electron Devices 40 (1993) 1215
[5] TESIM4, Fraunhofer-Institut für Mikroelektronische Schaltungen und Systeme, Institutsteil Dresden
[6] J. P. de Souza and H. Boudinov, J. Appl. Phys. 74 (1993) 6599
[7] S. Solmi, F. Baruffaldi, and R. Canteri, J. Appl. Phys. 69 , 2135 (1991)

W. Jiang
R. Grötzschel

Stopping cross sections and charge exchange of channelled MeV heavy ions

The remotely controlled two-axis goniometer was completed, installed and tested. The obtained reproducibility of the angular settings was measured to < 0.02° for both axes,sufficient for MeV ion channelling. A fast electrostatic beam deflection system for beam monitoring was completed. The electrostatic analyser (r=2 m / 30°), delivered by DANFYSIK, was installed and tested. The software for the CAMAC data acquisition and goniometer control was finished and used succesfully in a preliminary experiment. The first results indicate that the stress causes a bending of the 1 μm thick monocrystalline Si films, which demands beam spot diameters of < 100 μm for channeling.

supported by SMWK

K.-H. Heinig
M. Jentschel
*V. Konoplev**
*H. Börner***

Development of a nuclear method for the measurement of interatomic potentials

A joint research program with the ILL Grenoble has been established in order to develop the Crystal-GRID (Gamma Ray Induced Doppler broadening) method. On the basis of theoretical studies we predict the possibility to measure interatomic potentials in solids in the 100 eV region. For this aim ~10^4 trajectories of γ-ray induced recoils were calculated by the molecular dynamics method. Then, on the basis of the resulting field of recoil velocities $\mathbf{v}_i(t)$, theoretical spectra of Doppler broadened γ-lineshapes are calculated. Such simulations have been carried out for different single crystals like Si, Ti, TiO_2, and PbS. Moreover, the theoretical studies predict the possibility of more accurate measuring of lifetimes of nuclear states in the femtosecond range. Proposals for experiments at the Grenoble reactor, relying on the theoretical predictions, have been accepted for experiments in 1995.

supported by Saxonian Government

Collaboration: Institute of Electronics, Tashkent (Uzbekistan)*; ILL Grenoble (France)**

K.-H. Heinig
M. Jentschel
H. Kissener
*V. Konoplev**
*W. Wesch***
*H. Börner****

Theoretical prediction of a new method to determine lattice lokations of impurities in a crystal

Comprehensive computer simulations demonstrated the feasibility of Crystal-GRID (Gamma Ray Induced Doppler broadening) for the determination of lattice locations of impurities in crystals. Substantial differences in the Doppler broadened shapes of γ-lines from impurities occur if the impurities occupy different sites in the host lattice. These differences are sufficient to decide experimentally, which (of the theoretically predicted) lattice site is occupied by an impurity. This new possibilities to measure impurity locations have resulted in an approved proposal for experiments at the ILL Grenoble reactor. In order to facilitate the search of isotopes appropriate for the use as impurities in Crystal-GRID experiments, a catalouge of cross sections for the capture of thermal neutrons, γ-transition energies and probabilities etc. has been prepared by using the data base of the Brookhaven National Laboratory.

supported by BMFT

Collaboration: Institute of Electronics, Tashkent (Uzbekistan)*; FS University Jena (Germany)**; ILL Grenoble (France)***

K.-H. Heinig
*D. Stock**
*V.A. Zinovjev***
*A.V. Dvurechenskii***

Ion-induced surface damage and its thermal annealing - Molecular Dynamics (MD) simulations and studies using reaction-diffusion (RD) equations

Comprehensive MD simulations on the 225 eV Xe ion-induced damage of Si(001)-(2x1) surfaces were carried out in order to improve the understanding of the fundamental processes involved. Long-time runs (a few tens of nanoseconds) show how the surface crater anneals. 1 μs after the impact a monolayer deep depression as well as some adatoms paired to dimers and arranged in a row is observed. This result is in agreement with recently published STM studies. Using many impact points and directions, the statistics were improved and give more reliable input data for studies with RD equations. The sputter kinetics described by RD equations are also in good agreement with experimental results.

supported by BMFT

Collaboration: AT&T Bell Laboratories (USA)*; Institute of Semiconductor Physics, Novosibirsk (Russia)**

H. U. Jäger

Ion implanted boron in silicon - modeling of multiple implant/-anneal steps

For B implants in Si (E≈30keV), fluences above $1.5x10^{14}cm^{-2}$ lead to dislocation formation during a subsequent 900°C anneal. The boron peak concentration of $1x10^{19}cm^{-3}$ reached for this threshold dose is well below the solubility limit $c_{sol}≈6x10^{19}cm^{-3}$. Multiple implant/anneal steps provide a possibility to realize boron doping up to the solubility limit while still avoiding dislocation formation. Using our model for transient enhanced diffusion and electrical activation of ion implanted boron in silicon, we have simulated the total and electrically active boron profiles measured by Liefting *et al.* after a six-step implant/anneal cycle. The results confirm the applicability of the model to such complicated process sequences.

supported by BMFT

*Q.K.K. Liu**
*J.P. Biersack**
M. Posselt

Comparison of channeling trajectories and ranges calculated by the continuum potential approximation and Crystal-TRIM

The continuum potential approximation can be useful in investigations of such problems as electronic stopping in channels and total channeling ranges of ions, since about one order of magnitude in CPU time can be gained in comparison to binary collision simulations. In order to test the validity of the continum potential approximation, 300 keV proton implantation into the <110> channeling direction of the silicon crystal was studied. The obtained range profiles and some selected trajectories were compared with results of the Crystal-TRIM code which is based on the binary collision approximation. The agreement is excellent overall.

Collaboration: Hahn-Meitner-Institut, Berlin (Germany)*

R. Mathar
M. Posselt

Electronic stopping of heavy ions in the Kaneko theory

The Kaneko dielectric model of targets presents an improved foundation of the familiar effective charge theory of heavy ion electronic stopping. It establishes susceptibilities of the chemical shells of the target atoms, and finally should offer the possibility to calculate heavy ion stopping powers without scaling of experimental proton stopping powers. We focused on several refinements to achieve this aim; the most important was the removal of the target polarization around the ion nucleus inside a sphere which must be of the size of the (velocity dependent) ion radius. This model may be interpreted as a local blocking of target electrons by the electrons bound to the ion, and leads to an important reduction of heavy ion stopping powers.

supported by BMFT

M. Posselt

Dynamic simulation of damage accumulation during implantation of BF_2^+ molecular ions into crystalline silicon

The binary collision code Crystal-TRIM was extended in order to include the simulation of the damage buildup during BF_2^+ implantation. It was assumed that BF_2^+ ions dissociate upon entry into the target. BF_2^+ implantations can be therefore simulated by a sequence of triple implantations of one boron and two fluorine pseudoprojectiles each of which corresponds to a certain dose increment. The creation of radiation damage by boron and fluorine projectiles is described by statistical accumulation of local amorphous regions. The method was applied to 35 and 65 keV BF_2^+ implantations into (100)-Si at doses between 10^{13} and 10^{16} cm^{-2}. The comparison with recently published experimental data on the dose dependence of the shape of boron and fluorine depth distributions showed a good agreement, both for channeling and tilt-angle implantations.

supported by BMFT

Collaboration: Institut für integrierte Systeme der ETH Zürich (Switzerland), IBM Semiconductor R & D Center East Fishkill (USA)

Group of 21 authors, amongst them M. Posselt

Round Robin computer simulation of ion transmission through crystalline layers

Round Robin computer simulations were performed by 11 groups from all over the world using 6 different Molecular Dynamics (MD) codes and 6 different Binary Collision Approximation (BCA) codes. The process simulated is the transmission of 0.2 keV, 0.5 keV, and 1.0 keV B atoms through 9 monolayers of (100)-Si and the transmission of 1.0 keV Ar atoms through 5 monolayers of (100)-Cu. In all cases the energy distribution and the angular distribution of the transmitted atoms have been calculated with and without taking into account the interaction between the target atoms. The results of the simulations with the different MD codes agree with each other within the statistical error. The BCA results are compared with each other and with MD data. Deviations are discussed. It is concluded that the binary collision concept is still applicable for such low energies if simultaneous collisions are taken into account.

Collaboration: 11 computer simulation groups from all over the world. The project was coordinated by K. Gärtner, Institut für Festkörperphysik, FSU Jena (Germany)

Ch. Neelmeijer
W. Wagner
I. Sandner
I. Rietschel
*H.-P. Schramm**

External PIXE-RBS analysis of historical paintings

The external PIXE facility at the 5 MV tandem accelerator was completed by on-air RBS. The oil paintings "14 Nothelfer" (1), "Christus als Schmerzensmann" (1) and "Christus und Maria Magdalena" (2) of Lucas Cranach the elder were studied at various incident proton energies. Whereas the early works (1) show clearly arranged pigment layer structures, e.g. varnish on vermilion on white lead (one of the red colours), the later work (2) is characterised by pigment admixtures. Details of underdrawings and the white lead pattern were imaged by means of areal Infrared- and X-ray photography. The substantial examinations took place in correlation with art science. Coloured wood-engravings in G. Agricola's scientific book "De re metallica" were identified to consist of historical pigment material. The presence of organic dyestuff on the pigment basis layer was found by RBS.

supported by BMFT

Collaboration: Hochschule für Bildende Künste, Dresden (*)

U. Kreissig
S. Grigull
*R. Behrisch**
R. Grötzschel
*M. Harz***

Light element profiles in plasma-exposed surfaces by ERDA

The depth profiles of hydrogen isotopes and the light elements in plasma-exposed samples from the JET in Culham were measured by Heavy Ion ERDA using 30 MeV Cl ions. A new computer code was developed to obtain the relative amounts and the depth distributions of hydrogen isotopes and light elements in the near-surface region of the samples. The H and D concentrations are typically of the order of a few at %. Be and O concentrations of the order of 20 at % are measured on C samples, and similar concentrations of C and O are measured on Be samples within a layer of 100nm.

The ERDA technique was also applied to analyse several carbon and nitrogen based hard coating layers, as e.g. Ti_xN_y, C_xN_y and a-C:H, formed by plasma-assisted deposition methods. Most of the hard coatings contain significant amounts of hydrogen and oxygen, which strongly influence the mechanical properties.

Collaboration: IPP Garching (*), Institut für Festkörper- und Werkstofforschung Dresden, Technische Universität Chemnitz-Zwickau, Technische Universität Dresden (**)

D. Grambole
F. Herrmann

Trace element analysis by means of microbeam PIXE

The nuclear microprobe at the 5 MeV tandem accelerator was used to measure by PIXE the lateral element concentration in small crystals of pyrites and granites and in femoral cross sections of medieval human bones. The absolute element concentrations were calculated by the GUPIX programme.

Collaboration: HMI Berlin, Technische Universität Bergakademie Freiberg, Institut für Anthropologie der Universität Göttingen

D. Grambole
F. Herrmann

Hydrogen depth profiling by the ^{15}N resonance reaction method

The hydrogen concentration was measured using the 6.385 MeV resonance of the nuclear reaction $^{1}H(^{15}N,\alpha\gamma)^{12}C$ up to several micrometers depth in following materials:
TiC layers (vacuum arc deposition in CH_4 atmosphere on Ti) and a-C:H layers (sputtering deposition).
In larger depths, i. e. at higher incidence energy, the γ-ray yield of hydrogen was corrected by subtraction of that one of the carbon matrix.

Collaboration: Technische Universität Chemnitz-Zwickau, Universität Frankfurt/M., FHG Braunschweig

M. Friedrich
G. Sun

Accelerator mass spectrometry (AMS)

The activities for detection of 14-C by AMS were stopped at the end of 1994 and have been concentrated on the detection of 3-H. The installation of a special injection beam line and of a detection system for simultaneous measurement of the isotopes 1-H, 2-H and 3-H at the 3 MV Tandetron has been started.

supported by BMFT

Ion Beam Surface Modification

H. Reuther

High dose implantation of Si into iron studied by Mössbauer and Auger electron spectroscopy

Iron samples were implanted with high doses of Si at different energies ($2x10^{17}$ -$1x10^{18}$ cm^{-2}, 100, 200, and 300 keV). The resulting phases were determined by conversion electron Mössbauer spectroscopy (CEMS), the depth profiles were measured by Auger electron spectroscopy (AES). Depending on dose and energy a doping of nearly 50 at.-% Si could be reached. The high Si content seems to be responsible for the formation of the non-magnetic FeSi phase. This phase disappeared after annealing the samples at temperatures above 500 °C.

supported by DFG

R. Günzel
H. Reuther

Structural study of iron treated by plasma source ion implantation(PSII)

Iron samples were treated by PSII with 35 keV N_2^+ ions with doses between $1x10^{17}$ and $2x10^{17}$ cm^{-2}. AES depth profiles showed that besides nitrogen oxygen was also introduced into the samples. Phase analysis performed by CEMS proved that ϵ-Fe_2N, but no γ'-Fe_4N was formed.

Th. Chudoba
E. Wieser

Modification of microhardness and wear behaviour of light metals by high dose and high energy ion implantation

Implantation of O^+, C^+ and Ti^+ into Mg and Al with energies between 100 and 300 keV results in an increase of the microhardness near the surface ($\sim$0.1 - 0.2 μm) between 2.5 and 3.5 compared with a non-implanted sample. The effect of Ti is smaller than for O and C. The hardness improvement by oxygen implantation increases with increasing dose until the stoichiometric composition of the oxide is approached. By high energy implantation (1 - 2 MeV) deeper and broader regions of improved hardness are obtained. This results in a lower penetration depth of the indenter for a given load compared to the implantations at 100 to 300 keV. Wear tests using the pin on disc method are difficult for the soft materials Al and Mg because strong cladding occurs. However, using alcohol as lubricant for implantation of oxygen in Al at 200 keV (10^{18} cm^{-2}) a decrease of the cross section of the wear track by a factor 10 has been observed.

S. Reiß
K.-H. Heinig
*L. Maximov**
*A.I. Ryazanov**
*A.E. Volkov**

Modification of materials using high dose ion irradiation

Starting from computer experiments of precipitate nucleation and growth during ion implantation as well as subsequent Ostwald ripening, both processes were described by analytical theories. The general equations for the in-beam precipitate nucleation kinetics were formulated. Special attention was paid to define the dependence of the kinetic coefficients on microscopic parameters of the material. The self-organization process of a finite ensemble of precipitates, which we found recently, was also analysed. The period of the space modulation of the precipitate density is proportional to the diffusional screening length of the precipitate ensemble.

supported by BMFT

Collaboration: I.V. Kurchatov Atomic Energy Institute, Moscow (Russia)*

S. Reiß
K.-H. Heinig
*M.-O. Ruault**
*H. Bernas**
*J. Clayton**
*O. Kaïtasov**

Nucleation, growth and Ostwald ripening of $CoSi_2$ precipitates during Co ion implantation in Si

Experimental in-beam studies of nucleation, growth and Ostwald ripening were compared with computer simulations. A model was developed which describes these processes simultaneously within a mean field approximation. We find a good agreement in the evolution of the precipitate density, whereas the differences between the measured and calculated particle radius distributions are considerable. The comparison reveals that initially the evolution of the ensemble of $CoSi_2$ precipitates is mainly controlled by nucleation and growth. Ostwald ripening becomes important when a certain precipitate density has been built up.

supported by PROCOPE

Collaboration: CNRS Orsay (France)*

J. Teichert
L. Bischoff
E. Hesse
W. Skorupa
D. Panknin

Ion Beam Synthesis of $CoSi_2$ microstructures by writing FIB implantation

The maskless writing ion implantation with the focused ion beam (FIB) as an alternative method for ion beam synthesis of cobalt disilicide microstructures was demonstrated. The implantation was performed with 35 keV Co^+ and 60 keV Co^{++} ions into 400°C heated Si substrates at doses of about 10^{17} cm^{-2}. A subsequent two step annealing (600°C, 1h and 1000°C, 0.5h in N_2) led to a resistivity below 20 μΩcm. With the improved resolution of the IMSA-100 FIB a test gate structure, e.g. useable for a permeable base transistor was 'written', with a smallest feature size of 200 nm.

supported by BMFT

R.Kögler
W.Skorupa
D.Panknin
W. Matz
M. Betzl
F.Eichhorn
F.Prokert

Proximity gettering in Si by high energy implanted isovalent impurities

Isovalent impurities as C, Si and Ge were implanted into Si with ion energies in the MeV range. The measurement of reverse current of a diode reveale that the damage introduced by the high energy implantation can be used as a gettering centre for metallic impurities if the annealing temperature is sufficiently high. Metallic impurity gettering proceeds in C implanted layers in a depth position at the projected range (RP), whereas in Ge implanted layers the gettering occurs in a well defined depth layer between the surface and RP where no structural defects can be observed. Around RP a distinct band of dislocations was found which contains obviously no gettering sites.

The double-crystal X-ray instrument was used for high resolution diffraction studies on silicon single crystals. The lattice strain induced by the implantation of Ge and C was detected through the changes in lattice plane distances. By rapid thermal annealing the value of ($\Delta d/d$) is reduced from $3x10^{-3}$ to $2x10^{-5}$.

supported by BMFT

N. Hatzopoulos
D. Panknin
W. Skorupa
*D. Siapkas**
H. Hosack[+]

Structural, optical and electrical characterisation of double SIMOX structures formed by sequential high energy oxygen implantation into silicon

Separation by Implantation of Oxygen (SIMOX) technology at high (MeV) energies was used in order to form novel $Si/SiO_2/Si/SiO_2/Si$ structures which could potentially be used as Si based optical waveguides and phase modulators. Samples with such structure were realised by the successive implantation into Si of 9 and 3.8 MeV O^+ ions, followed by high temperature annealing at 1300°C for 12 hours. The structural properties of these samples are revealed by 1.4 MeV H^+ RBS/Channelling in combination with XTEM investigations, while the optical and electrical characterisation is carried out by FTIR reflection spectroscopy and Spreading Resistance profiling, respectively. The dose used for the implantation ($1x10^{18}$ O^+ cm^{-2}) was sufficient for the production of a continuous shallow (3.8 MeV) SiO_2 layer but not enough to form a continuous deep (9 MeV) SiO_2 layer. The Si crystalline quality is very high after annealing. All defects are to be found at the buried layers, in the form of pinned dislocations or twins. Both buried layers are of a resistive character, with the shallow layer having a rectangular resistance profile while the deep one exhibits a broad distribution. The optical measurements showed the buried layers are of rectangular shape with the shallow layer having a higher SiO_2 content than the deep layer.

Collaboration: University of Thessaloniki, Greece*; Texas Instruments, USA[+]

T. Henkel
V. Heera
R. Kögler
W. Skorupa

Ion beam induced interfacial amorphization (IBIIA) in silicon below room temperature (RT)

The temperature dependence of IBIIA in silicon has been investigated at temperatures between 80 K and RT. A low temperature regime of the interfacial amorphization was found below 300 K, where the IBIIA rate is nearly temperature independent. Above this transition temperature IBIIA depends on temperature with an activation energy of about 0.6 eV. A new interstitial diffusion model developed for the low temperature regime explains the dependence of the IBIIA rate on temperature and energy deposited into elastic collisions. According to this model an athermal diffusion of interstitials to the amorphous/-crystalline-interface, being induced by collision cascades, is suggested. The temperature dependence of the IBIIA rate in the high temperature regime can be explained by a radiation enhanced diffusion of point defects to the interface.

supported by DFG

H. J. Steffen
V. Heera
R. Kögler
W. Skorupa

Electron spectroscopy studies of SiC formation in C^+ ion implanted Si

Auger depth profiling and least-squares fitting of spectra revealed quantitatively the carbidic binding states of Si and C, as well as elemental Si in C^+ ion implanted amorphous Si. The Si LVV Auger line indicates the existence of Si binding states different from Si with 4 neighboring silicon and Si with 4 neighboring, tetrahedrally coordinated, carbon atoms. The C KVV spectrum suggests the existence of noncarbidic coordinations which might be carbon-carbon binding states. A subsequent high-energy Si^+ ion irradiation at 400 °C does not change the chemical states of the elements but an carbon enrichment within the implantation zone is observed and can be related to the ion-beam-induced epitaxial crystallization of the underlying Si. It was found that the depth dependent atomic density corresponds to the observed plasmon energies and amounts to the initial Si atom density raised by the embedded carbon.

Y. Pacaud
*A. Perez-Rodriguez**
G. Brauer⁺
W. Skorupa

Studies of damage induced by 200 keV Ge^+ ions implantation in 6H-SiC

Amorphized layers obtained for doses above $3x10^{14}$ cm^{-2} were investigated by Raman spectroscopy. Chemical disorder arises from the breaking of SiC bonds and the formation of SiSi and CC bonds, the amount of which increase with ion dose. Positron annihilation shows a considerable vacancy diffusion - up to 1μm deep for the high doses - in the material, TRIM calculation predicts a vacancy profile depth of 160 nm.

Collaboration: IBOS-Network 3 collaboration

*supported by *European HCM-project, +TUD WIP/-HEP-Programme*

H. Weishart
J. Schöneich
H. J. Steffen
W. Matz
F. Eichhorn
F. Prokert
W. Skorupa

Ion beam synthesis by tungsten implantation into 6H-SiC

In order to synthesize a conductive surface layer for metallization, 200 keV tungsten ions were implanted into 6H-SiC at room temperature. Subsequently, the samples were annealed in two steps at 500°C and 700°C or 950°C, respectively. The influence of dose and annealing temperature on the reaction of W with SiC was investigated by Rutherford Backscattering Spectrometry (RBS), X-Ray Diffraction (XRD) and Auger Electron Spectroscopy (AES). During implantation, sputtering becomes significant at a dose exceeding 1.0×10^{17} $W^{+}cm^{-2}$. Amorphous phases of tungsten carbide and silicide form already in the as-implanted samples. Hexagonal tungsten carbide crystallizes during annealing at 950°C; tungsten silicide, however, remains amorphous at this temperature. Hence, a mixture of polycrystalline tungsten carbide and amorphous tungsten silicide evolves under these conditions. The resistivity of 565 $\mu\Omega$cm at 1.0×10^{17} $W^{+}cm^{-2}$ is only one magnitude higher than the resistivity of the corresponding single crystalline materials.

R. Weber
W. Skorupa

Precipitation studies during Ion Beam Synthesis

The ripening of SiO_2 precipitates in oxygen implanted Si was investigated in dependence of the nucleation conditions. Oxygen was implanted into Cz-Si (100) at 200 keV to a fluence of 1×10^{17} $O^{+}cm^{-2}$. The substrate temperature varied from 200°C to 700°C. The annealing conditions (temperature of 1300°C for 2 hours in a nitrogen atmosphere), remained the same for all prepared samples. From Transmission Electron Microscopy, mean diameter, density, and volume concentration of the precipitates were obtained. Better statistics and a higher depth resolution can be achieved by Scanning Electron Microscope investigations of bevelled samples. For this kind of analysis, filtering, segmentation and reconstruction algorithms for an image processing system were established. Characteristic spatial information is extracted from the micrographs by applying correlation measurements. The influence of interstitials and strain on the precipitation process is roughly estimated by using a simple thermodynamical model for the growth and ripening stage.

supported by BMFT

L. Bischoff
K.-H. Heinig
J. Teichert
W. Skorupa

A new fabrication method for submicron $CoSi_2$ dots and wires using focused ion beam implantation and local melting by flash lamps

After implanting dots, stripes and other structures into Si(001) by means of a 35 keV Co^{+} microbeam of about 200 nm diameter at doses of 0.5, 1.0 and 3.0 x 10^{17} cm^{-2} flash lamp irradiation with millisecond pulses was successfully employed to form $CoSi_2$ microstructures with dimensions of about 100 nm and below. Promising applications of this new method are in the field of quantum devices.

V. Heera
R. Kögler
W. Skorupa
*J. Stoemenos**

Ion Beam Induced Crystallization of SiC - Kinetics and Morphology

As demonstrated by RBS/C and XTEM investigations, crystallization of amorphous SiC layers in single crystalline 6H-SiC was obtainedby means of ion beam irradiation at temperatures far below 1450°C, the threshold temperature for thermally stimulated solid phase epitaxy. Even at a temperature of 300°C an amorphous surface layer of 170 nm can be completely recrystallized. However, at such low temperatures ion beam enhanced spontaneous nucleation competes with ion beam induced epitaxial crystallization (IBIEC) and leads to a multilayer structure of crystalline and polycrystalline SiC. Due to this competition the IBIEC rate is a function of fluence. The formation of polycrystalline material can be avoided by applying temperatures above 1000°C, where IBIEC dominates, or by alternating low fluence IBIEC and post-amorphization of the remaining layer.

supported by DFG

Collaboration: Aristotele University of Thessaloniki, Greece (*)

Ion- and Plasma Assisted Deposition

D. Grambole
F. Herrmann

The new nuclear microprobe facility

The set-up of the nuclear microprobe at the tandetron accelerator was finished. The total length is about 6 m. The lens system is a quadrupole triplet by Danfysik and has a mass energy product of 45 MeV·amu, which enables the focussing of heavy ions. The samples are transferred via a lock to a five-axis-manipulator inside of a UHV scattering chamber and can be observed optically by means of a special long distance microscope with an optional CCTV camera and by SE imaging using a 10 kV electron microprobe.

supported by
BMFT, DFG,
SMWK

R. Küchler

Characterization of TiAlN and metal-carbon layers with surface acoustic waves

The change of the spreading velocity of ultrasonic surface waves by TiAlN and Me-C:H (metal-carbon layers) deposited on steel was measured by means of the sing around method. The residual stress in the layers was evaluated from the curvature of the bended sample. At known layer thickness and density, the influence of the residual stress in the TiAlN and Me-C:H coatings on the velocity (elastic modulus) was calculated using the nonlinear equations of motion. It has been found that a layer system can be characterized by an average Young's modulus, which was 332 GPa and 70 GPa for TiAlN and Me-C:H films, respectively.

supported by
DFG

A. Kolitsch

Implantation into a-C films

Hard amorphous carbon films prepared by neon ion beam assisted deposition on silicon wafers were investigated before and after modification by 20keV carbon ion beams of different fluences ranging from $1x10^{13}$ to $1x10^{18}$ carbon ions per cm^2. In the fluence range between $1x10^{15}$ and $1x10^{16}$ ions/cm^2, a steep increase of micro hardness and electrical resistivity is correlated with pronounced changes of the Raman signals (peak position, half widths and intensity ratio of graphite/disordered graphite peaks). All the observed effects can be explained by a shift of the bonding character to a higher sp^3 portion.

supported by
SMWK

A. Kolitsch
M. Plass
W. Fukarek

Synthesis of cubic Boron nitride by IBAD

First boron nitride films were deposited on Si substrates using an ion assisted process involving electron beam evaporation of B and simultaneous bombardment of the growing film by nitrogen and argon ions from a Kaufman source. The existence of the cubic phase within the layers was proven by IR reflection spectroscopy. A feature related to the TO reststrahlen band around 1100 cm^{-1} indicates the presence of c-BN. In addition, the films still contain non-cubic phase(s), as can be seen from the reflection peak around 1350 cm^{-1} corresponding to the in-plane stretching mode of h-BN.

supported by SMWK

A. Kolitsch
W. Matz

The preparation of AlN by IBAD

The deposition of aluminum nitride films by nitrogen ion assisted deposition was investigated in a wide range of low energies (200 to 1200eV) of the assisting nitrogen ions, at different deposition rates of the evaporated aluminum and in dependence on the resulting nitrogen/aluminum transport ratio at a fixed ion energy of 600eV. All prepared films are of good homogeneity and hardness. First investigations by X-ray diffraction show a very fine microcrystalline structure of hexagonal AlN for deposition using a high nitrogen ion current (N/Al transport ratio > 1), and additional reflections of metallic aluminum at nitrogen deficiency during the deposition (N/Al transport ratio $<< 1$). Surface investigations by atomic force microscopy (AFM) show very small crystallites of some nanometers to some ten nanometers size at all deposition conditions.

L. Bischoff
J. Teichert
E. Hesse
P. Schneider
*T. Geßner**
*B. Löbner**
*N. Zichner**

Application of the Focused Ion Beam for three dimensional structuring of micromechanical devices:

The Rossendorf Focused Ion Beam IMSA-100 was used for writing cobalt implantation across a topographical structured surface with a partly controlled focus. The experimentally determined depth of focus amounts to 28 μm. After a subsequent two step annealing, $CoSi_2$ - interconnection lines across a slope of about 300 μm were formed from the top to the bottom of an anisotropical etched groove in <100>-Si and analysed by SEM and electrical measurements. By using a dynamically controlled focus three-dimensional conducting features of high accuracy can be formed for applications in micromechanical devices.

supported by SMWK

Collaboration: Technische Universität Chemnitz-Zwickau (*)

M.T. Pham
S. Howitz
M. Bürger
U. Müller
T. Wegener

ISFET array with ion implantation fabricated silicate membranes

An array of ISFETs with aluminosilicate membranes (wCaO-xNa K_2O-yAl_2O_3-zSiO_2) of different sensitivities to H^+, Na^+, and K^+ was fabricated by ion implantation. The spectrum of signal responses obtained varies from approximately 10 to 50 mV per concentration decade. The sensor array including an Au microelectrode was packaged into a fluidic microcell made by a Si glass compound. An integrated ASIC version of the electronics is realized in collaboration with Zentrum für Mikroelektronik Dresden.

supported by SMWA

Collaboration: TU Dresden, Zentrum für Mikroelektronik Dresden

H. Seifarth
M. T. Pham
J. Hüller
D. Möller

Tantalum oxide films for ISFET-membranes

Tantalum pentoxide (Ta_2O_5) films were prepared by reactive RF-magnetron sputtering in an Ar/O_2 plasma (n= 2.0...2.15, $\varepsilon \approx 20$). Ta_2O_5 / thermal SiO_2 double layers on ISFET-equivalent EIS structures with stoichiometric Ta_2O_5 and an abrupt interface were fabricated. They exhibit a nearly ideal Nernstian behaviour with regard to the pH sensitivity and excellent long time stability. The implantation of Na (or K) and Al ions leads to a sensibilization of the membrane surface to alkali ions. In addition, Ta_2O_5, SiO_2 and Si_3N_4 were compared regarding their ability to act as entrapping matrix for the ion beam synthesis of silver halides and aluminosilicate membranes. The distribution of the implanted species and the ion sensitivity are found to depend appreciably on the oxygen content present in the matrix material. Si_3N_4 proves to be mostly favorable among them in view of achieving an implanted phase finely limited within a thin region.

M. T. Pham
J. Hüller
D.Möller

Ion beam synthesis of silver and arsenic sulfide into thin SiO_2-films

Ag_2S and AsS_2 embedded into a thin SiO_2 layer was fabricated synthetically by high dose ion implantation ($10^{16}...10^{17}cm^{-2}$) of the elemental species and subsequent annealing (RTA or furnace: 500 - 1000°C). As shown by AES and XPS investigations, the relative content of Ag_2S and AsS_2 in the SiO_2 matrix is below 10 %, which deviates considerably from that of commercially available bulk material (> 40%). Nevertheless, the ion sensing characteristics of the implanted membranes is comparable to that of bulk material. Preliminary results demonstrate the ability to couple the membranes to field effect microstructures. It is found, that the ion sensitivity can be adjusted by the implantation parameters.

supported by AIF

Collaboration: Institut Fresenius für Angewandte Festkörperanalytik Dresden

S. Howitz
M. Bürger
H. Fiehn
S. Steinbach
T. Vopel

The development of chemical micro analysis systems (FIM, μ-FIA)

The first prototype of an integrated **F**luidic- **ISFET**- **M**icrosystem (FIM) for the chemical analysis of electrolyte solutions has been realized. The modular designed FIM contains sensors (ISFET's, ion sensitive film electrodes), piezoelectrically driven micropumps, fluidic channels and signal processing components, which may be flexibly combined according to the measuring purpose. To enable a multiion analysis, the properties (slope, selectivity, adhesion etc.) of different casted PVC-based ion selective membranes for the determination of NO_3^-, NH_4^+, K^+ or Na^+ have been investigated. The problem of the mechanical fixation of the membranes on the transducer surface was solved by suitable designed spacer chips which are also used for coupling the sensors to the micro flow through cell. A Micro-**F**low-**I**njection-**A**nalysis (FIA)-system has been assembled.

supported by SMWA

Collaboration: FZR, Institut Medizintechnik GmbH Dresden

T. Wegener

Piezoelectrically driven fluid ejector

As a significant part of the actuatoric concept of the FIM system a fluid ejector based on a piezoelectric micropump has been developed and optimized for application in microanalytical systems. Its overall size is 10 mm x 15 mm. The micropump has been fabricated by an isotropic chemical etching of silicon and anodic bonding of the structured Si wafer with a Pyrex wafer. The displacement of the piezo ceramic leads to a decrease of the pump chamber volume. This causes the ejection of droplets in the range of 0.5 ...3.5 nl from the nozzle of the pump. The maximum pump yield is 100 µl/min (piezoactuator power supply: 60 V / 2 kHz).

Collaboration: TU Dresden

J. von Borany
J. Goerigk
W. Voitus
I. Beatus
U. Päprer

Fully ion implanted HP-Ge-detectors

Fully implanted planar HP-Ge- detectors were realized by boron and phosphorous ion implantation into high purity germanium (HP-Ge). Flash lamp annealing (t_p=20 ms) is performed to obtain complete electrical activation of the dopands and to avoid changes of the substrate net doping ($10^{10}cm^{-3}$) due to copper and hydrogen related acceptor states. HP-Ge-detectors up to 10 cm^3 volume with good detector performance for γ -spectroscopy (^{137}Cs - 662 keV, FWHM = 1,5 keV) both for n- and p-type material have been fabricated. Under full depletion conditions, dead layers below 1 μm are achieved on both detector sides. The development of pixel detectors for X-ray spectroscopy is beeing in progress as a first application of fully ion implanted planar HP-Ge-structures.

supported by BMFT

Collaboration: EURISYS MEASURES, Lingolsheim, France

B. Schmidt
G. Schnabel

Ultra thin membranes for ion beam experiments

Ultra thin free standing crystalline silicon and SiO_2-films in the thickness range ≤ 1μm have been prepared by standard semiconductor technology, in particular wet chemical selective and anisotropic etching of <100>-oriented silicon. The area was 1x1 up to 7x7 mm^2 and 1x1 mm^2 for c-Si and SiO_2, respectively. The disturbing rippening of the thin foils after etching and storage can be eliminated by a hydroflouridic acid dip which removes contamination and native oxid layers.The Si membranes are used and tested in channeling experiments and in scanning transmission ion microscopy. 100 nm free standing SiO_2 layers are used as matrices for in-situ TEM-investigations of ion beam synthesis.

Collaboration: FZR, University of Munich, University of Melbourne, CNRS Orsay

B. Schmidt,
J. von Borany

Monolithically integrated dE/dx-E-detector telescopes

High energy boron implantation has been used to realize $n^+np^+nn^+$-detector structures, which exhibit the combination of a transmission dE/dx-detector with a E-stop-detector. By B^+-MeV-implantation to form a buried pn-junction (E = 8 MeV, D = $5x10^{14}$ cm^{-2}, annealed at 900 °C for 30 min) a thin dE/dx detector of 10 μm thickness, vertically stacked on a 300 μm E-detector has been fabricated. The electrical contact to the buried p^+-layers was established applying anisotropic etching of 10 μm deep contact holes into <100>-oriented Si with a accuracy of the depth etching of (10.26 ± 0.07) μm.

J. von Borany
B. Schmidt

First test of high field region detectors for low energy heavy ion spectroscopy

Silicon p^+n-junction detectors with additionally MeV- implanted buried n^+-layers have been prepared to realize high field region detectors with internal electric field strength of $10 < F < 150$ kV/-cm. The detectors were tested with low energy heavy ions (1-10 MeV), leading to a significant enhancement of the pulse amplitude up to 25% for O^+- and Cl^+-ions compared to conventional silicon particle detectors. The signal enhancement for low energies is mainly determined by a field dependent reduction of the effective silicon dead layer window from 130 nm up to 35 nm between 12 kV/cm and 85 kV/cm, respectively. Above 100 kV/cm avalanche multiplication effects have been obtained.

S. Grigull
M. Harz
U. Kreissig
K. Lange
B. Schmidt

Ion drift behavior in borosilicate glasses during anodic bonding to silicon or metals

The electrical field induced drift of alkaline ions in the glass is a key mechanism in anodic bonding frequently employed in microsystem technology. Heavy Ion Elastic Recoil Detection (HIERD) has turned out to be the only reliable quantitative method for determining depth resolved alkali contents in technical glasses. Glass samples coated with thin Al-layers were treated by a drift process and analyzed ex-situ. Sodium ions in TEMPAX glass (Schott 8330) were found to start drifting already at a temperature of about 200°C. By applying a voltage of 400 V for 10 min at a temperature of about 225°C the glass was completely depleted of Na within a near surface layer of about 300 nm thickness. For identical drift parameters but a temperature of 300°C the depletion layer increases up to a thickness of about 1 µm. This result has to be considered in view to the typical applied bonding temperatures above 400°C. In addition, preliminary results were obtained for a Li-containing borosilicate glass, which was developed to meet the properties especially for anodic bonding at lower temperatures. Here, the alkali depletion starts at a temperature between 150°C and 250°C. At 250°C the thickness of the depletion layer amounts to about 500 nm.

supported by BMFT

Collaboration: TU Ilmenau

M.Harz

Thermally induced bend change of anodically bonded silicon and Pyrex wafers

Anodically bonded silicon and Pyrex-glass wafers bend after the bonding process due to different thermal expansion coefficients. For the first time it was found, that the bend of the wafer compound can be changed after bonding by annealing below the glass transition region. The change of the bend as a function of the annealing time and temperature has been observed *in situ* by means of optical trian-glometry. After annealing at temperatures of 390°C and 445°C for 24 hours the radius of curvature has changed from +6.73 m to -3.64 m and from +8.63m to -2.62 m, respectively. Furthermore, the *in-situ* experiment has shown, that a flat wafer compound can be rea-lized for suitable annealing parameters (390°C, 1h or 445°C, 15 min). The observed bending behaviour can be explained by the structural rela-xation of Pyrex glass.

Collaboration: TU Dresden

Structural Investigations

W. Matz
F. Prokert
M. Betzl
F. Eichhorn

Design of the FZR beam line at the ESRF (ROBL)

The conceptual design report for a bending magnet beam line at the ESRF with 3 experimental stations was prepared. The proposal was submitted to the ESRF and got its scientific approval.

Main activities for the design of the beam line optics and 2 experimental stations of the *RO*ssendorf *B*eam *L*ine (*ROBL*) were the estimations of physical demands and different technical solutions of mirrors and a monochromator set-up for synchrotron radiation. Energy resolution and intensity were calculated for different configurations also using the ray-tracing code SHADOW.

The design of a 6-circle goniometer the main equipment of the experimental station 2A was finished and a technical document prepared.

Collaboration: Institute of Radiochemistry of FZR; Central Department of Research and Information Technology of FZR; ESRF, Grenoble; University of Lausanne

M. Betzl
K. Walther
K. Ullemeyer
J. Heinitz

Texture investigations at the neutron time-of-flight diffractometer in Dubna

Neutron diffraction texture studies on fine and coarse grained quartzite were compared to electron back scattering data (by Adams, Pittsburgh). Differences in the ODF due to the inhomogeneity of the texture were explained by the integral character of neutron diffraction versus the grain-by-grain probing of electron back scattering.

In cooperation with the TU Chemnitz-Zwickau the structure of molten silver-tellur at the eutectic composition was investigated. For the first time we succeeded in the estimation of the short range order of $Ag_{49}Te_{51}$ between 470°C and 800°C.

The main activities were improvements of the texture machine. A new detector bank was designed (project SKAT) and the mechanical construction ordered. It will allow a drastic reduction of measuring time. The remote control was remade for a new data processing device on the base of a M68000 processor and OS/9 operating system.

A new 5-axis-goniometer for internal stress investigation was shipped to Dubna and equipped with electronics for remote control. In future texture and stress investigation will run simultaneously and independently by dividing the large neutron beam into two subbeams.

supported by BMFT

Collaboration: Joint Institute for Nuclear Research, Dubna; Universität Göttingen; RWTH Aachen; TU Clausthal-Zellerfeld; GeoForschungszentrum, Potsdam; TU Chemnitz-Zwickau; Institute of Physics of the Earth, Moscow

F. Eichhorn
A. Hempel

Test of a new double-crystal diffractometer and neutron small-angle scattering at hydrating cement

A new double-crystal diffractometer for small-angle scattering of thermal neutrons was installed at the BER-II reactor at the Hahn-Meitner-Institute Berlin. It main components are two perfect silicon crystals which can be bent to various radii down to a minimum radius of 10 m and a position sensitive detector. This enables the simultanous measurement of the whole small-angle scattering range without rotating the analyzer crystal step by step. The momentum transfer ranges between 10^{-4} nm^{-1} and $2x10^{-1}$ nm^{-1} with a variable but high resolution of $(0.1\text{-}5)x10^{-3}$ nm^{-1}. The instrument reached the design parameters and was tested by diffraction of neutrons on lithographic and holographic gratings.

Small-angle scattering experiments on hydrating cement pastes were performed to study the time dependence of the evolution of the microstructure during the hydration process. Measurements at 20, 30, 40, and 50°C show that already temperature differences of +10 degree significantly enlarge the speed of hydration. The final particle size reached after different times is independent on the temperature.

supported by BMFT

Collaboration: Hahn-Meitner-Institut, Berlin; Fraunhofer-Institut für zerstörungsfreie Prüfung, Saarbrücken/Dresden; Joint Institute for Nuclear Research, Dubna; Universität Osnabrück; Institute for Nuclear Physics, Řež

W. Matz
M. Betzl

X-ray diffraction phase analysis of powders

With the Institute of Radiochemistry an investigation of uranyl silicate $(UO_2)_2SiO_4x2H_2O$ was performed. A new preparation technique was developed there and among the different methods (XRD, IR, AAS, NMR, DTA) used for the characterisation of the synthesis products XRD was the most sensitive one concerning the phase purity. The determined crystal structure parameters agree satisfactory with the published data sets and are used also for the interpretation of EXAFS results.

For the WIP/HEP group the ideal density of the mixed crystals systems $Ba(Tb_xIn_{1-x})O_3$ and $Ba(Ce_xGd_{1-x})O_3$ was estimated from the lattice parameters. The materials are solid electrolytes and the density is essential for the assessment of ion conductivity.

For the VKTA investigations of the phase composition of sulfidic rocks and possible weathering products were performed. The results will help to understande the migration of waste substances in geological formations.

Collaboration: Institut für Radiochemie; TU Bergakademie Freiberg (WIP/HEP); Verein für Kernverfahrenstechnik und Analytik, Rossendorf

*M. Große**
F. Eichhorn

Small-angle scatterring on reactor pressure Vessel Steels

SANS and anomalous SAXS experiments were performed in order to characterize the initial state and the irradiation induced changes of precipitates in the reactor pressure vessel steel 15Kh2MFA used in VVER-440 reactors. The precipitates formed by irradiation were identified as vanadium rich particles. This supports the results of former positron annihilation experiments where vanadium carbide was assumed for the interpretation.

supported by BMFT

Collaboration: Institute of Safety Research of FZR (*); HASYLAB at DESY, Hamburg; Hahn-Meitner-Institut, Berlin

Ion Devices

M. Mäder
R. Grötzschel
W. Taubert
K. Brankoff

RBS and channeling investigations of thin layers

At the 2 MV van de Graaff accelerator the PDP-11 data acquisition and control system of the RBS/channelling facility was completely replaced by a PC based configuration.

The RBS was widely used for precise composition analyses of thin films of various silicides, TiN and ZrN, MoS_2 and others.

The crystalline structure of double layer structures of porous silicon and of CeO_2 on sapphire was investigated using channeling.

supported by SMWK

Collaboration: TU Chemnitz-Zwickau, IFW Dresden, BAM Berlin, IHP Novosibirsk, Universität München

H. Tyrroff
D. Henke
F. Nötzold
G. Franz
P. Hartmann
*G. Zschornack**
*R. Friedlein**
*S. Herpich**

ECR ion source (Joint project FZR - TUD)

A system for handling and retardation of highly charged ions from a 7.25 GHz source is put into operation. Current densities of about 5 $\mu A/cm^2$ at final energies of 500 eV are presently obtained. An experiment for crossing ion and electron beams is in preparation. Characteristic X-rays of Argon plasmas and Bremsstrahlung of the plasma electrons are used to determine plasma parameters like ion and electron density and the energy density distribution of the plasma electrons.

supported by BMFT, SMWK, VW-Stiftung

Collaboration: TU Dresden (*), Strahlenzentrum Universität Giessen, Universität Frankfurt

M. Friedrich
S. Turuc
W. Bürger

Operation and development of the electrostatic accelerators

The 2 MV VdG has been operated completely for ion beam analysis. After replacement of the titanium getter pumps by air-cooled turbomolecular pumps and new aligment of the beam line a stable accelerator operation has been obtained. Some troubles at the 5 MV tandem with the NMR device for the analysing magnets were solved. The 5 MV tandem has been applied for ion beam analysis, high energy implantation, surface modification, detector development and foil irradiation. The charging belt (Greengate) was changed after 14.000 hours. A 150 l/s turbomolecular pump has been installed inside the terminal and the pumping tube for the stripper gas has been removed. A leak at the stripper required some openings of the pressure tank.The 3 MV Tandetron required a lot of maintenance during the first time of operation. After the exchange of accelerating tubes in September 1994 a stable operation of 120 hours per week has been obtained for surface modification, high energy implantation and ion beam analysis. A stable beam for implantation was also realized at 150 kV terminal voltage.

E. Hesse
O.W.M. Stins
J. Teichert
L. Bischoff

Test of a retarding field energy analyser and measurement of the energy spread of liquid metal ion sources (LMIS) for gallium and lithium

A retarding field energy analyser has been successfully tested. By measuring the energy distribution of a thermoionic electron cathode a systematic spreading of ΔE_{FWHM} of 0.8 eV has been determined. This resolution is sufficient for the measurement of energy distributions of LMIS. The energy spread of a Ga-LMIS and a Li-LMIS have been measured depending on the ion current. The lowest E_{FWHM} values are 6.1 eV and 4.6 eV for the Ga-LMIS and the Li-LMIS, respectively. They were determined at the lowest investigated currents of 1.7 and 1.3 μA. With a chromatic angular intensity of 0.35 $\mu A/(sr(eV)^2)$ and 1.23 $\mu A/(sr(eV)^2)$ for the Ga-LMIS and the Li-LMIS, respectively, a significantly enhanced current density at the target of a FIB system is available for Li rather than Ga.

L. Bischoff
J. Teichert
G. Hofmann
W. Probst
E.Hesse

Improvement of the Focused Ion Beam Facility

The digital scan and image processing of the FIB facility system was supplemented by two high resolution scan amplifiers, which allow a scan field of 4096 x 4096 pixel with an increment of 50 nm at variable ion energies. Furthermore the semiconductor secondary elecron detector was replaced by a quadrant-anode microchannel plate for secondary electrons or ions. This system allows to process also topography or material contrast images.

The optimization of the ion optics led to a minimum spot size of a cobalt ion beam of about 100 nm with a current density of 8 A/cm^2.

J. Teichert
L. Bischoff
E. Hesse
*P.D. Prewett**
*J.G. Watson**

Development of an E x B mass separating system for the application of a focused ion beam for cluster beam deposition

An E x B double mass separator with Co-Sm permanent magnets was designed and fabricated according to the experiences with the IMSA-100. This system was implemented in the FIB 50 focused ion beam at the Rutherford Appleton Labs. The aim of this work is to study the cluster emission from a capillar type gallium liquid metal ion source and to use this technique for cluster deposition.

supported by DAAD
Collaboration: Rutherford Appleton Laboratories (*)

Publications

Barnitzke, W., Friedlein, R., Hentschel, R., Hiller, H., Schmidt-Böcking, H., Schneider, M., Stiebing, K., Streitz, H., Tyrroff, H., Wirth, H., Zippe, C., Zschornack, G.,
Status of the ECR ion source of the TU Dresden,
KVI Report 996 (1993) 249

Bischoff, L., Hesse, E., Panknin, D., Skorupa, W., Teichert, J.,
Writing implantation with a high current density focused ion beam,
Microelectronic Engineering 23 (1994) 115

Böhm, G., Günzel, R.,
50 k pulse generator for plasma source ion implantation,
J. Vac. Sc. and Technology B12 (1994) 821

Brauer, G., Eichhorn, F., Frisius, F., Kampmann, R.,
Investigation of neutron irradiated Soviet-type reactor pressure vessel steels by small angle neutron scattering,
Effects of Radiation on Materials: Proceedings of the 16th International Symposium (Aurora, CO, June 23-25, 1992), ASTM Publication 04-011750, Philadelphia, January 1994, p.503-515

Eichhorn, F., Häußler, F., Baumbach, H.,
Structural studies on hydrating cement pastes,
Journal de Physique IV, Colloque C 8, Suppl. J.Physique I, vol 3 (1993) 369-372

Einfeld, D., Büttig, H., Dienel, S., Gläser, W., Goetz, Th., Guratzsch, H., Hartmann, B., Janssen, D., Krug, H., Linnemann, J., Matz, W., Murphy, J.B., Neumann, W., Oehme, W., Picard, M., Plesko, M., Pröhl, D., Schlenk, R., Tomassini, D., Tyrroff, H.,
The synchrotron light source ROSY
Nucl. Instr. Meth. B 89 (1994) 74-78

Eremin, V., Ilyashenko, I., Strokan, N., Schmidt, B.,
Rekombination von Überschußladungsträgern in der Ionisationsspur schwerer Ionen in Si (in russisch),
Fisika i Tekhnika Poluprovodnikov Juni 1994

Eremin, V., Ivanov, A., Verbitskaya, E., Schmidt, B.,
Low temperature annealing of α-particle induced generation current in silicon pn-junction diodes,
J. Appl. Phys. 76 (7) (1994) 4072-4076

Eremin, V., Ivanov, A., Strokan, N., Verbitskaya, E., Schmidt, B., Li, Z.,
Relaxation of Radiation Damages in Silicon Planar Detectors,
Conf. Proceedings Vol. 46, "Large Scale Applications and Radiation Hardness of Semicon-ductor Detectors", Eds. A. Baldini and E. Focardi,
Società Italiana di Fisica, Bologna, 1994, pp. 181-190

Friedl, A., Fukarek, W., Möller, W., Koch, A.,
In situ characterization of plasma-deposited a-C:H thin films by spectroscopic infrared ellipsometry,
Rev. Sci. Instrum. 65 (1994) 2882

Friedlein, R., Herpich, S., Hiller, H., Tyrroff, H., Zschornack, G.,
Spektrometrie der Elektronenbremsstrahlung zur Bestimmung der Elektronenergieverteilungsfunktion im Plasma einer 7.25 GHz ECR-Ionenquelle, EAS-15, ISSN (1994) 0724-4975 Rietzlern

Friedrich, L., Huttel, E., Hentschel, R., H. Tyrroff, H.,
A 7.25 GHz ECR ion source with floating disk operation,
KVI Report 996 (1993) 19

Friedrich, M., Bürger, W., Grötzschel, R., Henke, D., Sun, G., Turuc, S., Hebert, D., Rothe, T., Stolz, W.,
Accelerator mass spectrometry at the Rossendorf tandem accelerators,
Nucl. Instr. Meth. B 92 (1994) 58

Gorski, N., Ostanevich, Y.M.,
Small-angle neutron scattering (SANS) determination of the volume occupied by a single molecule in the inverted micellar systems $AOT+X(H,D)_2O+C_{10}D_{22}$ by internal contrast variation technique,
Journ. de Physique IV (1993) 149-152

Gorski, N., Gradzielski, M., Hoffmann, H.,
Mixtures of nonionic and ionic surfactants. The effect of counterion binding in mixtures of tetradecyltrimethylamine oxide and tetradecyltrimethylammonium bromide,
Langmuir 10 (1994) 2594-2603

Günzel, R., Wieser, E., Richter, E., Steffen, H.J.,
Plasma source ion implantation of oxygen and nitrogen in aluminum,
J. Vac. Sci. Technol. B 12 (1994) 927

Hatzopoulos, N., Siapkas, D.I., Hemment, P.L.F., Skorupa, W.,
Formation and characterization of double SIMOX structures by sequential high and low energy oxygen implantation into silicon,
Proc. of the 6th Int. Symp. Silicon-on-insulator technology and devices, The Electrochemical Society, Vol. 94-11 (1994) 123

Hatzopoulos, N., Siapkas, D.I., Katsidis, C.C., Zorba, T., Hemment, P.L.F.,
Refractive index and compositional depth profiles in high energy SIMOX structures,
Proc. of the 6th Int. Symp. Silicon-on-insulator technology and devices, The Electrochemical Society, Vol. 94-11 (1994) 173

Häußler, F., Eichhorn, F., Baumbach, H.,
Small-angle neutron scattering on hardened cement paste and various substances for hydration,
Cement and Concrete Research 24 (1994) 514-526

Häußler, F., Eichhorn, F., Baumbach, H.,
Description of the structural evolution of a hydrating Portland cement paste by SANS,
Physica Scripta 50 (1994) 210-214

Heera, V., Kögler, R., Skorupa, W., Glaser, E.,
Ion beam induced epitaxial crystallization of single crystalline 6H-SiC,
Mat. Res. Soc. Symp. Proc. 316 (1994) 229; 321 (1994) 387

Heera, V., Kögler, R., Skorupa, W., Stoemenos, J.,
Amorphization and recrystallization of 6H-SiC by ion beam irradiation,
Mat. Res. Soc. Symp. Proc. 339 (1994) 197

Heinig, K.-H., Stock, D., Boettger, H., Zinovyev, V.A., Dvurechenskii, A.V., Alexandrov, L.N.,
Formation of double height Si (001) steps by sputtering with Xe ions - a computer simulation,
Mat. Res. Soc. Symp. Proc. 316 (1994) 1035

Heinitz, J., Isakov, N.N., Nikitin, A.N., Sukhoparov, Ullemeyer, K., Walther, K.,
A high-pressure device for in-situ measurements in a neutron beam,
Proc. of the 10th International Conference on Textures of Materials, Clausthal, Germany, 1993, Materials Science Forum 157-162 (1994) 131-136

Helming, K., Schwarzer, R.A., Rauschenbach, B., Geier, St., Leiss, B., Wenk, H.-R., Ullemeyer, K., Heinitz, J.,
Texture estimates by means of components,
Z. Metallkunde 85 (1994) 545-553

Hesse, E., Bischoff, L., Teichert, J.,
Development of a cobalt liquid alloy ion source,
J. Phys. D: Appl. Phys. 27 (1994) 427-428

Hesse, E., Naehring, F.K.,Teichert, J.,
A Li metal ion source with a narrow angle emission for writing beam lithography,
Microelectronic Engineering 23 (1994) 111

Howitz, S., Pham, M.T., Bürger, M., Fiehn, H., Vopel, T., Steinbach, A.,
A Fluidic- ISFET-Microsystem,
Proc. 5th Internat. Meet. on Chemical Sensors, Rome 11.- 14.07.1994, p. 257

Hüller, J., Pham, M.T., Vopel, T., Albrecht, J.,
Ion beam modification of ISFET-membranes for heavy metal ion detection,
Proc. 5th Intern. Meet. on Chemical Sensors, Rome 11.- 14.07.1994, pp. 283-286

Hytry, R., Möller, W., Wilhelm, R.,
Running waveguide discharge for inner coating of metal tubes,
Appl. Phys. Lett. 64 (1994) 3401

Isakov, N.N., Nikitin, A.N., Nikolayev, D.I., Ullemeyer, K., Heinitz, J.,
Teksturnje issledovanija geomaterialov na nejtronnom spektrometre vysokogo rasreschenija v LNF OIYaI,
Trudy meshdunarodnoi konferenzii "Geofizika i sovremennyi mir", (1993) 357-358

Jacob, W., Engelhard, M., Möller, W., Koch, A.,
Absolute density determination of CH radicals in an ECR methane plasma,
Appl. Phys. Lett. 64 (1994) 971

Kämpf, H., Franzke, H.-J., Betzl, M., Scheffzük, Ch.,
Texture investigation on halite and fluorite by neutron diffraction
Proc. of the 3rd Conference on the Mechanical Behaviour of Salt, Palaiseau, France (1994) 153-158

Keudell, A.v., Möller, W.,
Combined plasma-surface modeling for the deposition of C:H films,
J. Appl. Phys. 75 (1994) 7718

Kögler, R., von Borany, J., Panknin, D., Skorupa, W.,
Electrical effects of residual defects in Si after high energy implantation of Ge^+ ions and annealing,
Nucl. Instr. Meth. B 89 (1994) 350

Kreissig, U., R. Grötzschel, R., Behrisch, R.,
Simultaneous measurement of the hydrogen isotopes H, D, T and ^3He with HIERD
Nucl. Instr. Meth., B 85 (1994) 71

Küchler, R., Richter, E.,
Ultrasonic Surface Waves for Studying the Properties of Thin Films,
phys. stat. sol. (a) 146 (1994) 659

Laube, M., Ottermann, C., Wagner, W., Niederwald, H., Rauch, F., Bange, K.,
Composition of titania coatings deposited by different techniques,
Glastechnische Berichte 67 (1994) 87-92

Möller, W.,
Computer simulation of ion-beam assisted thin film growth (Extendet Abstract),
Nucl. Instr. Meth. B 89 (1994) 322

Möller, W.,
Plasma and surface modeling for the deposition of hydrogenated carbon films (Extendet Abstract),
Proc. TATF/HVITF '94, ed. by G. Hecht, F. Richter, and J. Hahn, DGM Informationsgesellschaft Oberursel (1994)

Möller, W., Fukarek, W., Lange, K., Keudell, A.v., Jacob, W.,
Mechanisms of the deposition of hydrogenated carbon films,
Proc. 16th Dry Process Symposium, Tokyo (1994)

Mücklich, A., Klimanek, P.,
Experimental errors in quantitative texture analysis from diffraction pole figures
Proc. of the 10th International Conference on Textures of Materials, Clausthal, Germany, 1993, Materials Science Forum 157-162 (1994) 275-286

Neelmeijer, C., Wagner, W., Schramm, H.P.,
Analysis of art objects by the combined application of three ion beam methods on air,
Proc. of 4th Int. Conf. Non-Destructive Testing of Works of Art,
ed. DGZfP e.V. Berlin (1994) 296-305

Neelmeijer, C., Wagner, W., Schramm, H.-P.,
Nondestructive pigment analysis in paint layers using ion beam methods in air,
Naturwissenschaften 81 (1994) 553

Nikitin, A.N., Sukhoparov, V.A., Heinitz, J. Walther, K.,
Structure Investigations of Piezoelectric Quartzites by Neutron Diffraction,
Journal of Experimental Mineralogy, Seismology and Geology 2 (1993) 152-153

Nikolayev, D.I., Walther, K.,
Absorption correction for non-standard geometry for pole figure measurements
Proc. of the 10th International Conference on Textures of Materials, Clausthal, Germany, 1993, Materials Science Forum 157-162 (1994) 381-386

Nikolayev, D., Ullemeyer, K.
A Note on Preprocessing of Diffraction Pole-Density Data,
J. Appl. Cryst. 27 (1994) 517-520

Panknin, D., Eichhorn, F., Wieser, E., Skorupa, W., Henrion, W., Albrecht, J.,
Electrical and optical properties of β-$FeSi_2$ after Co implantation and annealing,
Nucl. Instr. Meth. B 84 (1994) 172

Panknin, D., Henrion, W., Wieser, E., Voelskow, M., Skorupa, W., Vöhse, H.,
Electrical and optical properties of Co alloyed β-$FeSi_2$ formed by ion beam synthesis,
Mat. Res. Soc. Symp. Proc. Vol. 316 (1994) 723

Pham, M.T., Howitz, S., Bürger, M., Müller, U., and Wegener, T.,
A sensor array structure with ion beam fabricated membranes,
Proc. 5th Internat. Meet. on Chemical Sensors, Rome, 11.- 14.07.1994, pp. 1066-1069

Posselt, M.,
Channeling effects and defect accumulation in ion implantation,
Nuclear Instruments and Methods B90 (1994) 373

Posselt, M.,
Crystal-TRIM and its application to investigations on channeling effects during ion implantation,
Radiation Effects and Defects in Solids 130/131 (1994) 87

Reiß, S., Heinig, K.-H.,
Ostwald ripening during ion beam synthesis - a computer simulation for inhomogeneous systems,
Nuclear Instruments and Methods B84 (1994) 229

Reiß, S., Weber, R., Heinig, K.-H., Skorupa, W.,
Experimental study and modeling of structure formation in buried layers at ion beam synthesis,
Nuclear Instruments and Methods B89 (1994) 337

Reiß, S., Heinig, K.-H., Weber, R., Skorupa, W.,
Is self organisation during Ostwald ripening a crucial process in ion beam synthesis?
Mat. Res. Soc. Symp. Proc. 316 (1994) 819

Reuther, H.,
Mössbauer and Auger spectroscopic investigations of Fe-Si alloys produced by ion implantation
Surface Interface Anal. 22 (1994) 547

Reuther, H., Nikolov, O., Kruijer, S., Brand, R.A., Keune, W., Liljequist, D., Weber, S., Scherrer, S.,
CEMS and DCEMS investigations of Al-implanted iron,
Hyperfine Interactions 92 (1994) 1367

Schmidt, B., Borany, J. von ,Todt, U., Erlebach, A.,
Preparation and characterization of ultrathin crystalline silicon membranes,
Sensors and Actuators A 41-42 (1994) 689-694

Skrotzki, W., Dornbusch, J., Heinicke, F., Ullemeyer, K.,
Formation of oblique shape and lattice preffered orientation in a quartz band of a gneissic mylonite
Proc. of the 10th International Conference on Textures of Materials, Clausthal, Germany; 1993, Materials Science Forum 157-162 (1994) 1481-1486

Steffen, H.J.,
Use of valence-band AES to study thin film growth: oxide and diamond-like carbon,
Thin Solid Films 253 (1994) 269

Teichert, J., Bischoff, L., Hesse, E., Panknin, D., Skorupa, W.,
Formation of $CoSi_2$ wires by maskless implantation with the focused ion beam,
Mat. Res. Soc. Symp. Proc. 316 (1994) 741; 320 (1994) 153

Ullemeyer, K., Weber, K.,
Correction of phyllosilicate (002) X-ray pole figure measurements
Proc. of conference on "Textures of Geological Materials" Göttingen, Germany (1993)
DGM Informationsgesellschaft Verlag, Oberursel, 1994, 83-91

Ullemeyer, K., Helming, K., Siegesmund, S.,
Quantitative texture analysis of plagioclase
Proc. of conference on "Textures of Geological Materials" Göttingen, Germany (1993)
DGM Informationsgesellschaft Verlag, Oberursel, 1994, 93-108

Verbitskaya, E., Eremin, V., Malerenko, A., Strokan, N., Sukhanov, V., Schmidt, B., Borany, J. von ,
Precision semiconductor spectrometry of ions,
Semiconductors 27 (1993) 1127-1136

Verbitskaya, E., Eremin, V., Strokan, N., Kemmer, J., Schmidt, B., Borany, J. von,
Physical aspects of precise spectrometry of α-particles with silicon pn-junction detectors,
Nucl. Instr. and Meth. in Phys. Res. B 84 (1994) 51-61

Wagner, W., Rauch, F., Jeschkowski, U., Bange, K.,
Ion beam analysis investigations on multilayer devices for visible optics,
Thin Films, eds. G. Hecht, F. Richter and J. Hahn, DGM Informationsgesellschaft Verlag, Oberursel (1994) 453-456

Wagner, W., Rauch, F., Bange, K.,
Stoichometry of NiO_xH_y films determined by ion beam analysis,
Nucl. Instr. Meth. B89 (1994) 104-108

Wagner, W., Neelmeijer, C., Schramm, H.P.,
Paint layer studies using PIXE and RBS on air,
Proc. 4th Int. Conf. Non-Destructive Testing of Works of Art, ed. DGZfP e.V. Berlin (1994) 316-325

Wagner, W., Rauch, F., Jeschkowski, U., Bange, K.,
Ion beam analysis investigations on multilayer devices for visible optics,
Phys. stat. sol. 145 (1994) 619-623

Weber, R. Müller, R., Skorupa, W.,
Precipitation studies in oxygen- and nitrogen rich silicon formed by high dose implantation,
Nucl. Instr. Meth. B 84 (1994) 286-290

Weber, R., Skorupa, W.,
Experimental study of structure formation in ion beam synthesized buried layers,
Proc. of the 6th Int. Symp. Silicon-on-insulator technology and devices, The Electrochemical Society, Vol. 94-11 (1994) 57

Weber, R., Yankov, R., Müller, R., Skorupa, W., Reiss, S., Heinig, K.-H.,
Experimental studies of precipitation processes in oxygen implanted silicon,
Mat. Res. Soc. Symp. Proc. Vol. 316 (1994) 729

Conference Contributions

Aldridge, L., Bertram, W.K., Sabine,T., Eichhorn, F., Hempel, A.,
SANS spectra from hydrated cement pastes,
5th BENSC Users' Meeting , Berlin, November 18, 1994

Bayreuther, G., Bottyan, L., Deak, L., Gerdau, E., Korecki, J., Lauter, H., Leupold, O., Nagy, D.L., Pasyuk, V.V., Petrenko, A.V., Reuther, H., Richter, E., Röhlsberger, R., Rüter, D., Szilagyi, E., Szücs, I.,
Nuclear resonant $^{56}Fe/^{57}Fe$ mirror - an attempt,
4th Seeheim Workshop on Mössbauer Spectroscopy, Seeheim, 24.-28.5.1994

Beyer, R., Burghardt, H., Prösch, G., Thomas, E., Reich, R., Grambole, D., Herrmann, F., Weidner, G.,
Physical and electronic properties of thin siliconoxydnitride layers prepared by rapid thermal processing,
4th Int. Symp. on Trends and New Applications in Thin Films and 11th Conf. on High Vacuum, Interfaces and Thin Films,
Dresden, Jan. 1994

Bischoff, L., Teichert, J., Hesse, E., Panknin, D., Skorupa, W.,
Writing implantation with a high current focused ion beam to form $CoSi_2$-microstructures,
38th International Symp. on Electron, Ion and Photon Beams, EIPB '94,
New Orleans, USA, May 31 - June 03, 1994

Bischoff, L., Teichert, J., Hesse, E.,
Interconnection lines following the surface topography fabricated by writing focused ion beam implantation,
Int. Conf. Micro- and Nanoengineering '94, Davos, Switzerland, 26.9.-29.9.1994

Böhmert, J., Brauer, G., Große, M., Eichhorn, F.,
Characterization of irradiation-induced precipitates in VVER-type RPV steel 15Kh2MFA by anomalous small angle X-ray scattering (ASAXS),
International Group on Radiation Damage of Materials
5th Meeting (IGRDM-5), Santa Barbara (California), 1-6 May 1994

Borany, J. von , Goerigk, J., Voitus, W., Henck, R., Gutknecht, D., Fonné, C.,
Fully ion implanted HP-Ge-detectors for X-ray and γ-spectroscopic investigations,
IEEE Nuclear Science Symposium, 30.10.-5.11.1994, Norfolk, Virginia, USA

Brauer, G., Kolitsch, A., Schut, H., van Veen, A.,
Variable energy positron measurements at nitrogen ion bombarded steel,
Effects of Radiation on Materials: 17th International Symposium, Sun Valley, Idaho, 20.-23.6.1994

Chudoba, Th.,
Verbesserung der mechanischen und korrosiven Oberflächeneigenschaften von Magnesium durch Ionenimplantation,
VDI-Tagung Werkstofftechnik, Duisburg, 8.-10.3.1994

Eichhorn, F., Häußler, F., Hempel, A., Hempel, M., Baumbach, H.,
Microstructure of hydrated Portland cement paste investigated by small-angle neutron scattering,
15th European Crystallographic Meeting, Dresden, 28.08.-02.09.1994

Eichhorn, F., Hempel, A., Reichel, P.,
A neutron double-crystal diffractometer with a variable angular resolution,
2nd European Symposium on X-Ray Topography and High-Resolution Diffraction
Berlin, 5-7 September 1994 and
5th BENSC Users' Meeting, Berlin, November 18, 1994

Einfeld, D., Büttig, H., Gläser, W., Guratzsch, H., Janssen, D., Matz, W., Murphy, J.B., Neumann, W., Picard, M., Plesko, M., Pröhl, D., Rossmanith, R., Schlenk, R., Tomassini, D., Tyrroff, H.,
Dynamic Properties of the ROSY Optics,
4th European Particle Accelerator Conference, London, UK, 27 June -1 July 1994

Fiehn, H., Howitz, S., Pham, M.T., Wegener, T., Gehring, T., Bürger, M., Steinbach, A., Vopel, T.,
Components and technology for a Fluidic-ISFET-Microsystem,
Workshop on Micro Total Analysis Systems, University of Twente, Netherlands, 21.-22.11. 1994, Proc. pp. 289-293

Friedlein, R., Herpich, S., Lehnert, U.,Tyrroff, H., Zippe, C., Zschornack, G.,
X-Ray Spectroscopy on ECR Plasmas,
7. Int. Conf. Physics of Highly Charged Ions, Sept. 19-23, 1994, Vienna

Friedrich, M., Bürger, W., Grötzschel, R., Henke, D., Sun, G., Turuc, S., Hebert, D., Rothe, D., Stolz, W.,
Beschleunigermassenspektrometrie an den Rossendorfer Tandembeschleunigern,
58. Physikertagung, 14.-18.03.1994, Hamburg

Gärtner, K., Stock, D., Weber, B., Betz, G., Hautala, M., Hobler, G., Hou, M., Sarite, S., Eckstein, W., Jimenez-Rodriguez, J.J., Perez-Martin, A.M.C., Andribet, E.P., Konoplev, V., Gras-Marti, A., Posselt, M., Shapiro, M.H., Tombrello, T. A., Urbassek, H., Hensel, H., Yamamura, Y. Takeuchi, W.,
Round Robin computer simulations of ion transmission through thin crystalline targets,
2nd International Conference on Computer Simulation of Radiation Effects in Solids (COSIRES), St. Barbara, California, July 25 - 29, 1994

Goerigk, J., Borany, J. von , Voitus, W.,
Electrical activation of phosphorous implanted n^+-layers by means of different thermal annea-ling procedures for planar high purity germanium detectors,
NATO Advanced Study Institute, Seminar on Materials and Processes for Surface and Inter-face Engineering, 18.-29.07. 1994 Castera Verduzan, France

Große, M., Eichhorn, F., Böhmert, J., Brauer, G., Haubold, H.-G., Goerigk,G.,
Characterization of nanoscale precipitates in reactor pressure vessel steel 15Kh2MFA by small angle scattering experiments,
Euromat '94 (15th Conference on Materials Testing in Metallurgy and 11th Congress on Materials Testing), Balatonszeplak (Hungary), 30 May-1 June 1994

Große, M., Eichhorn, F., Böhmert, J., Brauer, G.,
Characterization of irradiation-induced precipitates by small-angle scattering experiments,
17th Symposium on Effects of Radiation on Materials, Sun Valley (Idaho), 20-23 June 1994

Große, M., Eichhorn, F., Böhmert, J., Brauer, G., Haubold, H.-G., Goerigk, G.
ASAXS and SANS investigations of the chemical composition of irradiation-induced precipitates in nuclear pressure vessel steels,
1st European Conference on Synchrotron Radiation in Materials Science, Chester, 3-8 July 1994

Grötzschel, R., (invited)
Composition analysis of thin surface layers by heavy ion ERD and RBS at a 5 MV tandem,
13th Int. Conf. on the Application of Accelerators in Research and Industry, Denton, Texas (USA), 7.-10.11.1994

Günzel, R., Reuther, H., Richter, E.,
Modification of pure Iron by Implantation of Nitrogen using Plasma Immersion Ion Implantation,
International Conference Plasma Surface Engineering, Garmisch-Partenkirchen, 20. - 23.9.1994

Harz, M.,
Mechanisch und thermisch induzierte Spannungen beim anodischen Bonden von Glas und Si-lizium,
11. Internationale Mittweidaer Fachtagung, Sektion E, Mikrosystemtechnik, FH Mittweida, September 1994

Hatzopoulos, N., Siapkas, D.I., Hemment, P.L.F., Skorupa, W.,
Formation and characterization of double SIMOX structures by sequential high and low energy oxygen implantation into silicon,
185th Meeting, The Electrochemical Society, 6th Int. Symp. on "Silicon-on-insulator technology and devices", San Francisco, USA, May 22-27, 1994

Hatzopoulos, N., Siapkas, D.I., Katsidis, C.C., Zorba, T., Hemment, P.L.F.,
Refractive index and compositional depth profiles in high energy SIMOX structures,
185th Meeting, The Electrochemical Society, 6th Int. Symp. on "Silicon-on-insulator technology and devices", San Francisco, USA, May 22-27, 1994

Häußler, F., Hempel, M., Eichhorn, F., Hempel, A., Baumbach, H.,
Hydrating cement pastes as a complex disordered systems,
Euroconference '94 on "Neutrons in disordered matter", Stockholm (Sweden), 9-13 June 1994

Heera, V., Kögler, R., Skorupa, W., Stoemenos, J.,
Amorphization and recrystallization of 6H-SiC by ion beam irradiation,
MRS Spring Meeting 94, San Francisco, April 6, 1994

Heera, V., Kögler, R., Skorupa, W., Stoemenos, J.,
Amorphization and recrystallization of 6H-SiC by ion beam irradiation,
10th Int. Conf. on Ion Implantation Technology, Catania, June 13-17, 1994

Heera, V., Stoemenos, J., Kögler, R., Skorupa, W.,
IBIEC of 6H-SiC,
IBOS-Network Meeting Dresden, 24.-25.9.94

Heinig, K.-H., (invited)
Ion-induced modifications of Si surfaces studied by MD calculations and reaction-diffusion equations
CECAM Workshop on Computer Simulation of the Growth of Semiconductor Materials, Lyon (France), May 30 - June 2, 1994

Heinig, K.-H., Stock, D., Zinovyev, V.A., Dvurechenskii, A.V., (invited)
Molecular Dynamics simulations applied to low energy ions in solids
2nd International Conference on Computer Simulation of Radiation Effects in Solids (COSIRES), St. Barbara, California, July 25 - 29, 1994

Heinig, K.-H., Konoplev, V., Börner, H.,
Prediction of a Crystal-GRID method by means of Molecular Dynamics simulations,
2nd International Conference on Computer Simulation of Radiation Effects in Solids (COSIRES), St. Barbara, California, July 25 - 29, 1994 and Gordon Research Conference on Particle-Solid Interactions, Plymouth (USA), July 31 - August 5, 1994

Heinig, K.-H., Konoplev, V., Jentschel, M., Börner, H.,
Crystal GRID: Eine neue nukleare Methode in der Festkörperphysik,
Arbeitstagung des BMFT-Verbundes "Festkörperphysik und Materialforschung mit nuklearen Methoden", Braunschweig, Oct. 4 - 6, 1994

Heinig, K.-H., Bischoff, L., Teichert, J., Skorupa, W.,
A new fabrication method for submicron $CoSi_2$ wires using focused ion beam implantation and local melting by flash lamps,
Symp. A, Mat. Res. Soc. Fall Meeting Boston (USA), Nov 27 - Dec. 2, 1994

Hempel, M., Hempel, A., Eichhorn, F., Häußler, F., Baumbach, H.,
Investigation of interfaces in hydrating cement pastes by small-angle neutron scattering,
European Physical Society, 14th General Conference Condensed Matter Division (GCCMD-14), Madrid, 28-31 March 1994

Hempel, M., Hempel, A., Häußler, F., Eichhorn, F., Baumbach, H.,
Strukturelle Veränderungen im Zementstein während des Hydratationsprozesses,
ibausil 12 (12. Internationale Baustofftagung), Weimar, 22.-24. September 1994,

Henke, D.,Tyrroff, H., Grötzschel, R., Wirth, H.,
Slow, highly charged ions from 7.25 GHz ECR ion source,
7. Int. Conf. Physics of Highly Charged Ions, Sept. 19-23, 1994, Vienna

Herrmann, F. Grambole, D.,
The New Rossendorf Nuclear Microprobe,
4th International Conference on Nuclear Microprobe Technology and Applications,
Shanghai (China), 10. - 14. 10. 1994

Hesse, E.,
Die Rossendorfer Ionenmikrostrahlanlage IMSA-100,
14. Treffen der Benutzergruppe Ionenimplantation Eaton,
Kirchheim-Heimstetten, 27.9.94

Howitz, S., Pham, M.T., Bürger, M., Fiehn, H., Wegener, T., Vopel, T., Gehring, T.,
Steinbach, A.,
Fluidik-ISFETs für die Analytik,
ACHEMA Frankfurt/Main, May 1994

Howitz, S., Pham, M.T., Vopel, T., Bürger, M., Fiehn, H., Wegener, T., Steinbach,
A., Hellfeld, T.,
Fluidik-ISFET-Mikrosystem,
7. Fachtagung Sensoren Technologie und Anwendung, Bad Nauheim, 14.-16. 03. 1994

Howitz, S., Pham, M.T., Wegner, T., Vopel, T., Steinbach, A., Bürger, M., Fiehn,H.,
Mikrosystem für chemische Analysen,
ACHEMA Frankfurt/Main, Mai 1994

Katsidis, C.C., Siapkas, D.I., Skorupa, W., Hatzopoulos, N., Panknin, D.,
Study of the high energy doping in Si and the formation process of doped high
energy SIMOX structures using FTIR spectroscopy,
10th Int. Conf. on Ion Implantation Technology, Catania, June 13-17, 1994

Kögler, R., von Borany, J., Panknin, D., Skorupa, W., Baither, D.,
Reverse currents of p+/n diodes after high energy implantation of C^{+} and Ge^{+} ions and
annealing,
10th Int. Conf. on Ion Implantation Technology, Catania, June 13-17, 1994

Kögler, R., Heera, V., Skorupa, W.,
IBIEC an 6H-SiC,
BMFT-Verbundtreffen, Braunschweig, Oct. 4-6, 1994

Kolitsch, A., Scheibe, H.J., Drescher, D.,
Modification of Laser-Arc DLC layers by ion beams
4th Internationales Symposium on Trends and new Applications in Thin Films,
Dresden, 7. -11.3.1994

Konoplev, V., Heinig, K.-H.,
Molecular Dynamics studies of self-interstitials in silicon using Stillinger-Weber and Tersoff potentials,
2nd International Conference on Computer Simulation of Radiation Effects in Solids (COSIRES), St. Barbara, California, July 25 - 29, 1994 and Gordon Research Conference on Point Defects, Line Defects, and Interfaces in Semiconductors, Plymouth (USA), July 31 - August 5, 1994

Konoplev, V., Uhlmann, S., Frauenheim, T., Heinig, K.-H.,
Classical and *ab-initio* Molecular Dynamics simulations of atomic configurations produced by a self-interstial in silicon,
Mat. Res. Soc. Fall Meeting, Symp. O, Boston (USA), Nov 27 - Dec. 2, 1994

Lange, K., Möller, W.,
Ratenbestimmende Teilchenflüsse aus Methan-Gleichspannungsentladungen zur Deposition dünner a-C:H-Schichten,
6. Bundesdeutsche Fachtagung Plasmatechnologie, Wuppertal, 2.-3.11.1994

Liu, Q., Biersack, J. P., Posselt, M.,
Comparison of channeling trajectories and ranges as calculated by the continuum potential approximation and by Crystal-TRIM,
2nd International Conference on Computer Simulation of Radiation Effects in Solids (COSIRES), St. Barbara, California, July 25 - 29, 1994

Mathar, R.J., Posselt, M.,
Effektivladungstheorie des elektronischen Stoppings schwerer Ionen im Festkörper,
Frühjahrstagung des Arbeitskreises Festkörperphysik bei der DPG, Münster, March 21 - 25, 1994

Mathar, R.J., Posselt, M.,
Elektronische Abbremsung schwerer Ionen im Festkörper,
Arbeitstagung des BMFT-Verbundes "Festkörperphysik und Materialforschung mit nuklearen Methoden", Braunschweig, Oct. 4 - 6, 1994

Mathar, R.J., Posselt, M.,
Effective charge theory of the electronic stopping of heavy ions in solids,
Gordon Research Conference on Particle-Solid Interactions, Plymouth (USA), July 31 - August 5, 1994

Matz, W., Nitsche, H., Bernhard, G., Prokert, F., Betzl, M., Schlenk, R., Pröhl, D., Möller, W., Brendler, V., Baraniak, L.,
A Project for a Radiochemical and Materials Science Beam Line at the ESRF,
1st European Conference on Synchrotron Radiation in Materials Science,
Chester, UK, 3-8 July 1994

Matz, W., Nitsche, H., Möller, W., Bernhard, G., Prokert, F., Schlenk, R., Pröhl, D., Betzl, M., Brendler, V., Baraniak, L.,
The Project for a Radiochemical and Materials Science Beam Line at the ESRF,
15th European Crystallographic Meeting, Dresden, Germany, 28 August-2 September 1994

Möller, W., (invited)
Plasma and surface modelling for the deposition of hydrogenated carbon films,
11th Conf. on High Vacuum, Interfaces and Thin Films, Dresden, 10.03.1994

Möller, W., (invited)
Plasma- und Oberflächenprozesse bei der Abscheidung amorpher C:H-Schichten,
Deutsche Fachtagung Plasmatechnologie, Wuppertal, 03.10.1994

Möller, W., (invited)
Mechanisms of the deposition of hydrogenated carbon films,
Dry Process Symposium, Tokyo/Japan, 11.10.1994

Neelmeijer, C., Wagner, W., Schramm, H.P.,
Analysis of art objects by the combined application of three ion beam methods on air,
4th Int. Conf. Non-Destructive Testing of Works of Art,
03.-08.10.1994, Berlin

Nikitin, A.N., Sukhoparov, V.A., Heinitz, J., Walther, K.,
Investigation of texture formation in geomaterials by neutron diffraction with high pressure chambers,
Neutron Scattering at High Pressure, Dubna, 5-7 October 1994

Nikitin, A.N., Sukhoparov, V.A., Heinitz, J., Walther, K.,
Investigations of texture formation in geomaterials by neutron diffraction with high pressure chambers,
XXXIInd Annual Meeting of the European High Pressure Research Group, Brno, 29 August-1 September 1994

Möller, W., Fukarek, W., Keudell A.V.,
Particle-solid interaction mechanisms during PECVD of hydrogenated carbon,
Gordon Research Conference on Particle-Solid Interactions, Plymouth (USA), July 31 - August 5, 1994

Neelmeijer, C., Wagner, W., Schramm, H.P., Thiel, U.,
"De re metallica" (G. Agricola) - IBA on air,
13th Int. Conf. Application of Accelerators in Research and Industry, 07.-10.11.1994, Denton (Texas), USA

Nomura, K., Reuther, H., Richter, E., Ujihira, Y.,
Magnetic structure of Fe-Si-Al films implanted with Al and N ions,
Eötvös Workshops in Science: Nuclear Techniques in Structural Chemistry,
Budapest, 31.8.-4.9.1994

Pacaud, Y., Skorupa, W.,
Study of defects induced by 200 keV Ge-Implantation in 6H-SiC,
IBOS-Network Meeting Dresden, 24.-25.9.94

Pecher, P., Jacob, W., Lange, K.,
Massenselektierte Ionenenergieverteilungen aus Methan-ECR-Plasmen,
6. Bundesdeutsche Fachtagung Plasmatechnologie, Wuppertal, 2.-3.11.1994

Posselt, M.,
Discussion of different phenomenological models for defect evolution used in dynamic computer simulations of ion implantation into crystalline targets,
2nd International Conference on Computer Simulation of Radiation Effects in Solids (COSIRES), St. Barbara, California, July 25 - 29, 1994 and
Gordon Research Conference on Particle-Solid Interactions, Plymouth (USA), July 31 - August 5, 1994

Posselt, M.,
3-D modeling of ion implantation into crystalline silicon: influence of damage accumulation on dopant profiles,
10th International Conference on Ion Implantation Technology, Catania, June 13 - 17, 1994

Posselt, M.,
Dynamic simulation of damage accumulation during implantation of molecular ions into crystalline silicon,
2nd International Conference on Computer Simulation of Radiation Effects in Solids (COSIRES), St. Barbara, California, July 25 - 29, 1994

Posselt, M., Heinig, K.-H.,
BC and MD simulations of low-energy channeling implantation,
2nd International Conference on Computer Simulation of Radiation Effects in Solids (COSIRES), St. Barbara, California, July 25 - 29, 1994

Prokert, F., Savenko, B.N., Balagurov, A.M.,
The Observation of Phonons in TSCC by Pulsed Neutron Diffraction
15th European Crystallographic Meeting (ECM15), Dresden, Germany, 28.8.-2.9.1994

Reiß, S., Heinig, K.-H.,
Computer simulations of mechanisms of the SIMOX process,
2nd International Conference on Computer Simulation of Radiation Effects in Solids (COSIRES), St. Barbara, California, July 25 - 29, 1994 and Gordon Research Conference on Particle-Solid Interactions, Plymouth (USA), July 31 - August 5, 1994

Reuther, H., (invited)
CEMS study of silicon implanted iron,
4th Seeheim Workshop on Mössbauer Spectroscopy, Seeheim, 24.-28.5.1994

Reuther, H.,
Untersuchungen an durch Ionenimplantation hergestellten Eisen-Silizium-Schichten,
8. Arbeitstagung Oberflächenanalytik, Kaiserslautern, 5.-8.9.1994

Reuther, H.,
CEMS-Untersuchungen an Silizium implantiertem Eisen,
VII. Mößbauer-Kolloquium, Freiberg, 28.-30.9.1994

Ruault, M.-O., Clayton, J., Reiß, S., Heinig, K.-H., Kaïtasov, O., Bernas, H.,
Study of nucleation and growth of $CoSi_2$ precipitates during the implantation stage of ion beam synthesis,

Mat. Res. Soc. Fall Meeting, Symp. A, Boston (USA), Nov 27 - Dec. 2, 1994 and Reunion annuelle du reseau francilien de microscopie electronique, Paris (France) Dec 12, 1994

Schellhorn,U., Hellwig, U., Danckert, O., Breer, S., Rupp, R.A., Gräbmeier, C., Finke, E., Kohlbrecher, J., Wiedenmann, A., Hempel, A., Eichhorn, F., Ioffe, A.,
Neutron optics based on holographic gratings,
5th BENSC Users' Meeting, Berlin, November 18, 1994

Schmidt, B., and Borany, J. von,
Silicon detectors with buried doping layers,
ALADIN - Workshop, Rathen, 25.-28.09.1994

Serre, C., Perez-Rodriguez, A. Romano-Rodriguez, A., Morante, J.R., Acero, M.C., Esteve, J., Kögler, R., Skorupa, W.,
Structural and spectroscopic analysis of high dose carbon ion implantation processes in silicon,
10th Int. Conf. on Ion Implantation Technology, Catania, June 13-17, 1994

Skorupa, W.,
Ge implantation into 6H-SiC: Damage, Amorphization and IBIEC,
IBOS-Network Meeting, Paris, 4.-5.2.94

Skorupa , W., (invited)
Ion Beam Processing for Silicon-on-Insulator, ,
NATO Advanced Research Workshop on "Physical and Technical Problems of SOI Structures and Devices", Yalta, Crimea, Ukraine, Nov. 1-4, 1994

Steffen, H.J., Heera, V., Kögler, R., Skorupa, W.,
Ion beam-induced SiC Crystallization of carbon implanted layers in Si(100) studied by electron spectroscopy,
41st National Symp. American Vacuum Society, Denver, USA, October 24-28, 1994

Teichert, J., (invited)
Maskless implantation using focused ion beams,
International Workshop Ion Micro Beams - Generation and Application,
Rottach-Egern, May 1994

Thomae, R.W., Seiler, B., Bender, H., Brutscher, J., Jakob, A., Klein, H., Maaser, A., Müller, J., Sarstedt, M., Weber, M.,
The Frankfurt PIII - Experiment,
International Conference on Ion Implantation Technology, Catania, Italien, 13.- 17. 6.1994

Thomae, R.W., Seiler, B., Bender, H., Brutscher, J., Günzel, R., Halder, J., Klein, H., Müller, J., Sarstedt, M., (invited)
High current ion implantation by plasma immersion technique,
Thirteenth International Conference on the Application of Accelerators in Research and Industry, Denton/Texas, 7.-10.11.1994

Uhlemann, J., Harz, M.,
Anlagen- und Verfahrenstechnische Entwicklungen zum anodischen Bonden,
11. Internationale Mittweidaer Fachtagung, Sektion E, Mikrosystemtechnik, FH Mittweida, September 1994

Wagner, W., Rauch, F., Jeschkowski, U., Bange, K.,
Ion beam analysis investigations on multilayer devices for visible optics,
4th Int. Symp. Trends and New Applications in Thin Films - TATF94 and 11th Conf. High Vacuum, Interfaces and Thin Films - HVITF94,
07.-11.03.1994, Dresden

Wagner, W., Neelmeijer, C., Schramm, H.P.,
External proton beam analysis of layered objects,
8. Arbeitstagung Angewandte Oberflächenanalytik AOFA8,
05.-08.09.1994, Kaiserslautern

Wagner, W., Neelmeijer, C., Schramm, H.P.,
Paint layer studies using PIXE and RBS on air,
4th Int. Conf. Non-Destructive Testing of Works of Art,
03.-08.10.1994, Berlin

Wagner, W., Neelmeijer, C., Schramm, H.P.,
External beam PIXE and RBS studies on paint layers,
13th Int. Conf. Application of Accelerators in Research and Industry,
07.-10.11.1994, Denton (Texas), USA

Weber, R., Skorupa, W.,
Experimental study of structure formation in ion beam synthesized buried layers,
"Materials and Processes for Surface and Interface Engineering", Chateau de Bonas, Castera-Verduzan, Gers, France, July 18-29, 1994

Weishart, H., Schöneich, E., Matz, W., Steffen, H.J., Skorupa, W.,
Ion beam synthesis by tungsten-implantation into 6H-SiC,
MRS Fall Meeting, Nov. 28 - Dec. 02, 1994, Boston, USA

Wieser, E.,
Ion beam surface modification studies at the Research Center Rossendorf,
1st Japanese-German Joint Symposium on Advanced Chemical Processing Technology,
TU Bergakademie Freiberg, 24.11.1994

Yankov, R.A., Komarov, F.F.,
Direct formation of thin film nitride structures by high intensity ion implantation of nitrogen into silicon,
NATO Advanced Research Workshop on "Physical and Technical Problems of SOI Structures and Devices", Yalta, Crimea, Ukraine, Nov. 1-4, 1994

Lectures

Betzl, M.,
Das Texturdiffraktometer NSWR am Impulsreaktor IBR-2 in Dubna,
Verbundgeräte-Beratung des Komitees für Forschung mit Neutronen
21.-22.1.1994, Max-Plank-Institut für Polymerenforschung, Mainz

Bischoff, L.,
Ionenstrahlsynthese von $CoSi_2$-Mikrostrukturen durch maskenlose Implantation mit dem feinfokussierten Ionenstrahl,
Eidgenössische Technische Hochschule Zürich, Institut für Teilchenphysik, 29.03.94,

Borany, J. von, Schmidt, B.,
Application of high energy ion-implantation for silicon radiation detectors,
EUROBALL LCP detectors meeting, 2.-3.05.1994, Bordeaux, France

Borany, J. von,
Fully ion implanted HP-Ge-detectors for an EUROBALL-stack-system,
GSI Darmstadt, 18.07.1994

Brutscher, J.,
Plasmaimmersionsimplantation in Rossendorf,
Winterseminar "Atom- und Beschleunigerphysik" des Instituts für Angewandte Physik der Universität Frankfurt/M., 27.2.-5.3.94

Brutscher, J.,
Dynamik der Randschicht bei der Plasmaimmersionsimplantation,
Vortrag Bundesdeutsche Fachtagung Plasmatechnologie Wuppertal, 2./3.11.94

Chudoba, Th.,
Ultramikrohärtemessungen mit dem DUH-202
FhG IWS Hemholzstraße, 9.2.94

Eichhorn, F., Hempel, A., Reichel, P.,
First experience with the double-crystal diffractometer S-V12 at the neutron guide 3B
4th Users Meeting at the Berlin Neutron Scattering Center (BENSC)
Hahn-Meitner-Institut Berlin, May 6-7, 1994

Friedrich, M.,
Operation and research at the Rossendorf electrostatic accelerators,
University of Lund, Dept. of Physics, June 17, 1994

Gorski, N.,
SANS-Untersuchungen an mizellaren Lösungen bei hohen hydrostatischen Drücken,
Universität Bayreuth, 09.03.1994

Grambole, D.,
Die Mikrostrahlanlagen an den Ionenbeschleunigern des FZR - Aufbau und Einsatz in der Materialanalytik,
Universität Leipzig, Fakultät für Physik und Geowissenschaften, Abt. Nukleare Festkörperphysik, July 13, 1994

Günzel, R.,
Ionenimplantation durch Plasmaimmersionsimplantation,
Erfahrungsaustausch "Niederdruckentladungen zur Oberflächenbehandlung" in Mühlleithen, 21. - 24.3.94

Harz, M., Schmidt, B., Kreissig, U., Grigull, S., Hüller, J.,
Statusbericht zum Teilvorhaben Si-Si-Fusion- und Si-Glas-Anodic-Bonding im Rahmen des BMFT- Verbundprojektes ANSYS, Förderkennz. 13MV0266, Speyer, 30.06.1994

Harz, M.,
Modellierung und Messung mechanisch und thermisch induzierter Spannungen in anodisch gebondeten Glas - Silizium - Verbindungen,
TU Dresden, Seminar Inst. f. Halbleiter- und Mikrosystemtechnik, Dresden, 05.05.1994

Heera, V.,
Ionenstrahlinduzierte epitaktische Kristallisation und Grenzflächenamorphisierung,
Hahn-Meitner-Institut, Berlin, 18.1.1994

Heera, V.,
Amorphisierung und Rekristallisation von 6H-SiC durch Ionenbestrahlung,
Uni Erlangen, FB Angewandte Physik, 18.11.1994

Heinig, K.-H.,
The GRID-method with single crystalline samples - new possibilities due to the structure in γ-lines,
ILL Grenoble (France), Feb. 17, 1994

Heinig, K.-H.,
Computer simulations of ion beam modifications of solids,
AT&T Bell Labs, Murray Hill (USA), Dec. 9, 1994

Howitz, S.,
Module des Mikro-Fluidhandlings,
Institut für Biotechnologie, Universität Würzburg, Februar 1994

Howitz, S.,
MST-Konzeption von μ-Fluidik-Systemen,
Kernforschungszentrum Karlsruhe, Dezember 1994

A. Kolitsch
Ion Implanter 1090-First User's Meeting,
Jyllinge, Dänemark, 1.-3. Juni 1994

Lange, K., Schmidt, B., Harz, M., Kreissig, U., and Grigull, S.,
Bericht zum Treffen Arbeitsgruppe Montagetechnik im Rahmen BMFT-Verbundprojekt ANSYS, Förderkennz. 13MV0266, Berlin, 23.09.1994

Matz, W.,
A beam line for radiochemistry and ion beam physics on a bending magnet source at the ESRF
9th CRG-Club Meeting, ESRF, Grenoble, February 24-25, 1994

Matz, W., Nitsche, H., Bernhard, G.,
Proposal for a beam line for radiochemistry and ion beam physics on a bending magnet source at the ESRF (Project ROBL),
Report to the ESRF Review Committee on the Rossendorf Proposal, Grenoble, April 30, 1994

Möller, W.,
Mechanismen und Modelle der plasmagestützten Abscheidung aus der Gasphase,
Physikalisches Kolloquium, Ruhr-Universität Bochum, 16.05.1994

Möller, W.,
Mechanisms and modeling of the plasma-enhanced deposition of hydrogenated carbon films from methane,
Technische Universität Eindhoven, Abt. für Physik, 08.07.1994

Möller, W.,
Mechanisms and modeling of the plasma-enhanced deposition of hydrogenated carbon films from methane,
Univ. of Illinois (USA), Coordinated Science Laboratory, 08.08.1994

Möller, W.,
Mechanisms and modeling of the plasma-enhanced deposition of hydrogenated carbon films from methane,
Argonne National Laboratory, Illinois (USA), 10.08.1994

Möller, W.,
Ionenbeschußeffekte bei der plasmagestützten Deposition von amorphen Kohlenstoffschichten,
FhI für Werkstoff- und Schichttechnologie, Dresden, 10.08.1994

Möller, W.,
Ion beam physics at Rossendorf/Dresden,
Univ. of Kyoto/Japan, Inst. of Technical Physics, 16.10.1994

Posselt M.,
Simulation of damage accumulation during ion implantation,
Institut für integrierte Systeme, ETH Zürich (Switzerland),
March 17, 1994

Schmidt, B.,
Anwendung der MeV-Ionenimplantation bei der Herstellung von Silicium-Sperrschichtdetek-toren (in russisch),
Institutsseminar PTI St. Petersburg, Russia, 10.06.19934

Schmidt, B.,
Ion implanted silicon pn-junction detectors with buried doped layers,
Institutsseminar Brookhaven National Laboratory, Brookhaven, USA, 14. 07. 1994

Skorupa, W.,
Ionenstrahlmodifizierung von einkristallinem Silizium durch Hochenergieimplantation,
Universität Augsburg, Sektion Physik, 21.07.1994

Skorupa W.,
Erzeugung von SiO_2- und Si_3N_4-Schichten durch Hochdosis-Ionenimplantation,
TU Dresden, Sektion Physik, 27.06.1994

Skorupa, W., Schmidt, B., Borany, J. von,
Anwendungen der MeV-Implantation,
Vortrag bei Fa. SILTEC, Seminar in Salem, Oregon (USA), Mai 1994

Steffen, H.J.,
Materialmodifikation und Analyse mit Ionenstrahlen,
Max-Planck-Institut für Metallforschung, Institut für Werkstoffwissenschaften,
Stuttgart, 20.06.1994

Teichert , J.,
Ionenoptischer Entwurf und experimentelle Ergebnisse eines achromatisch korrigierten Massenseparators für die Ionenfeinstrahlanlage IMSA-100 in Rossendorf,
Eidgenössische Technische Hochschule Zürich, Institut für Teilchenphysik, 29.03.94,

Ullemeyer, K., Weber, K.,
Gefügeentwicklung in einem Transpressionsregime
5. Symposium Tektonik-Strukturgeologie-Kristallingeologie, Göttingen, 7.-9. April 1994

Walther, K.,
Neutronendiffraktion mittels Flugzeittechnik
Hahn-Meitner-Institut, Berlin, 24.1.1994

Reports

Bischoff, L., Teichert, J., Hesse, E., Geßner, T., Löbner, B., Breng, U.,
Anwendung des feinfokussierten Ionenstrahles zur Fertigung mikromechanischer Bauelemente,
FZR Report-31, Februar 1994

Borany, J. von ,
n^+-Kontaktierung von HP-Ge-Detektoren,
Abschlußbericht zum BMFT-Fördervorhaben 06 DR 103 / TP3, November 1994

Große, M., Böhmert, J., Eichhorn, F., Haubold, H.-G., Goerigk, G.,
Resonante Röntgenkleinwinkelstreuung zur Untersuchung bestrahlungsinduzierter Ausscheidungen im Stahl 15Ch2MFA,
Jahresbericht 1993 HASYLAB am DESY Hamburg, 497-498

Howitz, S., Pham, M.T., Vopel, T., Steinbach, A., Bürger, M., Fiehn, H.,
Mikrosysteme für schwierige Messungen,
Chemische Industrie 6 (1994) 64-66.

Hüller, J.,
Entwicklung neuer Membranmaterialien für ionensensitive Feldeffekttransistoren durch Ionenstrahlsynthese,
Abschlußbericht zum AiF-Projekt 254 D, Januar 1994.

Pham, M.T., Howitz, S.,
Towards microinstrumentations for chemical analysis at the Research Center Rossendorf,
mst news, No. 11/1994

Prokert, F., Savenko, B.N., Balagurov, A.M.,
Thermal Diffuse Scattering in Time-of-Flight Neutron Diffraction Studied on SBN Single Crystals,
JINR Report E14-94-99, Dubna 1994

Stins, O.W.M.,
A retarding field energy analyser to measure the energy distributions of liquid metal ion sources,
FZR Report-35, August 1994

Zen En Ken, Isakov, N.N., Kirilov, A.S., Korobtschenko, M.L., Ostrovnoj, A.I., Resajev, W.E., Sirotin, A.P., Heinitz, J.,
Sistema nakoplenija, upravlenija i kontrolja spektrometra NSWR v standarte VME,
JINR Report R 13-94-73, Dubna, 1994

Laboratory Visits

Bischoff, L., Teichert, J.,
ETH Zürich, Switzerland,
March 27-29, 1994

Borany, J. von,
Instituto Nacional de Investigaciones Nucleares, Salazar, Mexico-D.F., Mexico,
12.09.-13.10.1994

Friedrich, M.,
University of Lund, Dept. of Physics, Lund, Sweden,
June 13-17, 1994

Heinig, K.-H.,
ILL Grenoble, France,
Feb. 10 - 18, 1994

Heinig, K.-H.,
AT&T Bell Labs, Murray Hill, USA,
Dec. 2 - 15, 1994

Pacaud, Y.,
Trinity College, Dublin, Irland,
July 21-30, 1994

Posselt M.,
Institut für Integrierte Systeme der ETH Zürich, Switzerland,
March 14 - 25, 1994, Oct. 24 - Nov. 4, 1994

Protze, A.,
Argonne National Laboratory, Argonne IL, USA,
Sept. 19-Oct. 28, 1994

Reiß S.,
Kurchatov Atomic Energy Institute, Moscow, Russia,
Sept. 4 - 11., 1994

Schmidt, B.,
Physico-Technical Institute, St. Petersburg, Russia,
25.05.-15.06.1994

Schmidt, B.,
Brookhaven National Laboratory, Instrumentation Division, Upton, Long Island, USA,
11.07.-15.07.1994

Steffen, J.,
Wayne State University, MI; Eastern Michigan University, MI, USA,
Oct. 20-21, 1994

Patents

Fuhr, G., Howitz, S.,
Kryokonservierung und Tienftemperaturbearbeitung von biologischen Zellen,
P 4 438 232.4, Oktober 94

Harz, M., Engelke, H.,
Verfahren zur Veränderung der Durchbiegung von anodisch gebondeten flächigen Verbund-körpern aus Glas und Metall oder Halbleitern,
P 44 36 561.6, 6.10.1994

Heinig, K-H., Reiss, S., Schmidt, B., Skorupa, W.,
Verfahren zur Herstellung röhrenförmiger Mikrostrukturen in Festkörpern
Patentanmeldung EP 94 106 815.7, 2.05.1994

Howitz, S., Pham, M.T.,
Chemischer Mikro-Analysator,
Patentanmaldung P 4 405 004.6

Howitz, S., Pham, M.T.,
Mikro-Fluiddiode,
Patentanmeldung P 4 405 005.4

Howitz. S., Pham, M.T.,
Mikro-Fluidmanipulator,
Patentanmeldung P 4 405 026.7

PhD Thesis

Hesse, E.,
Eine Lithium-Flüssigmetallionenquelle für die Lithographie mit schreibendem Ionenstrahl,
07.12.1994, TU Dresden

Diploma Theses

Bürger, M.,
Fluidlabormeßsystem mit ISFET-Sensoren,
Januar 1994, TU Dresden

Gehring, T.,
Konzeption und Realisierung von Eignungsuntersuchungen an mikromechanischen Aktuatoren (Ventilen und Pumpen) hinsichtlich ihrer Anwendbarkeit in Mikro-Fluidiksystemen,
Oktober 1994, TU Dresden

Wegener, T.,
Optimierung von piezoelektrisch getriebenen Schalldruckpumpen,
August 1994, TU Dresden

Meetings organized by the institute

European Meeting of the EMRS Network III "Ion Beam Processing of Semiconductors",
Chair Persons: Skorupa, W., Pacaud, Y.,
23./24.09.94, Rossendorf

Meeting of german experts to the deposition of c-BN,
Chair Person: Möller, W.,
07./08.06.94, Rossendorf

Seminar of the Institute

Dr. C.W. Allen, Argonne National Laboratory,
In situ transmission electron microscope studies of irradiation-influenced phase transformations,
01.03.1994

Dr. A. Anders, Lawrence Berkeley Laboratory,
Vakuumbogen-Ionenquellen: Plasmaphysik und Anwendungen,
02.06.1994

Prof. D. G. Armour, Univ. Salford,
The technology and application of ultra-low energy ion beams,
18.01.1994

Dr. R. Behrisch, MPI für Plasmaphysik, Garching,
Die Plasma-Wand-Wechselwirkung bei den Versuchen zur kontrollierten thermischen Fusion,
07.04.1994

Prof. J. Biersack, HMI Berlin,
Energieverlust und Reichweite von extrem hochgeladenen niederenergetischen Ionen (z.B. 300 keV Xe^{44} - > SiO_2),
11.05.1994

Prof. W. Bolse, Universität Göttingen,
Materietransport im ionenbestrahlten Festkörper,
14.07.1994

Prof. M. Döbeli, Paul-Scherrer-Institut, ETH Hönggerberg,
C- und Ge-Clusterbestrahlung von kristallinem Si,
08.12.94

Prof. V. Dose, MPI für Plasmaphysik Garching,
Inverse Photoemission,
28.04.1994

Prof. H. Ehrhardt, Universität Kaiserslautern,
Schichtwachstumsmodelle superharter metastabiler Phasen,
01.12.94

Prof. J. Fink, IFW Dresden,
Fullerene und Fullerenverbindungen,
09.06.1994

Prof. E. Förster, Max-Planck-Arbeitsgruppe "Röntgenoptik", Jena,
Röntgenoptik geborgener Kristalle,
24.03.1994

Prof. F. Fujimoto, Universität Tokyo,
Untersuchung der Wasserstoffbelegung von kristallinen Wolframoberflächen mittels $H(^{15}N,\alpha\gamma)^{12}C$-Resonanzreaktion,
03.02.1994

Prof. W. Heiland, Universität Osnabrück,
Experimente zur Wechselwirkung hochgeladener Ionen mit Festkörpern,
21.04.1994

Dr. W. Jäger, KFA Jülich,
Quantitative Hochauflösungs-Elektronenmikroskopie von Si-Ge-Heterostrukturen,
06.05.1994

Prof. R. Kassing, Gesamthochschule Kassel,
Mikrosystemtechnik,
15.12.94

Dr. V. Konoplev, Universität Alicante,
Molecular dynamics studies of defects and their migration in silicon,
10.11.1994

Dr. D.L. Nagy, KFKI Budapest,
Mößbauer-Streuung bei streifendem Einfall: Eine tiefenselektive analytische Methode,
10.02.1994

Dr. J. Pezoldt, TU Ilmenau,
Kontrollierte lokale polytype Phasenübergänge: Prinzipien und Anwendungen am Beispiel von SiC,
03.11.1994

Dr. R. Reiß, Otto-Schott-Institut für Glaschemie, FSU Jena,
Ein- und mehrstufige Abdruckverfahren für die Elektronenmikroskopie,
31.03.1994

Dr. A.A. Rempel, Institut für Festkörperchemie, Jekaterinburg,
Nonstoichometric transition metal carbides - crystal structure, order-disorder phase transformation and properties,
17.02.1994

Dr. T. Diaz de la Rubia, Lawrence Livermore National Laboratories,
An assessment of fundamental aspects of radiation damage production and accumulation in metals and alloys,
09.09.1994

Prof. F. Saris, FOM Amsterdam,
Exploring the iron/nitrogen phase diagram,
24.11.94

Prof. S. Schiller, FEP Dresden,
Forschungsprofil des Fraunhofer-Institutes für Elektronenstrahl- und Plasmatechnik,
27.01.1994

Dr. A. Weber, FhI Schicht- und Oberflächenphysik, Braunschweig,
Abscheidung von kubischem Bornitrid,
26.05.1994

Prof. E. Weber, Universität Berkeley,
GaN - ein neues Material für blaue Laser,
11.07.1994

Dr. R. Wiedemann, TU Bergakademie Freiberg,
Eigenspannungen in Hartstoffschichten,
23.06.1994

Prof. W. Witthuhn, FSU Jena,
Radioaktive Atome - Sonden im Halbleiter,
16.06.1994

Departments of the Institute

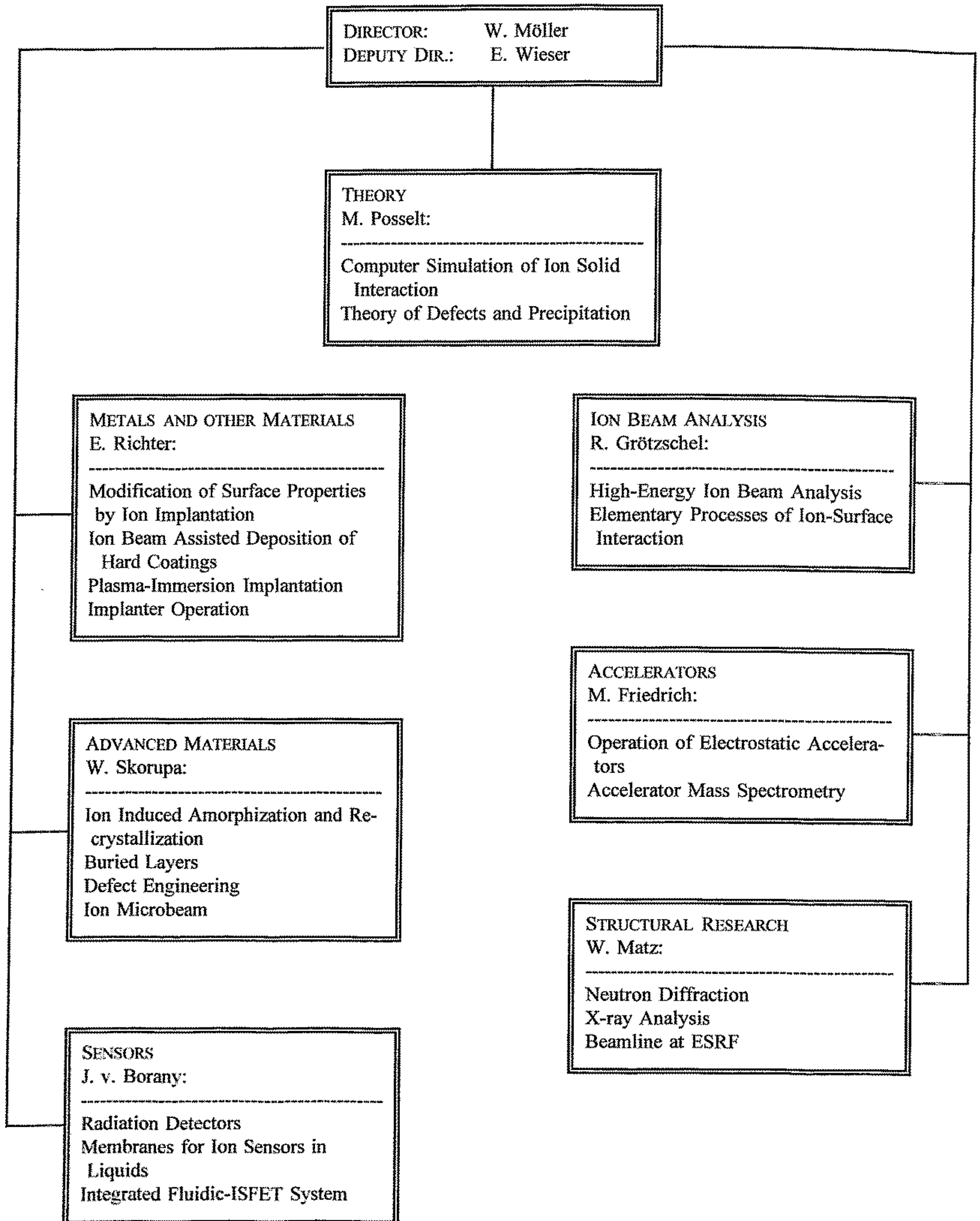

List of Personnel

Director: Prof. W. Möller **Deputy Director:** Prof. E. Wieser

Scientific Staff:
Permanent:

Dr. M. Betzl
Dr. L. Bischoff
Dr. J. von Borany
Dr. W. Bürger
Dr. F. Eichhorn
Dr. M. Friedrich
Dr. W. Fukarek
Dr. D. Grambole
Dr. R. Grötzschel
Dr. R. Günzel
Dr. V. Heera
Dr. K.-H. Heinig
Dr. H.-U. Jäger
Dr. A. Kolitsch
Dr. R. Kögler
Dr. U. Kreißig
Dr. W. Matz
Dr. A. Mücklich
Dr. C. Neelmeijer
Dr. D. Panknin
Dr. M.T. Pham
Dr. M. Posselt
Dr. F. Prokert
Dr. H. Reuther
Dr. E. Richter
Dr. B. Schmidt
Dr. J. Schöneich
Dr. H. Seifarth
Dr. W. Skorupa
Dr. J. Steffen
Dr. J. Teichert
Dr. H. Tyrroff
Dr. M. Voelskow

Post Docs:

Dr. J. Brutscher
Dr. H. Weishart
Dr. N. Schell

Stipendiaries:

Dr.N. Pessoa Barradas
Dr. I. Tyschenko

Projects:

M. Bürger
Dr. H. Fiehn
D. Henke
Dr. S. Howitz
Dr. J. Hüller
R. Küchler
M. Mäder
Dr. Y. Pacaud
I. Ritschel
Prof. I. Sandner
Dr. M. Seidel
Dr. A. Steinbach
T. Vopel
Dr. W. Wagner
Dr. K. Walther

PhD Students:

K. Albe
F. Brenscheidt
T. Chudoba
M. Dobler
J. Goerigk
S. Grigull
N. Hatzopoulos
A. Hempel
T. Henkel
E. Hesse
M. Jentschel
W. Jiang
S. Mändl
R. Mathar
D. Möller
U. Müller
M.F. Plass
G. Sun
S. Reiß
R. Weber

Guests:

Dr. C.W. Allen
Prof. J. Biersack
K. Brand
Dr. A. Deshkowskaya
Dr. N. Donkov
Prof.A. Dvurechenskii
Prof. F. Fujimoto
Dr. N.N. Isakov
Dr. V. Konoplev
Dr. I. Loader
Dr. V. Magula
M. Marik
Prof. L. Maximov
Dr. C.S. Murthy
Dr. D.L. Nagy
Dr. K. Nomura
Dr. J. Pezoldt
Prof. A.I. Ryazanov
J. Rozinek
Dr. E. Szilagyi
Prof. Y. Trushin
Dr. A. E. Volkov
Dr. J.G. Watson
A. Wiebert
Dr. R. Yankov
Dr. V. Zinovjev

Technical Staff:
Permanent:

J. Altmann
R. Aniol
I. Beatus
W. Boede
K.-D. Butter
W. Gäßner
B. Gebauer
H.-J. Grahl
P. Hartmann
F. Herrmann
G. Hofmann
R. Hüller
M. Iseke
S. Klare
R. Kliemann
L. Kumpf
G. Küster
D. Maul
M. Mißbach
I. Morawitz
K. Müller
F. Nötzold
W. Probst
A. Protze
E. Quaritsch
P. Reichel
B. Richter
M. Roch
E. Rost
C. Rußig
B. Scheumann
H. Schluttig
E. Schmidt
G. Schnabel
J. Schneider
A. Scholz
J. Schröter
C. Schulenberg
H. Seifert
U. Strauch
K. Thiemig
S. Turuc
A. Vetter
A. Weise
I. Winkler

Projects:

G. Franz
H. Hempel